

1. REPORT NUMBER CA13-2416	2. GOVERNMENT ASSOCIATION NUMBER	3. RECIPIENT'S CATALOG NUMBER
4. TITLE AND SUBTITLE Seismic Responses of MSE Walls Using Accelerated Alternative Backfill Materials with Recycled Tire Shreds and Lightweight Expanded Aggregates		5. REPORT DATE August 1, 2013
		6. PERFORMING ORGANIZATION CODE
7. AUTHOR Ming Xiao, Fariborz Tehrani, Manoochehr Zoghi		8. PERFORMING ORGANIZATION REPORT NO. CSU Fresno/CA13-2416
9. PERFORMING ORGANIZATION NAME AND ADDRESS Department of Civil and Geomatics Engineering California State University, Fresno Lyles College of Engineering 2320 East San Ramon Avenue, M/S EE94 Fresno, CA 93740		10. WORK UNIT NUMBER
		11. CONTRACT OR GRANT NUMBER 65A0449
12. SPONSORING AGENCY AND ADDRESS California Department of Transportation Division of Research, Innovation and System Information, MS-83 Engineering Service Center, MS 9-2/5i 1227 O Street Sacramento CA 95814		13. TYPE OF REPORT AND PERIOD COVERED Final Report 5/16/2012 – 7/16/2013
		14. SPONSORING AGENCY CODE

15. SUPPLEMENTARY NOTES
 Prepared in cooperation with the State of California Department of Transportation.

16. ABSTRACT
 Tire derived aggregates (TDA) and lightweight aggregates (LWA) have been increasingly used as lightweight backfills for embankments and retaining walls. However, with the innovative backfills for accelerated construction, the mechanically stabilized earth walls have yet to be fully tested and understood under seismic conditions. The objective of this project is to investigate the seismic performances of MSE walls with TDA and LWA as backfills, respectively, and provide design and construction recommendations for these types of MSE walls in seismic regions. Shake table tests and numerical model were used to achieve the objectives. One-dimensional shake table testing was conducted on model MSE wall that was 1.5 m tall, 1.5 m wide, and 1.3 m deep. Simulated full-scale Loma Prieta earthquake, Northridge earthquake, and sinusoidal sweep-frequency motions (0.2 to 6.0 Hz) were used in the shake table testing and numerical analyses. Flexible boundary condition was incorporated in the tests, and seismic design was used to design the internal stability of the MSE wall. Lateral deflections, vertical deformations, lateral pressures on backfill, and vertical stresses in the back, and accelerations in the backfill were recorded. A model was developed in PLAXIS environment to replicate the experimental studies. The numerical model verified the validity of using the spring-supported boundary condition in the shake table testing. It was concluded from this project that when properly designed, MSE walls with TDA backfill can sustain strong seismic shaking without excessive deformation and lateral spreading. When comparing the seismic performances, TDA is clearly a more suitable backfill material than LWA in seismic regions. The comparison between the numerical and the experimental results warrants further studies to improve the material characteristics and modeling techniques.

17. KEY WORDS Seismic responses, MSE retaining wall, Tire derived aggregates (TDA), Lightweight aggregates (LWA)	18. DISTRIBUTION STATEMENT No restrictions. This document is available to the public through the National Technical Information Service, Springfield, VA 22161
19. SECURITY CLASSIFICATION (of this report) Unclassified	20. NUMBER OF PAGES 86
	21. COST OF REPORT CHARGED

DISCLAIMER STATEMENT

This document is disseminated in the interest of information exchange. The contents of this report reflect the views of the authors who are responsible for the facts and accuracy of the data presented herein. The contents do not necessarily reflect the official views or policies of the State of California or the Federal Highway Administration. This publication does not constitute a standard, specification or regulation. This report does not constitute an endorsement by the Department of any product described herein.

For individuals with sensory disabilities, this document is available in Braille, large print, audiocassette, or compact disk. To obtain a copy of this document in one of these alternate formats, please contact: the Division of Research and Innovation, MS-83, California Department of Transportation, P.O. Box 942873, Sacramento, CA 94273-0001.

Final Report No. CA 13-2416

**Seismic Responses of MSE Walls Using Accelerated Alternative
Backfill Materials with Recycled Tire Shreds and
Lightweight Aggregates**

Ming Xiao

Fariborz M. Tehrani

Manoochehr Zoghi

Department of Civil and Geomatics Engineering
Lyles College of Engineering
California State University, Fresno
August 2013

Final Report submitted to the California Department of Transportation (Caltrans) under contract No. 65A0449

Table of Content

1. INTRODUCTION AND BACKGROUND REVIEW	1
(1) Problem Statements.....	1
(2) Background Review	2
2. SHAKE TABLE TESTING.....	4
(1) Materials.....	4
(2) Large-scale Direct Shear Testing of TDA and LWA.....	6
(3) Experimental Setup and Instrumentation	7
(4) Boundary Conditions	11
(5) Selection of Input Seismic Excitations	13
(6) Seismic Design of Model MSE wall.....	15
(7) Test Program	15
3. NUMERICAL ANALYSES	15
(1) Model Development.....	15
(2) Flexible Boundary Verification	21
4. RESULTS	24
(1) TDA backfill, Loma Prieta earthquake	25
a) Shake table test.....	25
b) Numerical model.....	27
(2) TDA backfill, sinusoidal motions	32
a) Shake table test.....	32
b) Numerical model.....	34
(3) TDA backfill, Northridge motions.....	44
a) Shake table test.....	44
b) Numerical model.....	46
(4) TDA backfill, sinusoidal motions	51
a) Shake table test.....	51
(5) LWA backfill, Loma Prieta earthquake	53
a) Shake table test.....	53
b) Numerical model.....	55
(6) LWA backfill, sinusoidal motions	59
a) Shake table test.....	59
b) Numerical model.....	62
(7) LWA backfill, Northridge earthquake	68
a) Shake table test.....	68
(8) LWA backfill, sinusoidal motions	71
a) Shake table test	71
b) Numerical model.....	74
(9) Post-Shake Evaluation of LWA	74
5. CONCLUSIONS.....	78
6. DESIGN and CONSTRUCTION RECOMMENDATIONS.....	79
7. REFERENCES.....	80

1. INTRODUCTION AND BACKGROUND REVIEW

(1) Problem Statements

As the nation's highway and bridge infrastructure age, the necessity of repairing and replacing them often means more traffic congestion. According to the Federal Highway Administration (FHWA 2006), vehicle miles of travel increased by 80% and licensed drivers increased by 31% from 1980 to 2000. Meanwhile, lane miles increased only by 3.8% and over 40% of all bridges are more than 40 years old with a design life of often 50 years when they were built. Although highway construction is unavoidable, excessive construction time must be minimized because it is costly and exposes highway workers to traffic and the motorists to prolonged substandard conditions. To prevent this gridlock and to preserve and maintain our highway system with the least impact on the motoring public, accelerated construction techniques are gaining popularity across the country. The FHWA has been actively promoting the applications of accelerated bridge construction (ABC). Proven benefits include minimized traffic disruption, improved work zone safety, and reduced on-site environmental impacts. The annual reports of the Accelerated Construction Technology Transfer of the FHWA (ACTT 2005, 2006, 2007) recommended a variety of accelerated construction techniques, such as using mechanically stabilized earth (MSE) walls and utilizing alternative accelerated backfills, e.g., recycled materials or flowable fill.

MSE walls are widely used in retaining embankments in highway systems. The MSE walls/abutments are easier to construct and more economical than their conventional counterparts—reinforced concrete abutments. Reinforced segmental retaining walls have shown the advantage of safety, environmental friendliness, savings in labor costs, equipment, and time. By and large, they performed well with no evidence of visual damage or with only minor damages during the past major earthquakes, such as the 1994 Northridge earthquake (M=6.7) (Sandri 1994), the 1989 Loma Prieta earthquake (M=7.1) (Eliahu and Watt 1991; Collin et al. 1992), and the 1995 Kobe earthquake (M=6.9) (Tatsuoka et al. 1996). However, major repairs or complete collapse were also reported for some MSE walls in the 1999 Chi-Chi earthquake (M=7.6) (Huang and Tatsuoka 2001; Ling et al. 2001) and in the 1995 Kobe earthquake (Tatsuoka et al. 1997). With the innovative backfill alternatives for accelerated bridge and embankment construction, the MSE walls have yet to be fully tested and understood under seismic conditions. The transient seismic pressure of the alternative fill materials on the modular facing, the dynamic settlement, the horizontal deflection of wall face, the time responses of horizontal accelerations, and the tensile stresses of reinforcement during earthquakes are the unknowns and therefore the focuses in this proposed study.

One type of recycled materials that has gained wide attention in the past two decades is waste tires. The Turner-Fairbank Highway Research Center of the FHWA (TFHRC 2010) estimated that approximately 280 million tires are discarded each year by American motorists, 40% of which are disposed in landfills, stockpiles, or illegal dumps. In California, approximately 44.8 million reusable and scrap tires are generated annually with a little fewer than 250,000 waste tires remaining in stockpiles throughout California (CalRecycle 2010). These stockpiles pose a potential threat to public health, safety, and the

environment. Tire shreds, also known as tire derived aggregates (TDA), are pieces of processed and shredded waste tires that can be used as lightweight and quick fills for embankments, subgrades, bridge abutments, and retaining walls backfills. Constructed on weak and compressible foundation soils, embankment retaining walls using tire shreds that are reinforced with geosynthetics result in less overburden pressure, efficient drainage, and cost.

Another alternative backfill material, lightweight expanded clay and shale aggregates, is produced in rotary kiln at temperatures over 1200°C. Its lightness, durability, and mechanical properties make it an appropriate alternative material for many geotechnical applications including earth-retaining structures. Expanded clay and shale aggregates provide excellent permeability and satisfactory internal friction as backfill materials. Replacing conventional sand fills with these alternative aggregates reduces the lateral loads acting on the MSE wall and facilitates construction through the reduction of compaction needs (Tehrani 1998). Moreover, durability and chemical neutrality of expanded aggregates would reduce corrosion of steel anchors and bars in MSE walls.

With the alternative backfill, however, the performances of MSE walls have yet to be fully tested and understood under seismic conditions. Specifically, the horizontal deflections of wall face, the dynamic vertical settlement of the MSE wall, the transient vertical effective stress within the wall, and the acceleration responses are unknown and therefore the focus of this research.

(2) Background Review

Shake table tests on MSE retaining walls have been conducted to study the seismic behavior and to provide earthquake design recommendations for the past 35 years since Richardson and Lee pioneered the tests on metallic-reinforced earth walls (Richardson and Lee 1975). The recent studies include the large-scale shaking table tests on modular-blocks and geocell reinforced soil (GRS) retaining walls (2.5m tall) (Ling et al. 2005, 2008) and the centrifuge tests on bar mat MSE walls (Siddharthan et al. 2004). Despite the active research on seismic performance and design of MSE retaining walls, two understudied aspects hinder the nation's and the Department's accelerated bridge construction (ABC) efforts. These are: (1) lack of guidelines for the seismic design and construction of MSE walls for embankments and (2) lack of experimental data and observations of accelerated alternative backfill materials under earthquake loadings. Ling et al. (2004) found through parametric study on the behavior of MSE retaining walls that the backfill soil properties, seismic motions, and reinforcement layouts are the three major design concerns (in the order of significance) under earthquake loading.

Tire-derived aggregates (TDA) of different sizes have been widely studied as alternative backfills for the past twenty years and vast literature references are available (e.g., Humphrey and Manion 1992; Humphrey 1998; Bosscher et al. 1992; Tweedie et al. 1998; Strenk et al. 2007; Tandon et al 2007). These studies have expanded our knowledge on the mechanical characteristics and in-situ performance of embankments or retaining walls using tire shreds or chips. Mixture of shredded tires and sand is another popular backfill

alternative and its static responses (stress, deformation, strength) have also investigated (e.g., Foose et al. 1996; Bosscher et al. 1997; Lee et al. 1999; Wartman et al. 2007). In contrast to the relatively rich literature on the static behavior of tire shreds, scarce experimental data are available on the seismic performances of MSE walls with tire shreds/chips as backfills. Tsang (2008) is one of few researchers who have studied a rubber-soil mixture backfill under seismic conditions. In his shake table tests, it was found that site response of the backfill was nonlinear and helped absorb incident seismic waves. Furthermore, Tsang (2008) raised concern for the resonance effects of the new backfill, which should be experimentally tested. The recent underwater shake table tests on gravity type model caisson, protected by a cushioning tire chips, found the tire chips substantially reduced the seismic load against the caisson wall (Hazarika et al. 2008).

Another less studied accelerated backfill alternative is lightweight expanded clay and shale aggregates. Application of this material as backfill substantially reduces the pressure at retaining elements due to its lightness and high internal friction angle. Further, its excellent drainage and permeability characteristics would improve the stability of slopes (Tehrani 1998). Holm and Valsangkar (2001) and Watn et al. (2004) have also reported the mechanical properties of lightweight expanded aggregates as backfill materials and have discussed various case studies of such applications. Tehrani (1998) concluded that the application of these materials yields numerous savings in design and construction of retaining elements and improves the performance of the supported infrastructure.

The principal **objectives** of this proposed research are: (1) to investigate the seismic behaviors of MSE walls with two alternative types of accelerated construction backfills (tire shreds and lightweight aggregates) and (2) to provide recommendations for the seismic design and construction of the MSE walls using the two types of backfills. Shake table tests and calibration and design using existing software will be conducted. This project supports the Department's mission and goals of improving mobility across California by providing alternative approaches to accelerated construction of MSE walls using fast backfill materials. Moreover, the application of recycled and environmentally friendly materials as alternative backfill materials will contribute to the preservation and enhancement of California's resources and assets as an excellent indication of the Department's stewardship.

Shake table tests and numerical model are used to achieve the objectives. Seven tasks were conducted in this research:

- Task 1: Shake table tests with TDA, using simulated Loma Prieta and Northridge earthquakes.
- Task 2: Shake table tests with TDA, using sinusoidal frequency sweep motion (0.2 ~ 6 Hz).
- Task 3: Shake table tests with LWA, using simulated Loma Prieta and Northridge earthquakes.
- Task 4: Shake table tests with LWA, sinusoidal frequency sweep motion (0.2 ~ 6 Hz).
- Task 5: Recommendations for seismic design and construction using experimentally calibrated Plaxis software.

Task 6: Development of design recommendations for the MSE walls using TDA and LWA, based on the experiments and numerical model simulation.

Task 7: Prepare and submit final report to Caltrans.

2. SHAKE TABLE TESTING

(1) Materials

The TDA were provided by the California Department of Resources Recycling and Recovery (CalRecycle). Figure 1 shows a photo of the TDA and Figure 2 shows their size distribution. The TDA can be categorized as Type A. The LWA was obtained from Utelite Corporation (Centerville, UT) in 2012. Figure 3 is a photo of the LWA. The material's grain size distribution is shown in Figure 4. The physical and mechanical characteristics of LWA are listed in Table 1. Geogrid was used as the MSE wall reinforcement, as shown in Figure 5. It is uniaxial (with design tensile strength in one direction only) and was obtained from Tensar International, Inc., who labels the geogrid as LH800. In the laboratory-scale shake table tests, we intentionally selected a low tensile strength geogrid. The LH800 geogrid has the lowest ultimate tensile strength of 35 kN/m in all geogrid products of Tensar International, Inc.



Figure 1. Photo of tire derived aggregates (TDA)

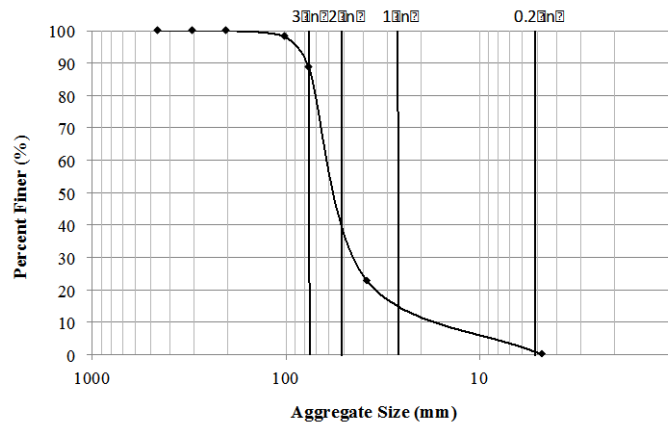


Figure 2. Size distribution of TDA



Figure 3. Photo of lightweight aggregates (LWA)

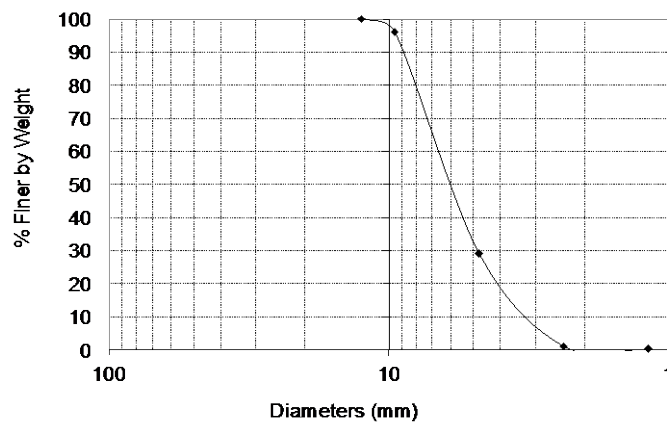


Figure 4. Size distribution of LWA

Table 1. Characteristics of LWA

Optimum water content	5%
Maximum dry unit weight	68.7 lb/ft ³ (10.8 kN/m ³)
Static cohesion	0
Static internal friction angle	30°
Specific gravity	1.74



Figure 5. Photo of geogrid (Tensar LH800)

(2) Large-scale Direct Shear Testing of TDA and LWA

The shear strengths of the TDA and LWA are needed in the seismic design of the model MSE wall that is tested on the shake table. Due to the large aggregate sizes of the TDA and LWA, standard direct shear device cannot be used to obtain their shear strengths. A large-scale direct shear device was designed and constructed, as shown in Figure 6.

The shear box is comprised of two half-boxes. The dimensions of each box are 79 cm wide, 80 cm long, and 61 cm tall. The upper box was bolted on the frame of a compression rig and was stationary. The lower box had guide rails on its bottom; it was driven by a horizontal hydraulic piston and can slide smoothly in the horizontal direction. Each box was constructed using strong structural steel frame to withstand large vertical and horizontal loads. The walls of the shear box were made of 2.54 cm (1.0 inch) plywood to ensure no flexing of the sidewalls. Smooth plastic sheets were lined on the inside of the four walls of the shear boxes to reduce vertical friction, so that the entire normal force can be applied to the materials in the lower box. The vertical load was applied by a vertical hydraulic piston. The hydraulic jack was positioned on a concrete slab as a loading plate. The horizontal displacement of the lower box was driven by a horizontal hydraulic piston. The maximum horizontal displacement was 18 cm. A linear variable displacement transformer (LVDT) was connected between the fixed frame and the movable lower box to record the lateral displacements. A load cell was connected between the hydraulic piston and the steel frame of the lower box to measure the horizontal shear resistance force during a shear test. Another load cell was positioned between the vertical piston and the loading plate to measure the vertical overburden force. The LVDT and the two load cells were connected to a data acquisition system to automatically record the displacement, the horizontal shear resistance force, and the vertical overburden force during a shear test. The shear test results are shown in Table 2.

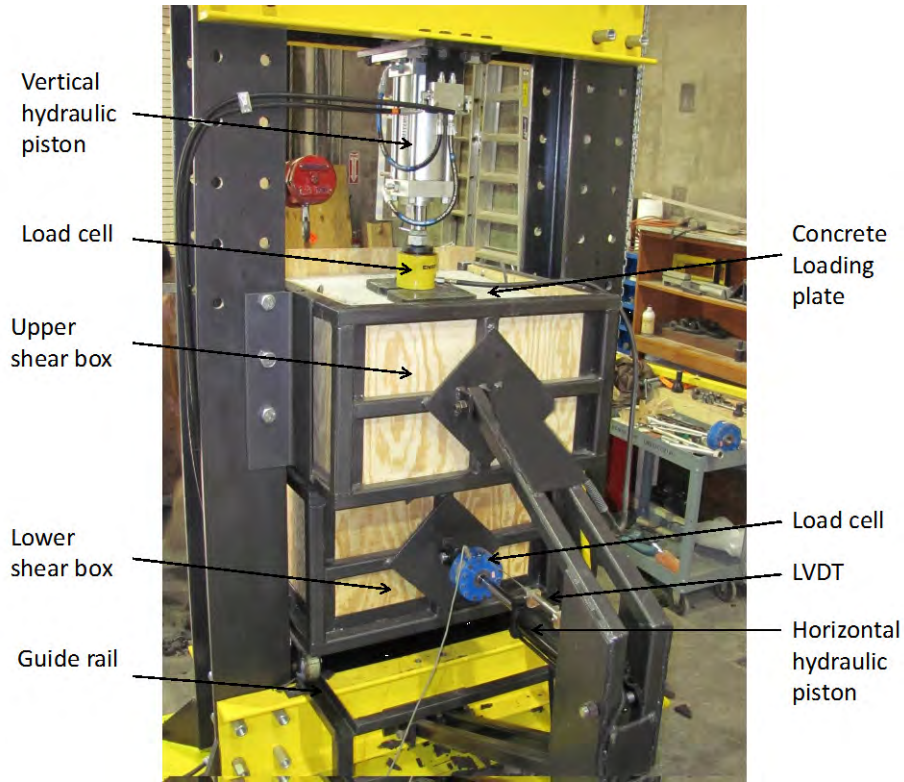


Figure 6. Large-scale direct shear test device

Table 2. Direct shear test results

Material	TDA	LWA
Cohesion	24.37 kPa (509 psf)	11.0 kPa (230 psf)
Friction angle	27.0°	47.7°

(3) Experimental Setup and Instrumentation

A section of short MSE wall was built in a 1.5 m (wide) × 1.87 m (long) × 1.8 m (tall) rigid steel box that was anchored on a 2.4 m × 2.1 m one-dimensional shake table. The load capacity of the shake table is 177.9 kN (20.0 tons); the actuator provides 244.6 kN (55 kips) hydraulic fluid driving force; and the maximum travel distance of the table is ±12.7 cm (± 5 inch). The shake table is capable of replicating recorded historical earthquake motions that are within its allowable displacement range. Figure 7 is a photo of the shake table and the box with a retaining wall built inside.



Figure 7. Shake table test of MSE wall

Figure 8 illustrates the configuration of the MSE wall and the instrumentations used in the model test. The MSE wall was 1.5 m high, 1.5 m long, and 1.3 m deep, and had five equal-thickness layers. Geogrid was used as wrap-around reinforcement. A concrete slab was anchored to the top of the wall to simulate a small surcharge of 3.4 kN/m^2 . Three linear potentiometers were used to measure the horizontal deflections of the wall face at the bottom, middle, and the top layers, as shown in Figure 9. The potentiometers were fixed to an inertial frame outside of the shake table, and an inelastic wire connected each potentiometer to the geogrid at the three designated levels. The fourth potentiometer was connected to the shake table in order to measure the actual seismic motions generated by the actuator. The dynamic vertical stresses in the backfill were measured using dynamic soil stress cells, which were placed flat at the bottom of layers 2 and 5 (as shown in Figure 10). Two other stress cells were mounted to the sidewall at the top and bottom sections, respectively, to measure the dynamic lateral pressures on the backfill. Wire-free accelerometers were embedded in each of the five layers and were close to the wall face in order to measure the acceleration responses of the backfill, as shown in Figure 11. One accelerometer was attached to the shake table and one to the box to measure their acceleration responses as well. A delayed-start timer was set in each accelerometer, and the data recording (100 data points per second) started automatically at a predetermined time when the shake table test was run. The vertical settlements of the MSE wall during the shaking were measured by LVDT transducers that were anchored on the box above the concrete slab (Figure 12). The potentiometers, the LVDTs, and the dynamic stress cells were connected to the National Instrument data acquisition system, which automatically recorded the readings during the shaking. In the shake table tests using TDA, the TDA was compacted dry in each reinforcement layer, the density after compaction was 689 kg/m^3 (43 lb/ft^3). In the shake table tests using LWA, the LWA was compacted at optimal water content of 5% to reach 95% of maximum dry density of 1100 kg/m^3 . To prevent the LWA from seeping out of the geogrid at the wall face, a non-woven, needle-punched geotextile was used to cover the wall face. The geotextile was not used as reinforcement.

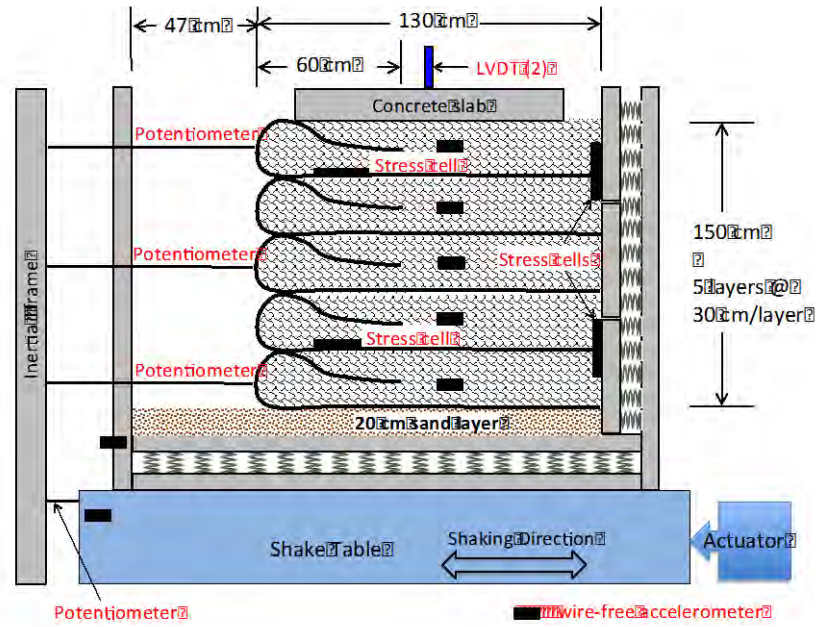


Figure 8. MSE wall configuration and instrumentation layout



(a) TDA backfill



(b) LWA backfill

Figure 9. Linear potentiometers to measure lateral movements of MSE wall



(a) TDA backfill



(b) LWA backfill

Figure 10. Dynamic pressure cell embedded in MSE wall



(a) TDA backfill



(b) LWA backfill

Figure 11. Accelerometer embedded in MSE wall



(a) TDA backfill



(b) LWA backfill

Figure 12. LVDT on constructed MSE wall to measure wall settlements

(4) Boundary Conditions

The rigid boundary of the steel-frame box did not represent the true boundary condition of the slurry wall and its confining soil. To address this boundary condition, spring-supported wood panels were installed at the bottom and on two sides of the box, as shown in Figure 7. The idea was to create a flexible boundary that has the same *dynamic stiffness* of dense sand. Gazetas (1991) derived the dynamic stiffness of foundations embedded in homogeneous half-space:

$$K_{dynamic} = K_{static} k(\omega) \quad (1)$$

where: $K_{dynamic}$ = dynamic stiffness, K_{static} = static stiffness, and $k(\omega)$ = dynamic stiffness coefficient.

(a) *To calculate static stiffness (K_{static}):*

In vertical (z) direction:

$$K_{static(z)} = K_z \left[1 + \left(\frac{1}{21} \right) \left(\frac{D}{B} \right) (1 + 1.3\chi) \left[1 + 0.2 \left(\frac{A_w}{A_b} \right)^{2/3} \right] \right] \quad (2)$$

In horizontal (y) direction, i.e., in the direction of shaking:

$$K_{static(y)} = K_y \left[1 + 0.15 \left(\frac{D}{B} \right)^{0.5} \right] \left\{ 1 + 0.52 \left[\left(\frac{h}{B} \right) \left(\frac{A_w}{L^2} \right) \right]^{0.4} \right\} \quad (3)$$

where: K_z and K_y = static stiffness for arbitrarily shaped foundations on the *surface* of homogeneous half-space in z and y directions, respectively; and

$$K_z = \left(\frac{2GL}{1-\nu} \right) (0.73 + 1.54\chi^{0.75}) \quad (4)$$

$$K_y = \left(\frac{2GL}{2-\nu} \right) (2 + 2.5\chi^{0.85}) \quad (5)$$

where: G = shear modulus of foundation soil, and

$$G = \frac{E}{2(1+\nu)}$$

L = half of the length of the foundation base,

B = half of the width of the foundation base,

D = foundation embedment = height of the shake table box in this research,

d = height of foundation that is actually in contact with soil = height of the shake table box minus the freeboard in this research,

$h = D - d/2$,

E = modulus of elasticity,

ν = Poisson's ratio,

$$\chi = \frac{A_b}{4L^2} \quad (6)$$

where: A_b = base contact area = $(2L)(2B)$,
 A_w = area of the four sides of the embedded foundation = $d(2L+2B)$.

(b) To calculate the dynamic stiffness coefficient, $k(\omega)$:

In z direction when $\nu \leq 0.4$:

$$k_z(\omega) = k_z \left[1 - 0.09 \left(\frac{D}{B} \right)^{3/4} a_0^2 \right] \quad (7)$$

where: k_z = dynamic stiffness coefficient for arbitrarily shaped foundations on the *surface* of homogeneous half-space in z direction,

$$a_0 = \frac{\omega B}{V_s} \quad (8)$$

where: ω = frequency, and V_s = shear wave velocity. a_0 ranges from 0 to 2. In this research, due to the lack of shear wave velocity data, take average value $a_0 = 1.0$ to account general soil condition. In y direction, $k_y(\omega)$ also depends on D/B and a_0 and can be determined using Eq (7).

In this research, the calculation of the dynamic stiffness is shown in the Table 2:

Table 2(a). Initial parameters in calculating dynamic stiffness of flexible boundary

Given parameters							Derived parameters		
L (cm)	B (cm)	D (cm)	d (cm)	h (cm)	E (N/cm ²)	ν	G (N/cm ²)	a_0	χ
83	75	180	160	80	3500	0.4	1250	1.0	0.90

Note: $E = 3500 \text{ N/cm}^2$ is typical value for dense sand.

Table 2(b). Calculation of dynamic stiffness of the bottom boundary (z direction)

k_z , using a_0 as 1.0 and the chart of Gazetas (1991)	$k_z(\omega)$	K_z (N/mm)	$K_{\text{static}(z)}$ (N/mm)	$K_{\text{dynamic}(z)}$ (N/mm)
0.8	0.661	74606	144441	95500

Table 2(c). Calculation of dynamic stiffness of side boundary (y direction)

$k_y(\omega)$, using a_0 as 1.0 and the chart of Gazetas (1991)	K_y (N/mm)	$K_{\text{static}(y)}$ (N/mm)	$K_{\text{dynamic}(y)}$ (N/mm)
0.75	55683	181036	135777

Heavy-duty compression springs in parallel were used to achieve the required stiffness on the three boundaries. Each spring's stiffness coefficient is 1386.5 N/mm, the free length is 10 cm, and the maximum travel distance is 20 mm. To simulate dense sand behind the TDA backfill, 187 springs were needed on one side of the box, and 126 springs were needed at the bottom. The total maximum weight of the MSE wall in the box was approximately 35,590 N (or 8,000 lb). At the maximum compression of 20 mm, the bottom spring-supported panel can support 1910,000 N, much more than the vertical load in the box. In the horizontal direction, if assuming a very large acceleration of 10 g, the horizontal inertia force would be 355,900 N; while the side spring-supported panel at full compression of 20 mm can sustain 2715,540 N, 7.0 time of the inertia force. So the springs would not be fully compressed.

To simulate the cyclic stress variation with depth, the vertical spring-supported board on each side consisted of three panels. To reduce the friction between the slurry wall and the front and back sides of the walls of the box, smooth Plexiglas sheets were attached to the plywood walls of the box, so that the sides of the slurry wall were in contact with the Plexiglas sheets.

(5) Selection of Input Seismic Excitations

In this research, the 1989 Loma Prieta earthquake ($M = 7.1$) and the 1994 Northridge earthquake ($M = 6.7$) were simulated. The earthquake's displacement-time history and acceleration-time history data were obtained from the Pacific Earthquake Engineering Research (PEER) Center Library of UC Berkeley and implemented into the input file to the MTS® control system of the shake table. Figure 13 shows the match of the displacement-time histories of the input file and the measured displacements (output) of the simulated Loma Prieta earthquake and Northridge earthquake by the shake table. Figure 14 shows the match of the acceleration-time histories of the input file and the measured acceleration (output) of the simulated Loma Prieta earthquake and Northridge earthquake by the shake table.

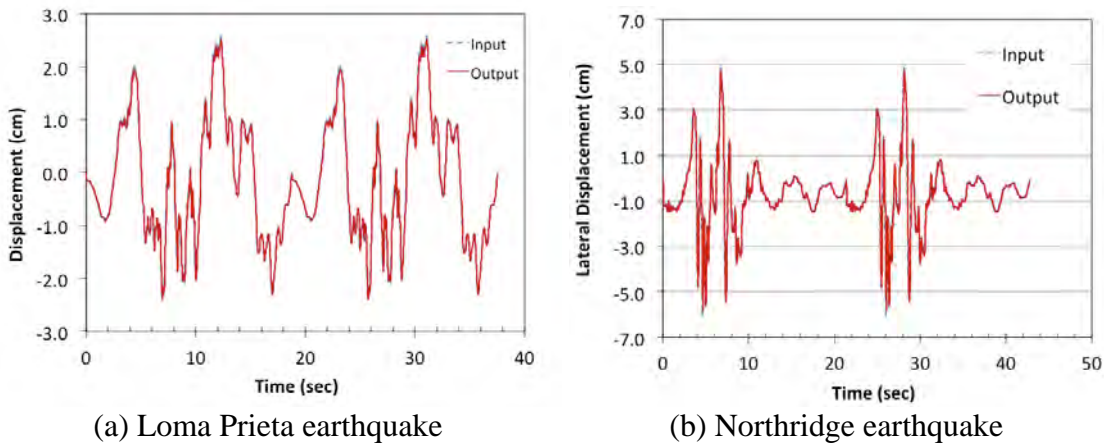


Figure 13. Input and measured (output) displacement ~ time histories of the simulated earthquake by the shake table

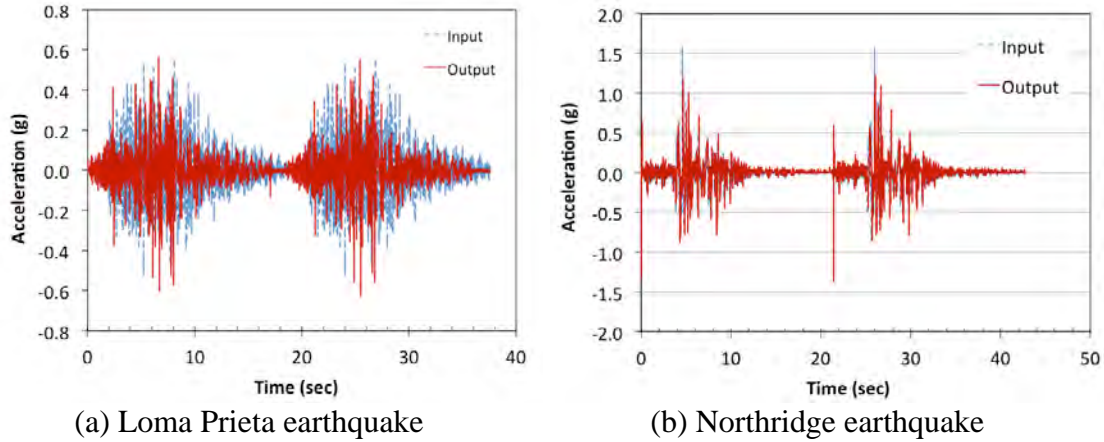
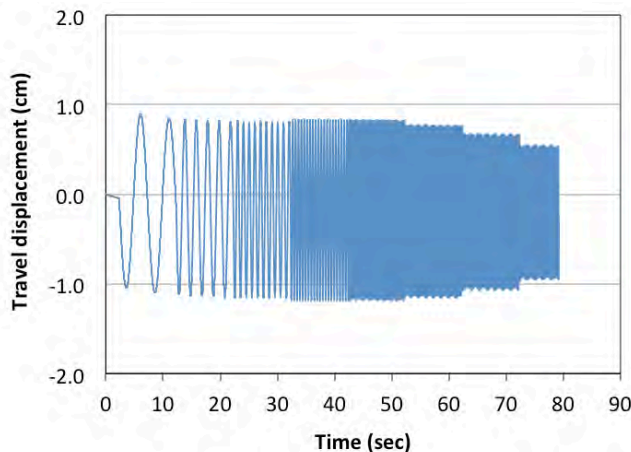
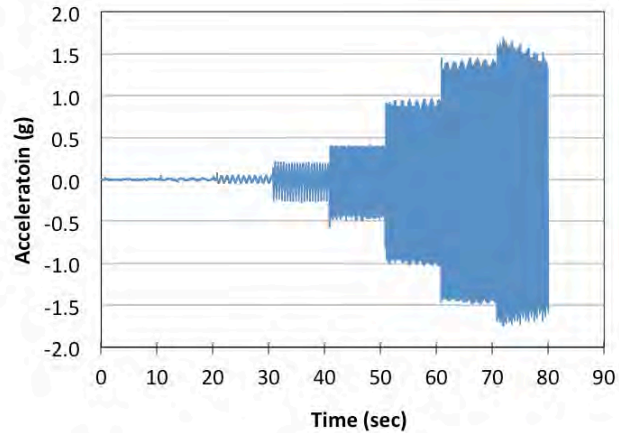


Figure 14. Input and measured (output) acceleration ~ time histories of the simulated earthquake by the shake table

Low-amplitude (~ 1.0 cm) sinusoidal excitations were also used to investigate the fundamental seismic responses of the MSE walls. The vibration frequency increased in steps and was 0.2, 0.5, 1, 2, 3, 4, 5 and 6 Hz, with each frequency lasting 10 sec. This frequency range covers the dominant frequency range in most earthquakes. Figures 15 shows the measured displacement-time history and acceleration-time history of the sinusoidal motions of the shake table. The purpose of using the sinusoidal sweep frequency motions was twofold: (1) to determine whether the natural frequency of the MSE walls with TDA and LWA fall into the dominant frequency range of earthquakes, (2) to shake the MSE wall till failure if the scaled Loma Prieta and Northridge earthquake motions could not fail the MSE walls, so that the failure mechanisms of the slurry wall can be further investigated. Moreover, sinusoidal waves can be easily input into numerical model for future model development.



(a) Measured displacement ~ time history



(b) Measured acceleration ~ time history

Figure 15. Sinusoidal sweep-frequency motions by the shake table

(6) Seismic Design of Model MSE wall

The model MSE wall with TDA or LWA backfill was designed using two seismic design guidelines by Elias et al. (2001) and Bathurst and Cai (1995). Due to the boundary condition of the model MSE wall, external stability (overturning, sliding, and bearing capacity) was not examined. Internal stability against pullout, tensile overstress, and internal sliding failures was evaluated to determine the geogrid reinforcement length and layer thickness. In the design, a low total reduction factor for geogrid's tensile strength was used: $\text{IRF} = 1.33$; and creep reduction factor was not considered, because creep occurs in long term. In the seismic design, $c = 0$, $\phi = 27^\circ$ were used for TDA, and $c = 0$, $\phi = 30^\circ$ were used for LWA. The adhesion and external friction angle between the TDA and geogrid were assumed to be 0 and 27° , respectively; the adhesion and external friction angle between the LWA and geogrid were assumed to be 0 and 30° , respectively. Both design methods yielded the factors of safety of the internal stability larger than 1.1 for the MSE wall configuration shown in Figure 8.

(7) Test Program

Test #	Backfill	Seismic motion	Note
Test 1	TDA	Simulated Loma Prieta earthquake	
Test 2		Sinusoidal sweep-frequency motions	Immediately after Loma Prieta motion
Test 3		Simulated Northridge earthquake	
Test 4		Sinusoidal sweep-frequency motions	Immediately after Northridge motion
Test 5	LWA	Simulated Loma Prieta earthquake	
Test 6		Sinusoidal sweep-frequency motions	Immediately after Loma Prieta motion
Test 7		Simulated Northridge earthquake	
Test 8		Sinusoidal sweep-frequency motions	Immediately after Northridge motion

3. NUMERICAL ANALYSES

(1) Model Development

The goal of numerical model development is to analyze the proposed MSE retaining wall model using PLAXIS software. PLAXIS implements the finite element method in engineering analysis of geotechnical systems. It incorporates the Hoek-Brown model as a standard material model and allows for analysis with multiple nodes. PLAXIS considers the effect of soil-structure interaction and, therefore, can model a wide range of problems from simple linear analysis to highly complex linear simulations.

A model has been developed in PLAXIS environment to replicate the experimental studies on shake table. This model incorporates soil characteristics as well as structural components, including geogrids and anchors. Further, additional elements have been introduced to model presence of springs and plates in the real experiment. Figure 16 presents the basic geometry and components of the model. Generation of this PLAXIS model includes following general steps.

Geometry

The geometry of the model follows the dimensions of shake table proto-type as discussed in Task 1. Therefore, the outcome of the numerical analysis for this model is expected to be subject to the same limits of experimental studies. An additional layer of sand is added at the bottom of proto-type to accurately model the interaction between backfill materials and existing soil in the field.

Boundary conditions and fixities

The boundary conditions and fixities allow horizontal and vertical motions, except for the base and side of the model, where the body of the MSE system is attached to the rigid steel frame and is subject to base excitations.

Structural components and elements (geogrids, plates, and springs)

Geo-grids are defined using PLAXIS features into the backfill area. The geo-grid elements are embedded in the backfill material and are not connected to any other elements, except for the brief friction contact between lower and upper layers in the front of the MSE system. Plates are defined to replicate plywood presence beneath and behind the backfill. Plywood plates are defined at the back of the MSE system in three different segments to model experimental layout. Springs are also modeled after the experimental prototype to replicate boundary conditions. Thus, the interpretation of preliminary results is limited to these defined boundary conditions. Springs are located at equal spacing to model equivalent number of springs per unit width of the system.

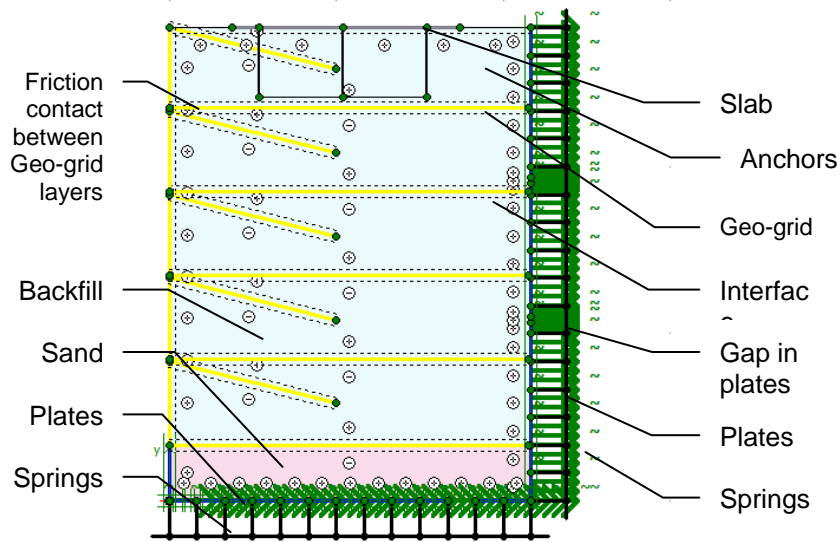


Figure 16 Geometry of the MSE model

Material properties

Properties of various materials, including backfill, geo-grids, plywood, and springs, have been incorporated in the model. Properties of backfill materials, including TDA and LWA, were obtained from shear testing, manufacturer specifications, and previous literature studies.

The type of backfill that was tested in the lab is composed of a tire shred mixture. This Tire Derived Aggregate (TDA) is a form of accelerated backfill material. The properties of this backfill material, which were determined through lab experiments, include a unit weight of 6.283 kN/m^3 , a friction angle of 35 degrees, a cohesion of 22.89 kN/m^2 and an E value of 2534 kPa . The E value was based on a large-scale compression test of the TDA, as shown in Figure 17. The curve shows a hardening effect as the TDA was compressed and the density increased, i.e., the E value increased with the compression and density. The E value was calculated based on the 15% and 30% strain, considering the relatively large compressional deformations of TDA. At each strain, the tangent and the secant Young's moduli were calculated: at 15% strain, tangent $E = 919.7 \text{ kPa}$, secant $E = 497.7 \text{ kPa}$; at 30% strain, tangent $E = 2533.5 \text{ kPa}$, secant $E = 1036.4 \text{ kPa}$. Comparison between experimental and analytical results indicated that the secant modulus obtained from the static compression testing is an underestimated value for dynamic response. Future tests at different strain rates might allow us to gain a better understanding of TDA response.

The properties for the bottom layer of sand were determined through testing conducted in the lab. These properties include a unit weight of 15 kN/m^3 , a friction angle of 35 degrees, a cohesion of 10 kN/m^2 and an E value of 35000 kPa .

The springs in the lab model are implemented to simulate dense sand. Therefore the spring stiffness that was used as an input value in PLAXIS 2D was calculated and compared to

the E value for dense sand. Numerical values have been discussed and tabulated in experimental studies.

The types of geogrids used for the project are Tensar LH800. Geogrids for this project were modeled using the geogrid option in PLAXIS 2D. The only input value required in PLAXIS 2D for geogrids is EA. The EA for the geogrids used in the design of this MSE wall was 280 kN/m. This value was provided by the Tensar website where geogrid specifications are shown.

Elastic properties of minor materials, such as plywood plates, have been obtained from typical values and simple engineering calculations. Three quarter inch thick plywood was used for the right side and bottom of the MSE wall. To model this plywood in PLAXIS the plate option was used. Assuming a low-grade species of plywood an E value of 1500 ksi was selected. With this the moment of inertia and area of the plywood could be calculated and the input values for PLAXIS 2D are an EI of 5.958 kN m²/m and an EA of 1.97x10⁵ kN/m.

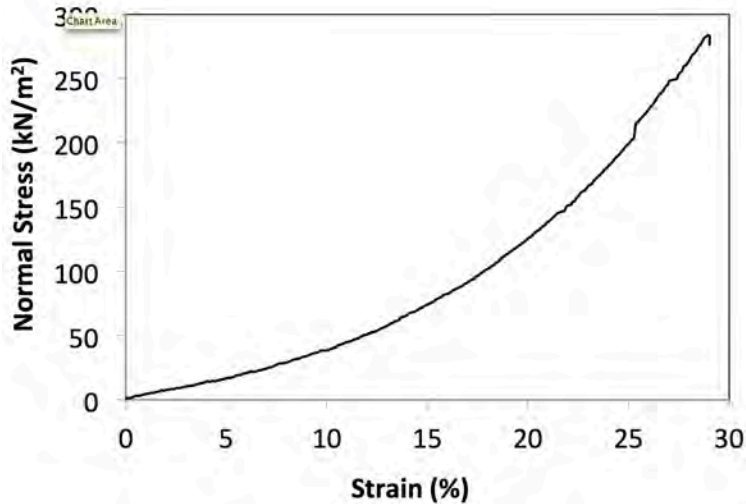


Figure 17. Compression curve of the TDA

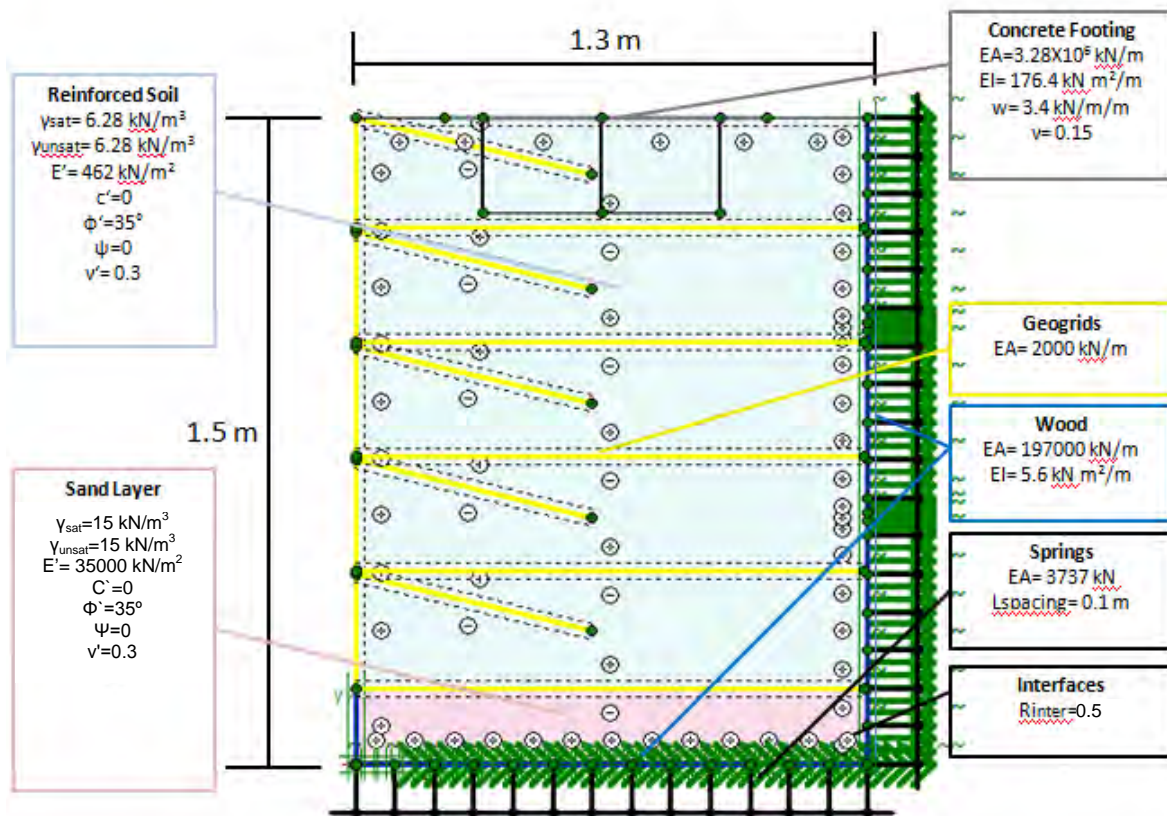


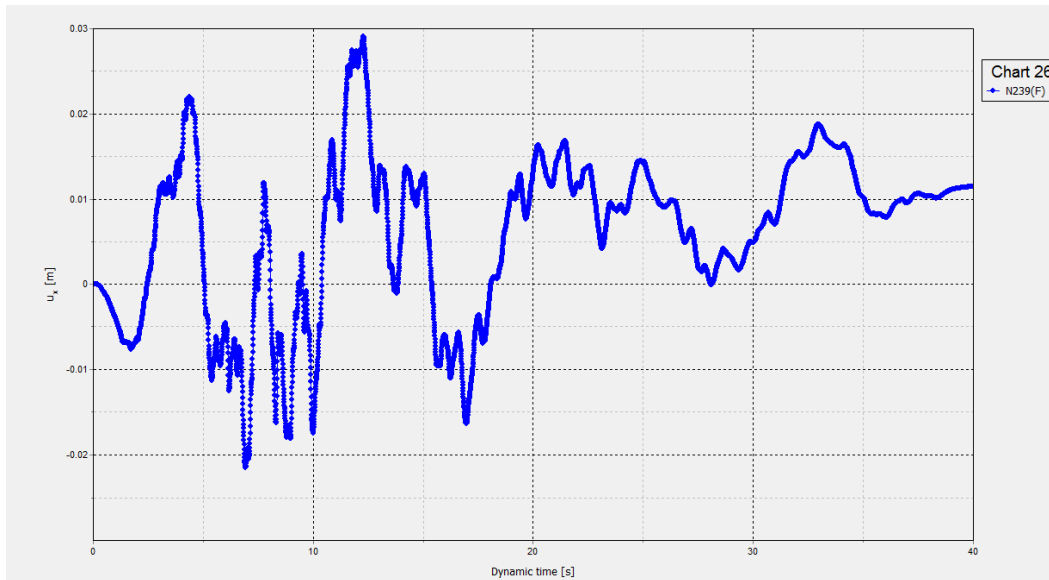
Figure 18. Material Properties

Loading

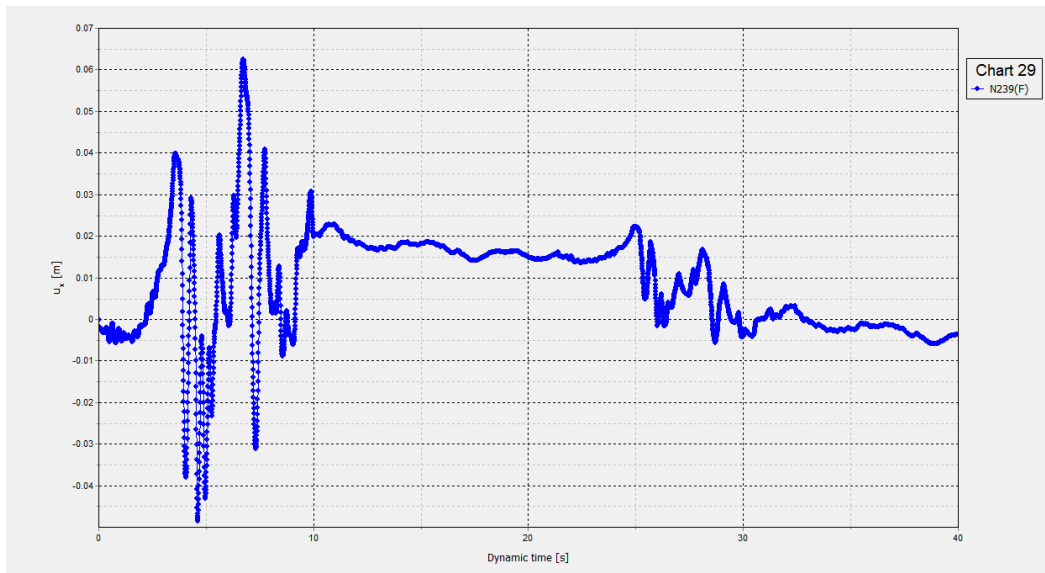
A surcharge was placed on the backfill to replicate concrete slab, when applicable. The concrete slab on the top of the MSE wall was modeled as a plate in PLAXIS 2D. The surcharge from the 6 inch concrete slab is 3.38 kPa and the modulus of elasticity for the concrete is 2.153×10^7 kPa. This gives an EI of $176.37 \text{ kN m}^2 / \text{m}$ which is one of the inputs required for this material in PLAXIS 2D. The other input value required for plates is EA which was $3.28 \times 10^6 \text{ kN/m}$ for the concrete slab.

A harmonic load containing various frequencies was defined based on lab simulations and applied to the model as base excitation. Further, the model was analyzed for the effects of Northridge and Loma Prieta earthquake records.

In the numerical analyses, the Loma Prieta earthquake and the Northridge earthquake were simulated. The entire duration of the earthquake record was used without repeating. The two earthquake excitations were shown in Figure 19.



(a) Loma Prieta earthquake



(b) Northridge

Figure 19. Earthquake excitations used in the Plaxis modeling

Interfaces

Interaction between backfill materials and structural elements, such as geo-grid and plywood, is defined through interface modeling. The interface was modified to reduce the friction by 50% per expert recommendations.

Mesh Generation

PLAXIS utilizes a mesh generation routine to finalize the model. Mesh generation was accomplished using 15-node plain-strain coarse elements as shown in Figure 20.

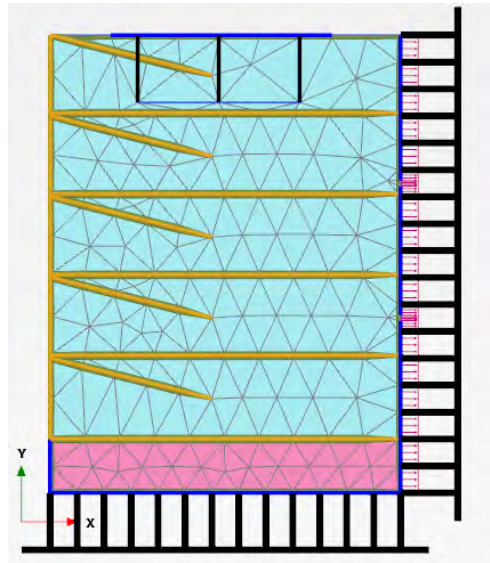


Figure 20. Mesh generation using PLAXIS

Results indicate output at various nodes on the model. Table 3 shows the coordinate of the nodes.

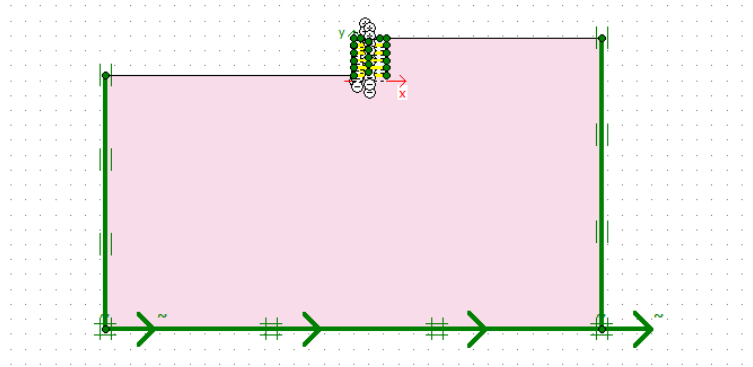
Table 3. Coordinates of output nodes

Result	X	Y
LVS	0.24	0.25
HVS	0.14	1.43
LHS	1.29	0.51
HHS	1.29	1.51
L1	0.71	0.35
L2	0.71	0.66
L3	0.7	0.92
L4	0.67	1.22
L5	0.69	1.6
GA	0	0.6

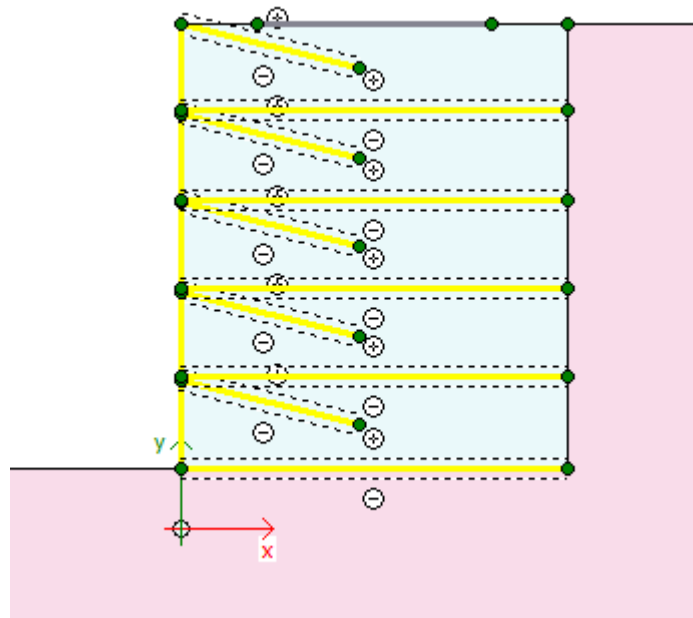
(3) Flexible Boundary Verification

The lab model without springs was analyzed for dynamic loading using PLAXIS 2D for the same harmonic loading and earthquake excitation as the lab MSE wall. The springs that were used to simulate dense sand were removed and replaced with dense sand in the Plaxis model. And the steel anchors used to secure the concrete slab during the application of the base excitation were removed. These anchors could be removed in the full scale analysis because for the lab model the application area of base excitation was very close in proximity to the concrete slab which caused the slab to jump up constantly during the

excitation. Because for the lab model without springs the base excitation is much farther down in the soil these anchors could be removed without affecting the slab. Figure 21 shows the configuration of the lab model without springs.



(a) General View



(b) Close-up View

Figure 21. Lab Model No Springs-Configuration, General View

A coarse mesh was used for this analysis along with a 15-node triangular element for the finite element calculations. Figure 22 shows the corresponding mesh for this configuration.

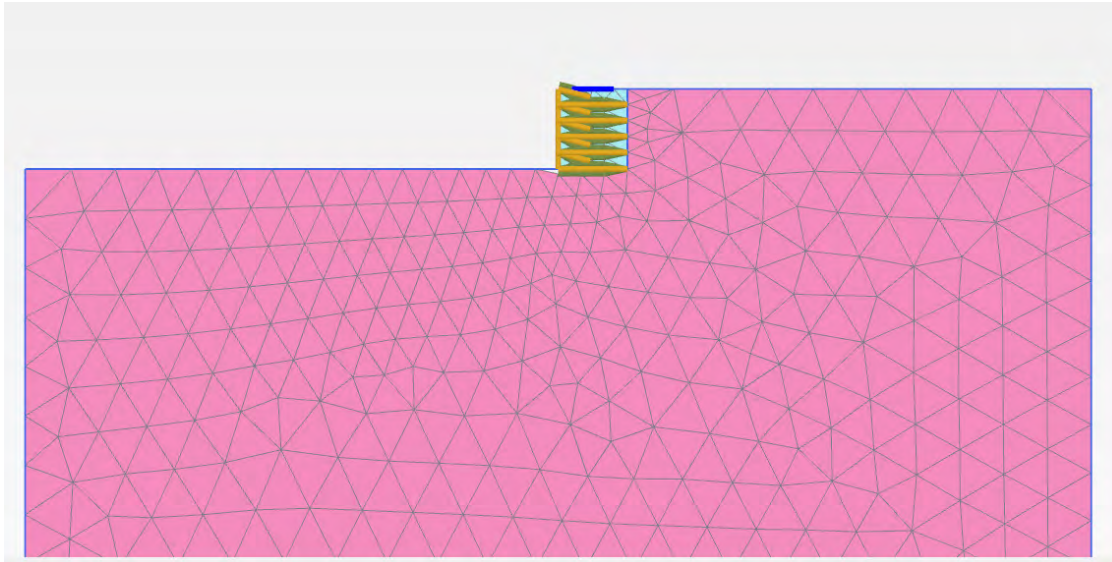


Figure 22. Mesh Generation for the No Springs-Configuration

Boundary Conditions

Two types of boundary conditions were tested: (1) springs that were used to simulate dense sand as used in the shake table tests, and (2) absorbent boundaries where the springs were replaced with sand of large depth. Springs were used in the lab model while no testing was conducted on MSE walls with different boundary conditions due to constraints of lab experimentation. Therefore, PLAXIS 2D was used to compare the behavior of MSE walls with these two types of boundary conditions. Table 4 shows the displacements of the MSE wall subject to sinusoidal motion with a frequency of 6 Hz for both types of boundary conditions. It can be seen that the displacements of the model are approximately equal for both types of boundary conditions. This is consistent with the idea that springs can be used to simulate dense sand if the proper stiffness is calculated for the springs. This stiffness, which is presented in the methodology section of this report, was derived based on the characteristics of dense sand.

Table 1. Boundary Condition Comparison

	Equivalent Springs	Absorbent Boundaries
Bottom Layer Displacement (m)	0.008	0.007
Middle Layer Displacement (m)	0.005	0.005

4. RESULTS

The test results are presented in the following sequence:

- (10) TDA backfill, Loma Prieta earthquake
 - c) Shake table test
 - d) Numerical model
- (11) TDA backfill, sinusoidal motions
- (12) Shake table test
- (13) Numerical model
- (14) TDA backfill, Northridge earthquake
 - c) Shake table test
 - d) Numerical model
- (15) TDA backfill, sinusoidal motions
 - a) Shake table test

- (16) LWA backfill, Loma Prieta earthquake
 - c) Shake table test
 - d) Numerical model
- (17) LWA backfill, sinusoidal motions
 - c) Shake table test
 - d) Numerical model
- (18) LWA backfill, Northridge earthquake
 - e) Shake table test
- (19) LWA backfill, sinusoidal motions
 - a) Shake table test

In each shake table test, five types of results are presented:

- Lateral deflections of MSE wall
- Vertical deformations of MSE walls
- Lateral pressures on backfill (top, middle, bottom layers)
- Vertical stresses in backfill
- Maximum accelerations in MSE wall and their time of occurrence

In each numerical model simulation, four types of results are presented:

- Deformed mesh
- Lateral displacement and velocity (top and bottom layers)
- Lateral pressures on backfill (top and bottom layers)
- Vertical stresses in backfill (top and bottom layers)

(1) **TDA backfill, Loma Prieta earthquake.**

(a) **Shake Table Test**

After the shake table testing, the MSE wall with TDA backfill did not have noticeable damage. And there were no excessive settlement and lateral spreading of the wall. Figure 23 shows the lateral deflections (displacements) of the MSE wall measured at the top, middle, and bottom layers in the shake table test. It shows increased lateral deflections from the bottom toward the top of the wall. In the first cycle of the simulated Loma Prieta earthquake, the maximum horizontal deflection was approximately 1.7 cm. Figure 24 shows the vertical deformations of the MSE wall in the shake table testing. The two LVDTs recorded similar settlements in the repeated Loma Prieta earthquake simulations, and the maximum vertical deformation was approximately 0.8 cm.

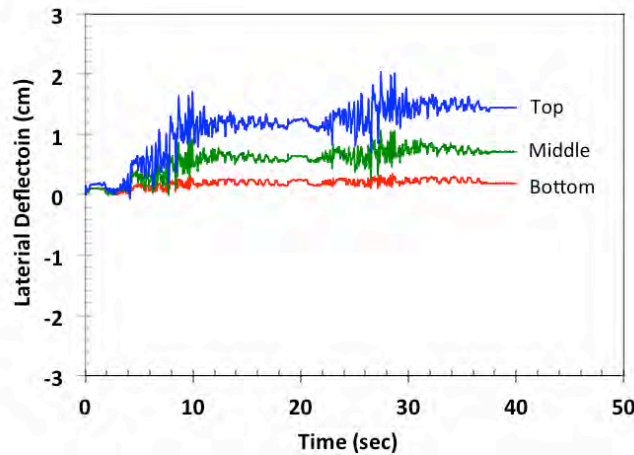


Figure 23. Lateral deflections of the MSE wall with TDA backfill, from Loma Prieta earthquake

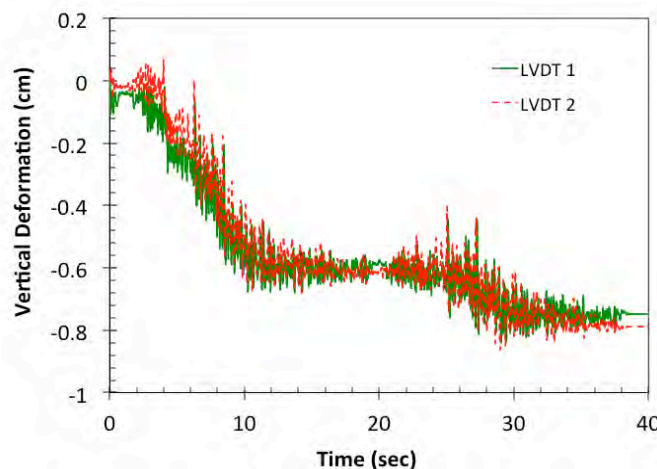


Figure 24. Vertical deformations of the MSE wall with TDA backfill, from Loma Prieta earthquake

Figure 25 presents the lateral pressures on the TDA backfill, and Figure 26 shows the vertical stresses in the TDA backfill.

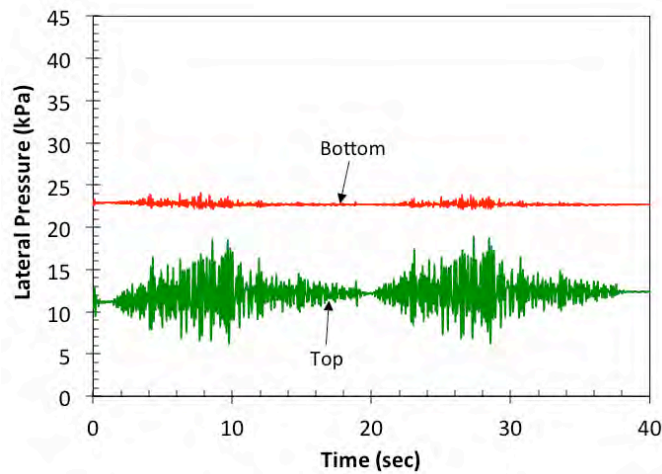


Figure 25. Lateral pressures on the TDA backfill of the MSE wall, from Loma Prieta earthquake

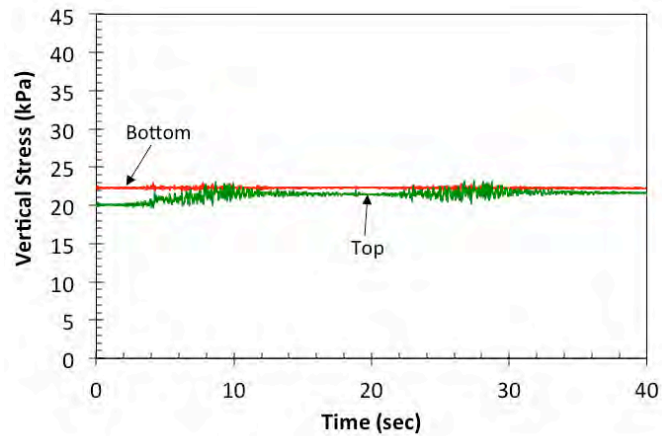


Figure 26. Vertical stresses in the TDA backfill of the MSE wall, from Loma Prieta earthquake

The accelerometers recorded the acceleration ~ time histories of each layer, the table and the box. The maximum accelerations and their time of occurrence are listed in Table 5. Non-linear distribution of accelerations with the depth of the wall was observed.

Table 5. Maximum accelerations and time of occurrences

Location	Layer 1 (bottom)	Layer 2	Layer 3	Layer 4	Layer 5 (top)	Table	Box
Acc (g)	0.727	0.848	0.795	0.644	0.533	0.587	0.624
Time (sec)	9.77	8.42	9.73	9.69	7.89	27.28	27.29

(b) Numerical Model

The response of the MSE system with TDA backfill to the Loma Prieta earthquake record is shown using time history of deformation and stress at various layers.

While, the general deformed shape confirms to experimental observations, the analytical results indicate higher deformations in comparison to experimental results. It appears that material characteristics, including the modulus of elasticity, have great impact on numerical analysis. Therefore, simplifications in estimating input values and testing procedures could be the source of observed discrepancy.

Further, lack of convergence in PLAXIS is manifested in high frequency fluctuations in the response time histories, even though; such short-duration noises do not have substantial impact on average results.

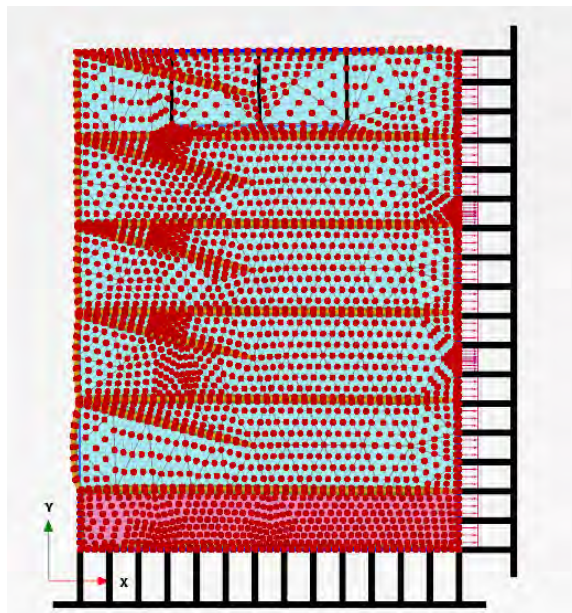


Figure 27 Typical deformed mesh (Loma Prieta)

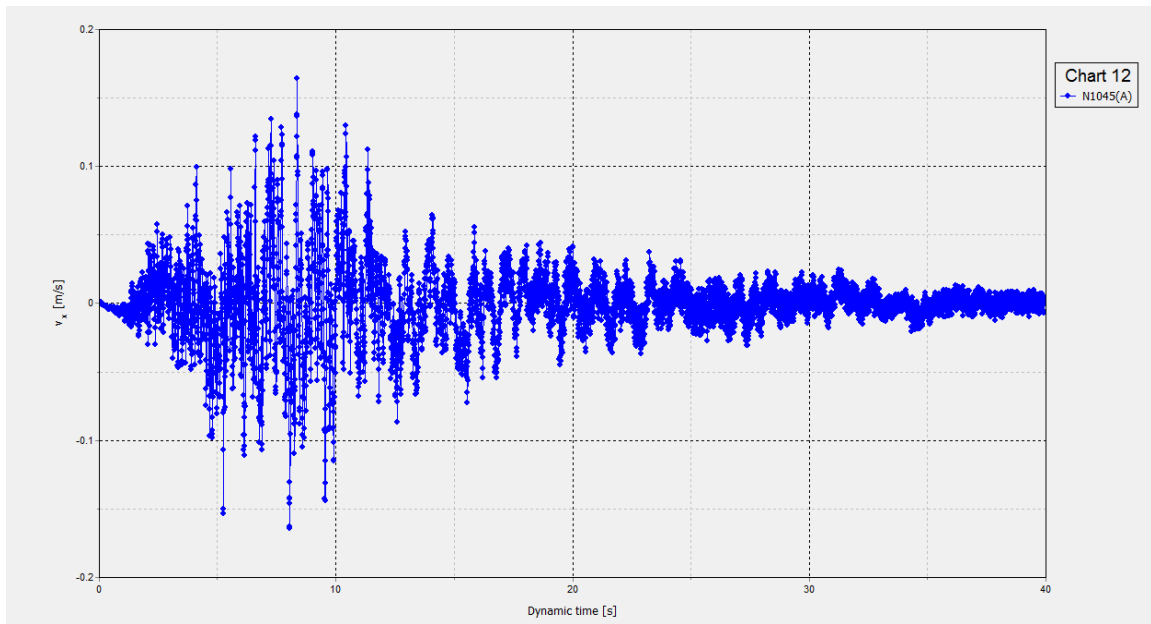
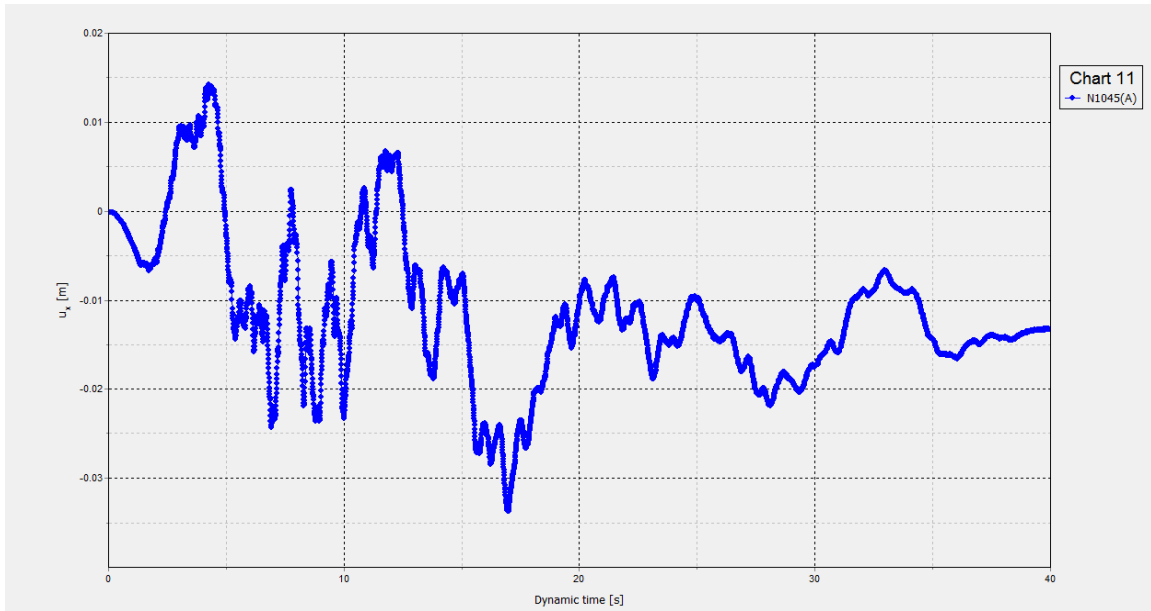


Figure 28 Time history of lower layer response to Loma Prieta earthquake (top: displacement, bottom: velocity)

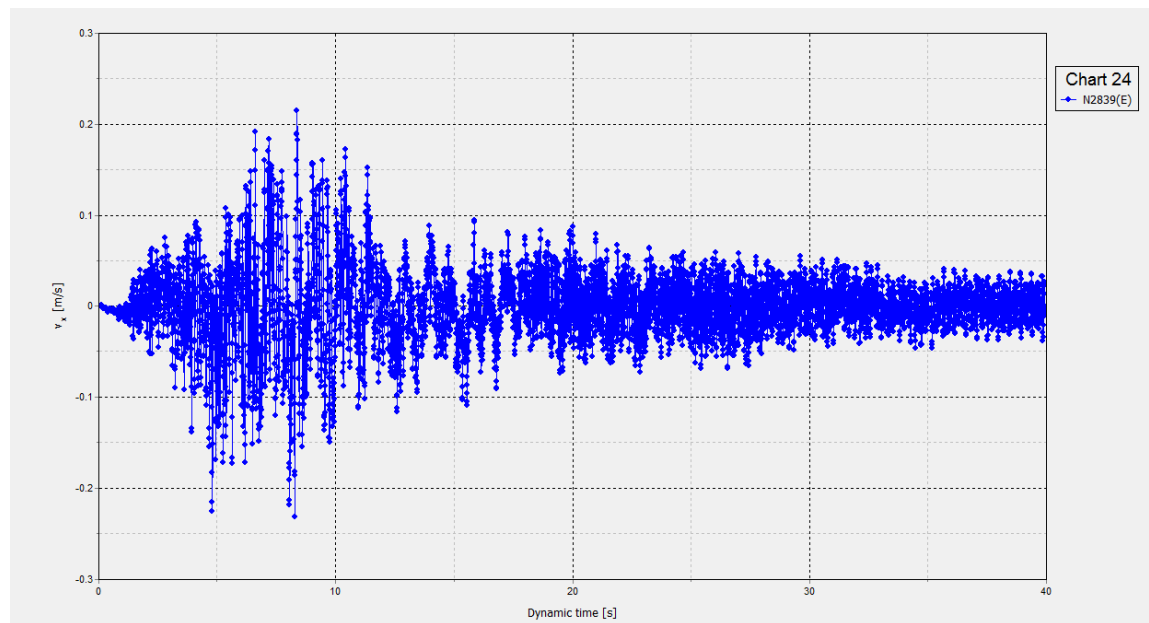
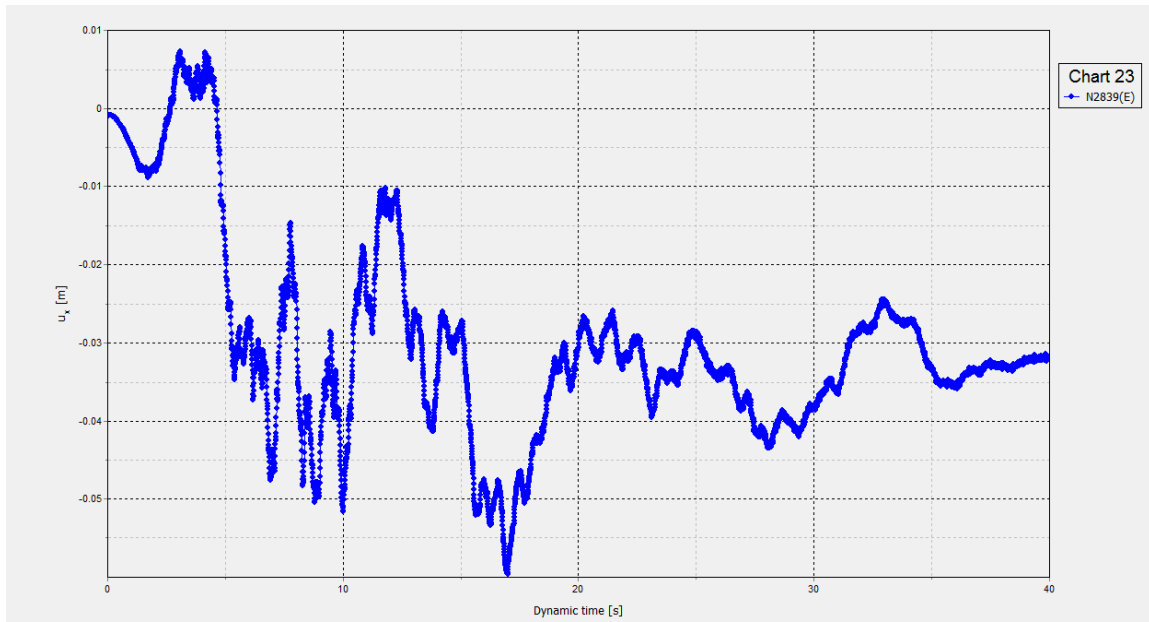


Figure 29 Time history of upper layer response to Loma Prieta earthquake (top: displacement, bottom: velocity)

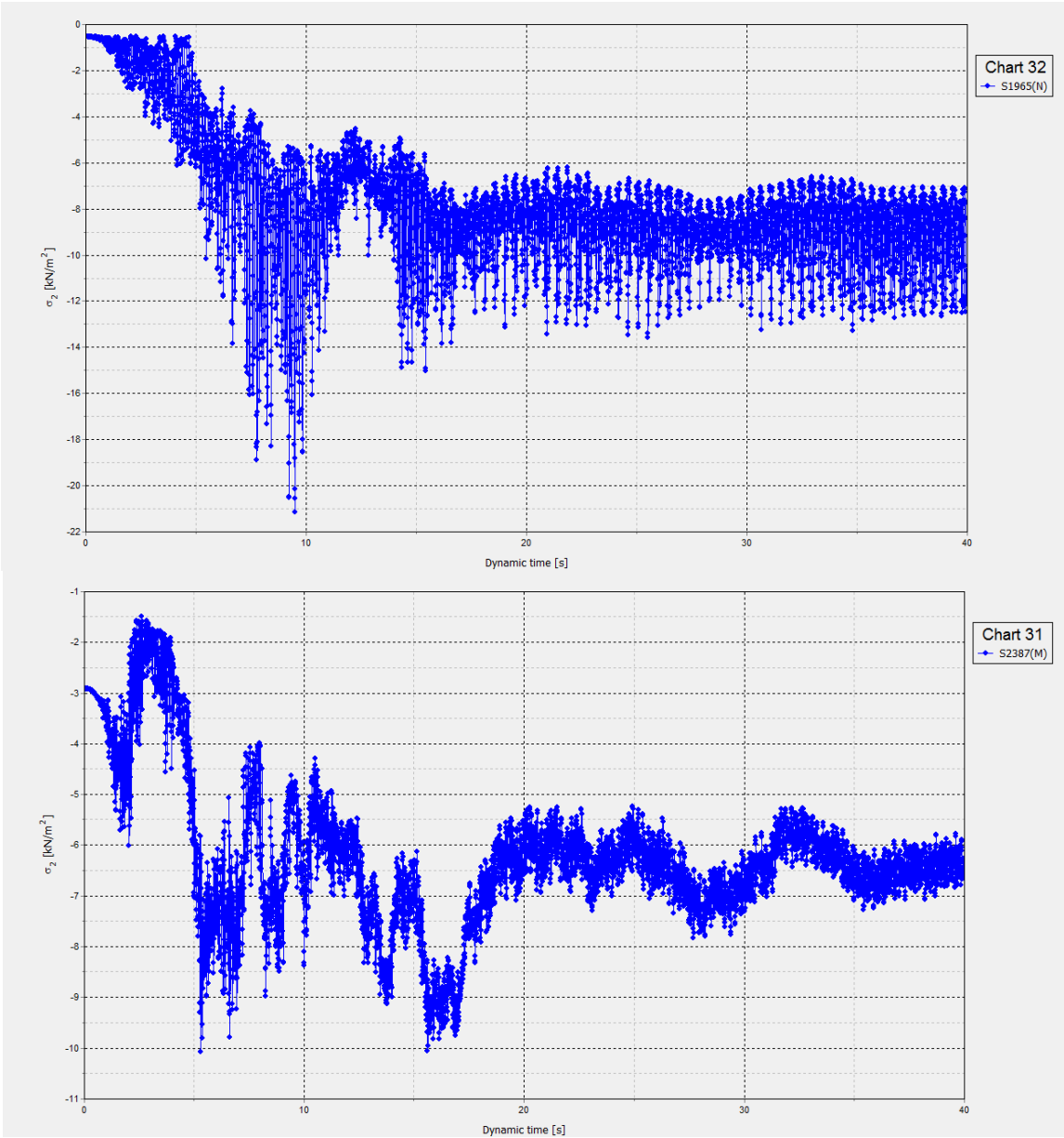


Figure 30 Time history of horizontal stress to Loma Prieta earthquake (top: upper layer, bottom: lower layer)

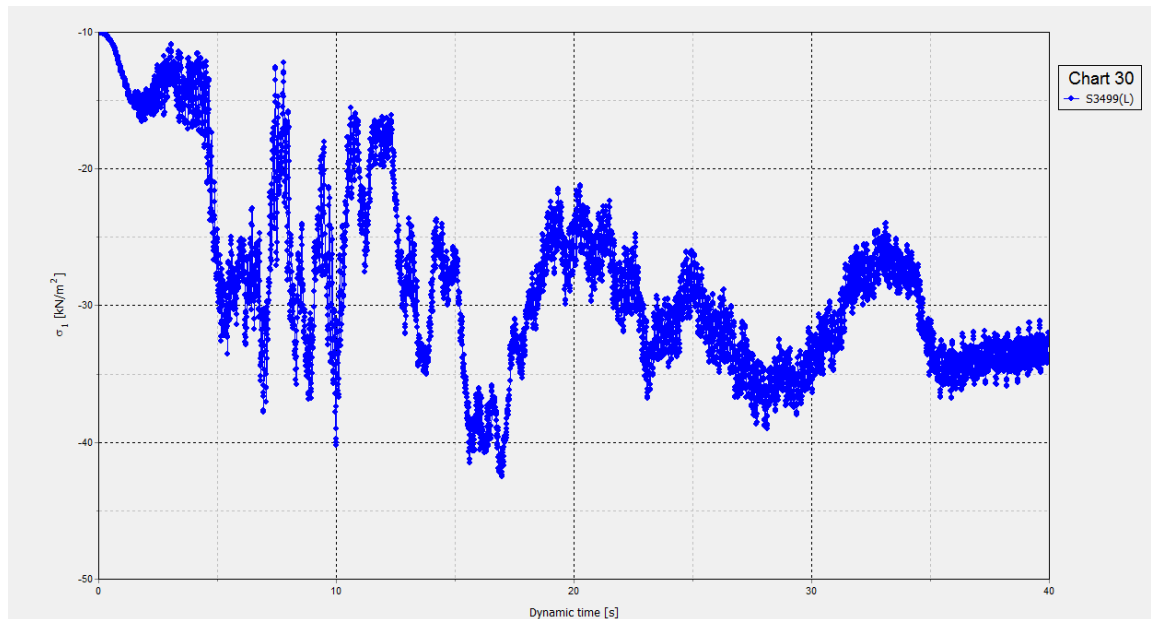
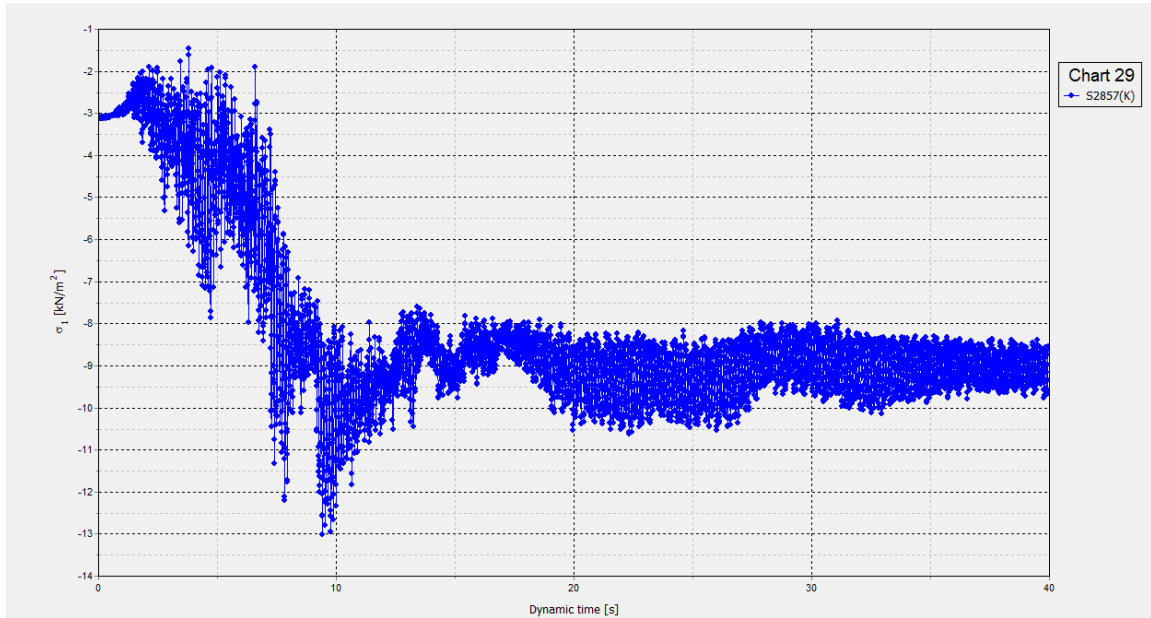


Figure 31 Time history of vertical stress to Loma Prieta earthquake (top: upper layer, bottom: lower layer)

(2) TDA backfill, sinusoidal sweep-frequency motions

(a) Shake Table Test

Immediately after the simulated Loma Prieta earthquake, sinusoidal sweep-frequency motions were run on the same MSE wall. After the strong shaking, the MSE wall with TDA backfill did not have noticeable damage. Figure 32 shows the lateral deflections (displacements) of the MSE wall measured at the top, middle, and bottom layers in the shake table test. It shows increased lateral deflections from the bottom toward the top of the wall and increased lateral deflection with the frequency. The maximum horizontal deflection was approximately 6.8 cm. Figure 33 shows the vertical deformations of the MSE wall in the shake table testing. The two LVDTs recorded similar settlements in the sinusoidal motions, and the maximum vertical deformation was approximately 2.4 cm.

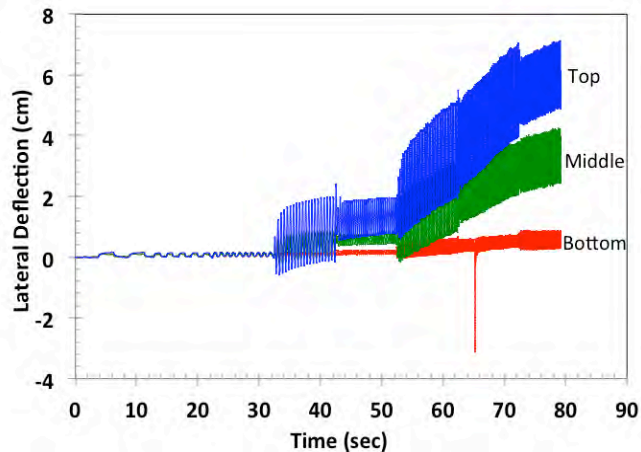


Figure 32. Lateral deflections of the MSE wall with TDA backfill, from sinusoidal sweep-frequency motions, after Loma Prieta earthquake

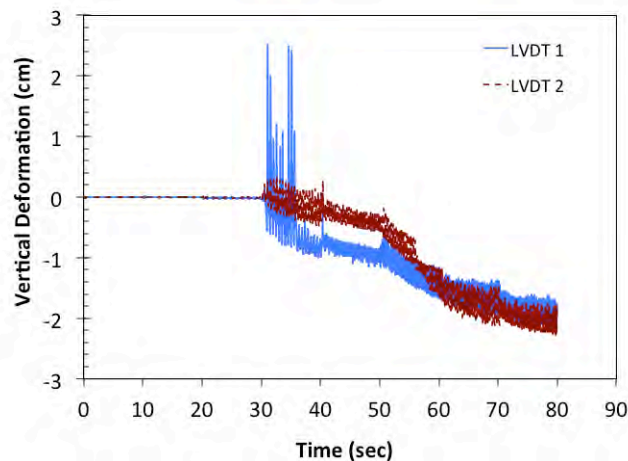


Figure 33. Vertical deformations of the MSE wall with TDA backfill, from sinusoidal sweep-frequency motions, after Loma Prieta earthquake

Figure 34 presents the lateral pressures on the TDA backfill, and Figure 35 shows the vertical stresses in the TDA backfill.

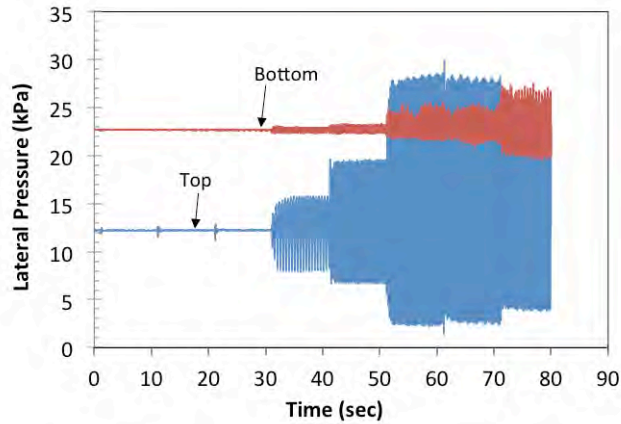


Figure 34. Lateral pressures on the TDA backfill of the MSE wall, from sinusoidal sweep-frequency motions, after Loma Prieta earthquake

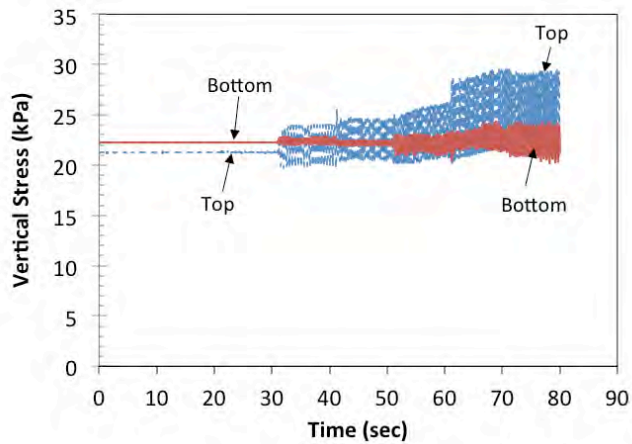


Figure 35. Vertical stresses in the TDA backfill of the MSE wall, from sinusoidal sweep-frequency motions, after Loma Prieta earthquake

The accelerometers recorded the acceleration ~ time histories of each layer, the table and the box. The maximum accelerations and their time of occurrence are listed in Table 6. The accelerations showed a decreasing trend from the bottom to top, except for the top layer.

Table 6. Maximum accelerations and time of occurrences

Location	Layer 1 (bottom)	Layer 2	Layer 3	Layer 4	Layer 5 (top)	Table	Box
Acc (g)	2.167	1.976	1.736	1.222	1.441	2.287	1.734
Time (sec)	72.34	71.2	70.45	50.68	72.87	78.27	71.99

(b) Numerical Model

The response of the MSE system with TDA backfill to the harmonic load is shown using time history of deformation, velocity, and stresses at various layers.

The results indicate an increase in maximum deflection of model as the frequency is increased from 0.2 Hz to 6 Hz. This qualitative outcome confirms experimental observations. The following figure shows the deformed mesh after three phases of analysis with PLAXIS 2D. The maximum deformation recorded through PLAXIS 2D is 1.642 cm and 9.46 cm for 0.2 Hz and 4 Hz, respectively.

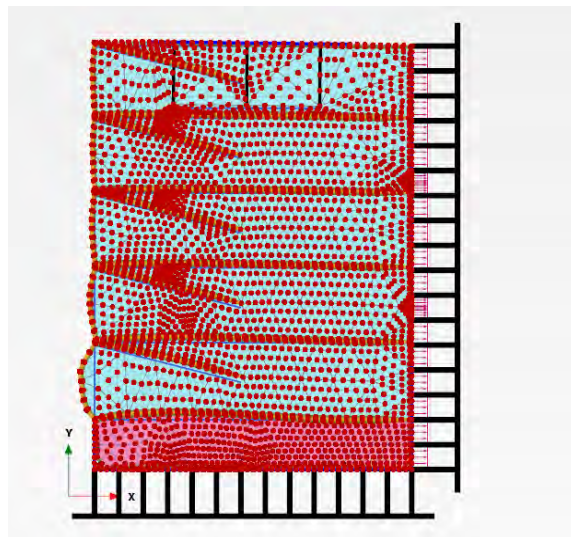


Figure 36 Typical deformed mesh, 0.2 Hz

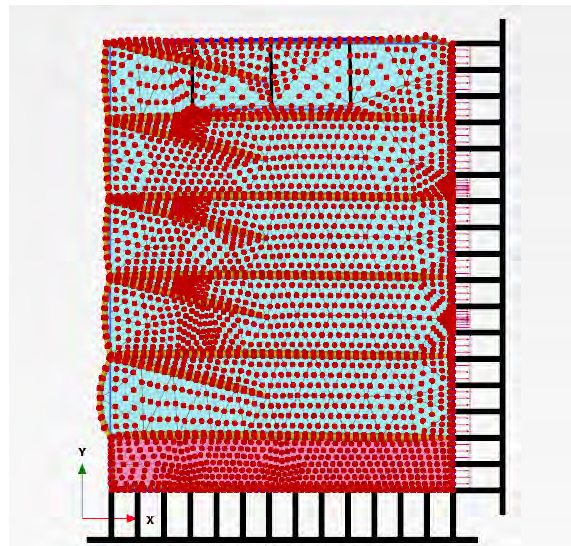


Figure 37 Typical deformed mesh, 4 Hz

Closer observations reveal that overall PLAXIS results for displacement and velocity follow a harmonic pattern, even though, results include noises in velocity time history due to lack of convergence. The lateral displacements obtained from PLAXIS 2D for this frequency are identical for the bottom, middle and top layers of the model. With the lower frequencies this is always the case, and can be seen in the next sections, but for the higher frequencies, because the model is more vigorously shaking back and forth the layers begin to observe different values of displacement. Further, the following figures show the velocity at the bottom and top layers of the model. As with the displacement curves, the curves of velocity have similar values for all the layers due to the low intensity of the excitation.

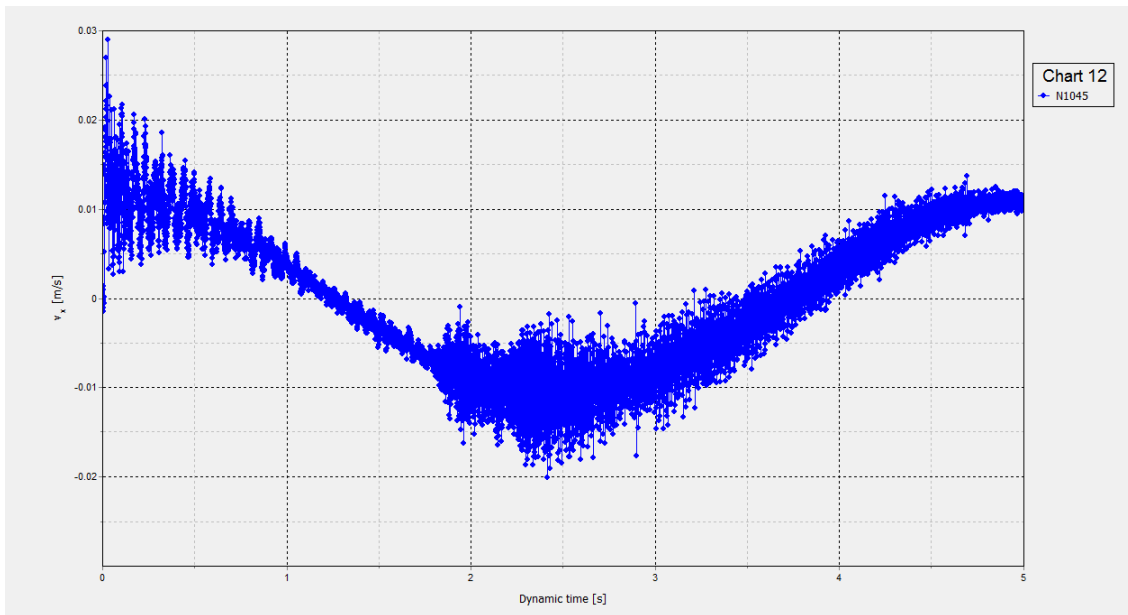
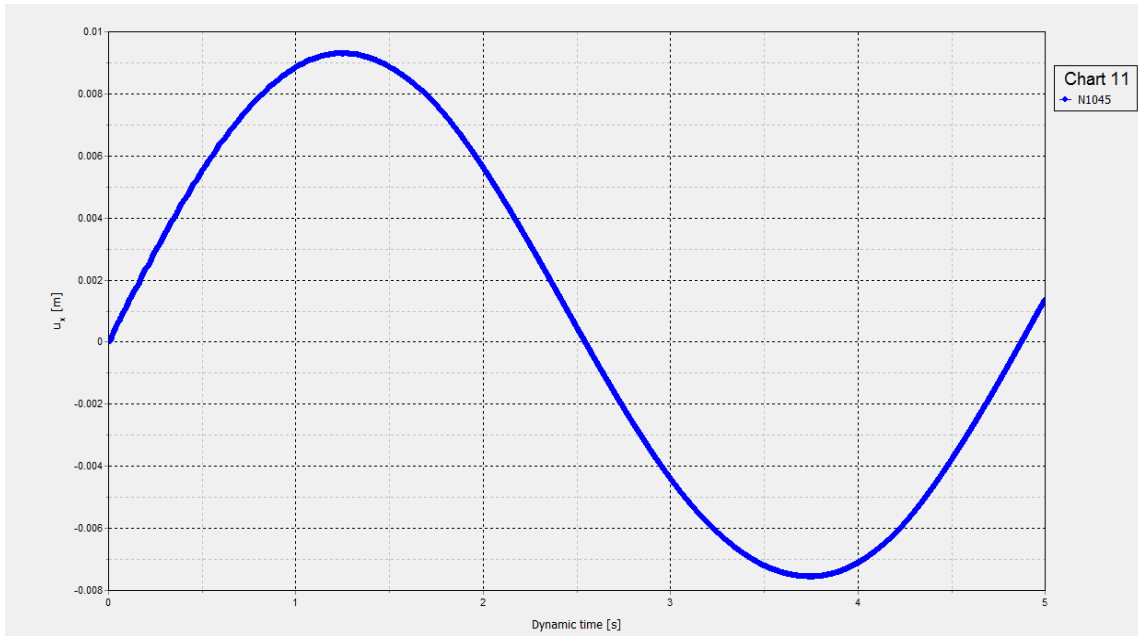


Figure 38 Time history of lower layer response to 0.2 Hz (top: displacement, bottom: velocity)

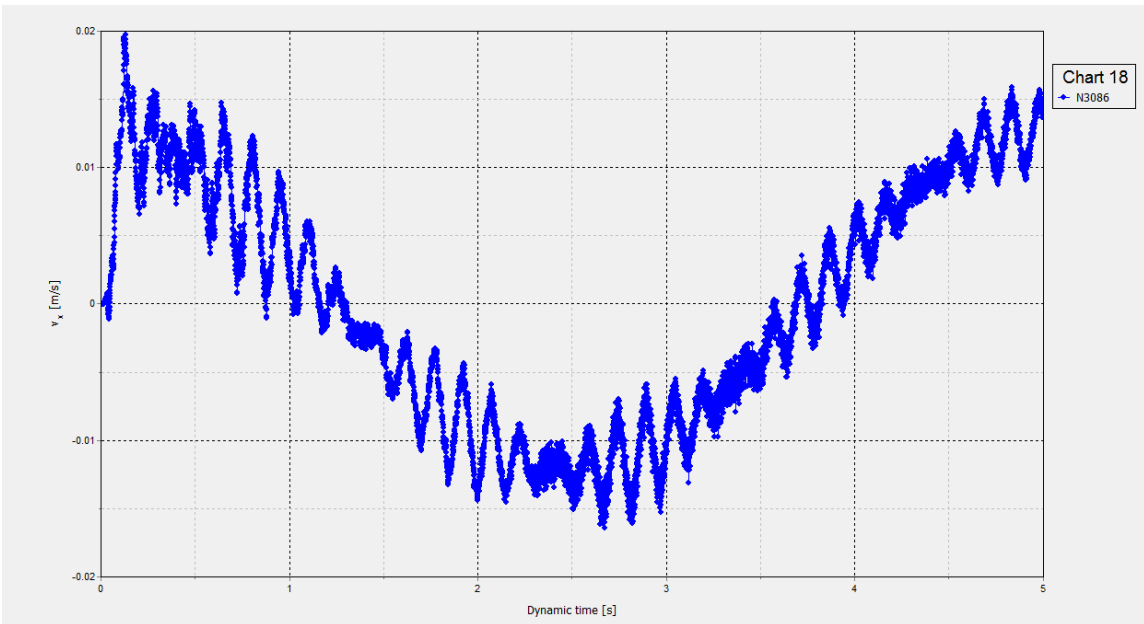
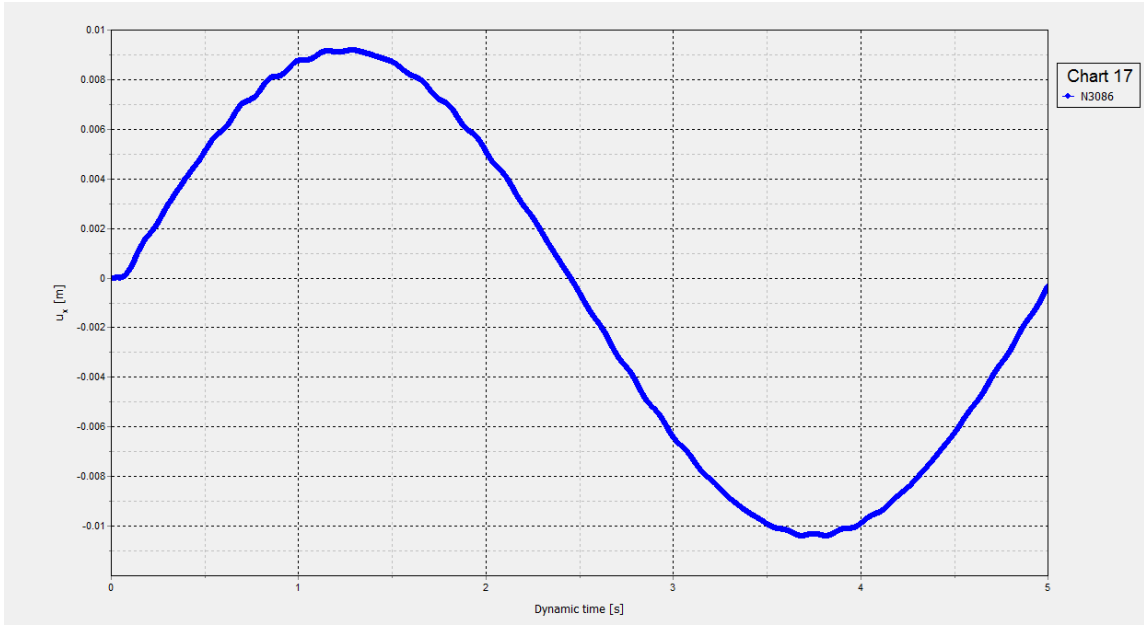


Figure 39 Time history of upper layer response to 0.2 Hz (top: displacement, bottom: velocity)

Time histories of horizontal and vertical stresses are subject to the same convergence issues as for velocity. Nevertheless, the average values indicate acceptable results.

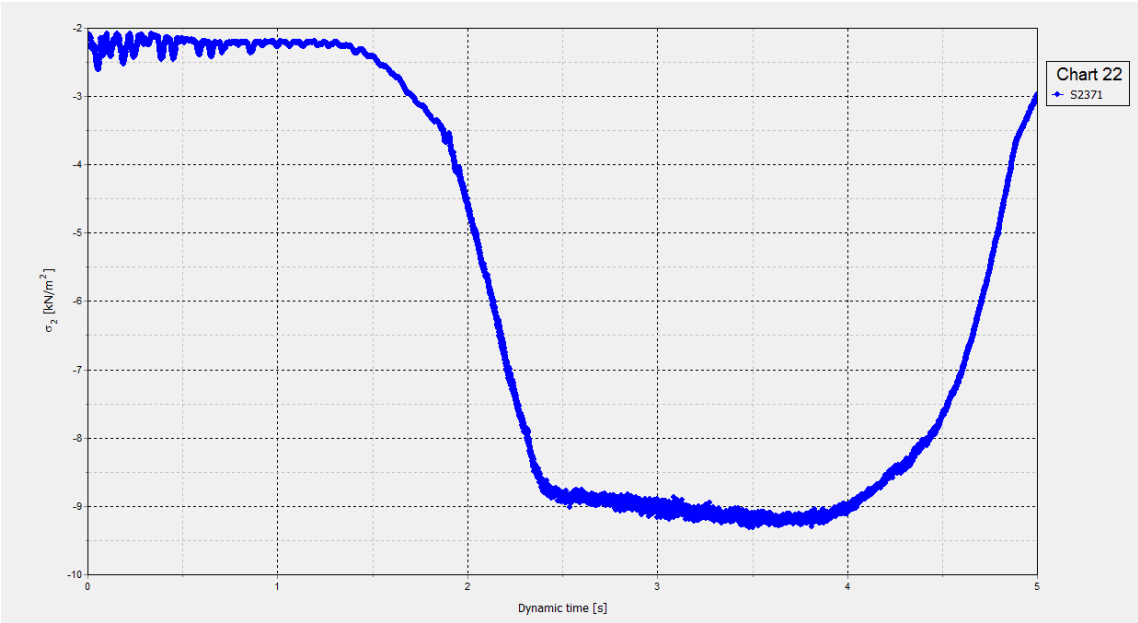
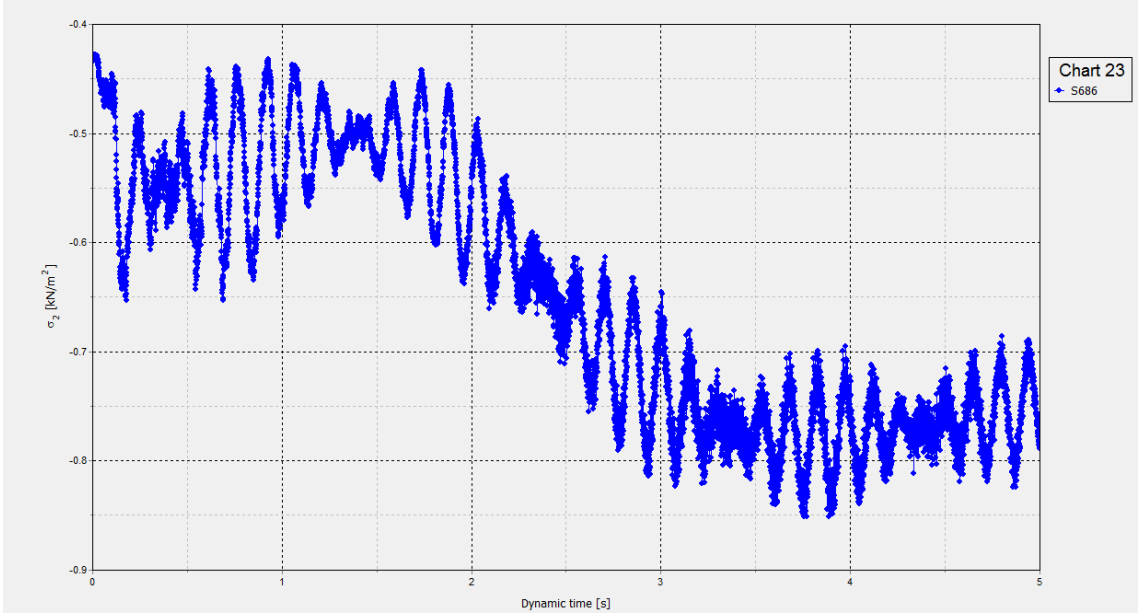


Figure 40 Time history of horizontal stress to 0.2 Hz (top: upper layer, bottom: lower layer)

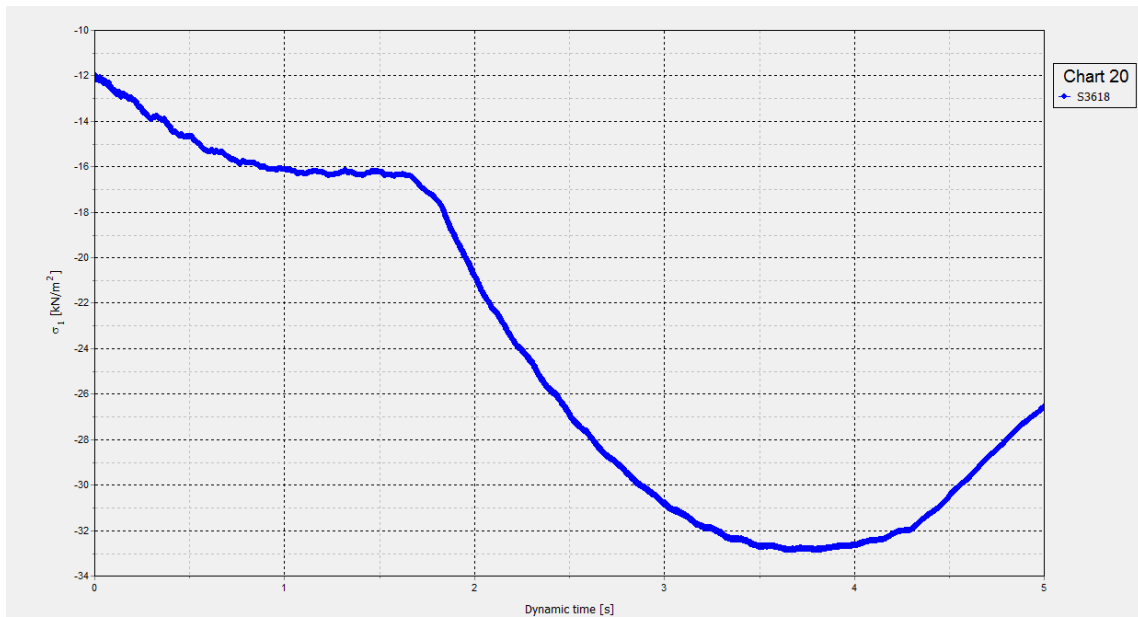
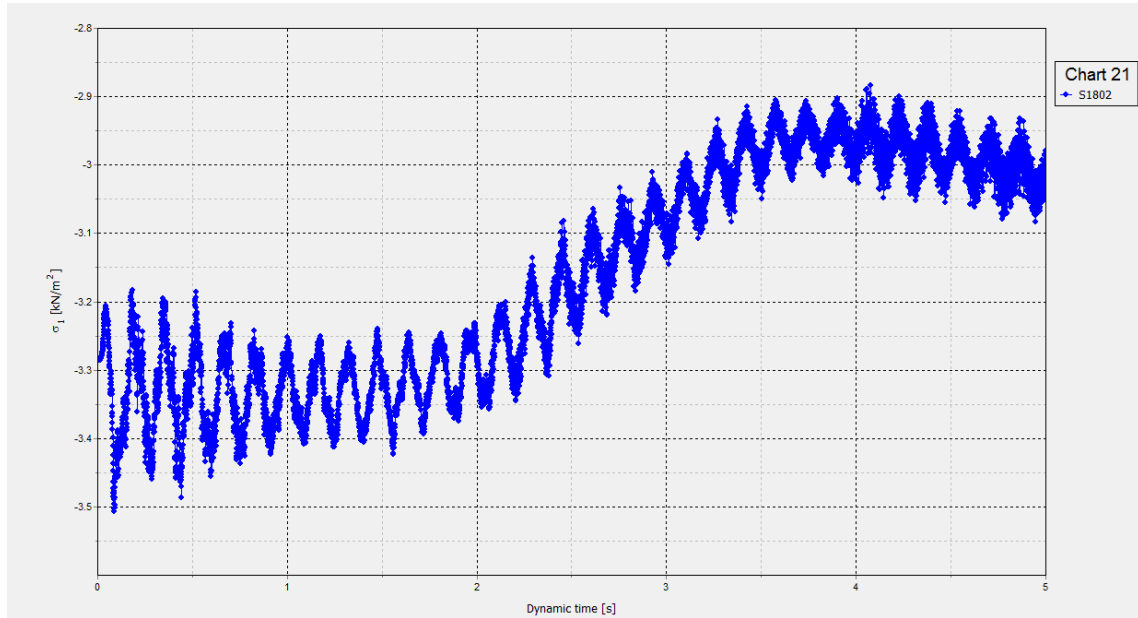


Figure 41 Time history of vertical stress to 0.2 Hz (top: upper layer, bottom: lower layer)

Comparing results for 0.2 and 6 Hz frequencies indicates how number and length of time steps during numerical analysis affects the apparent quality of resulted graphs.

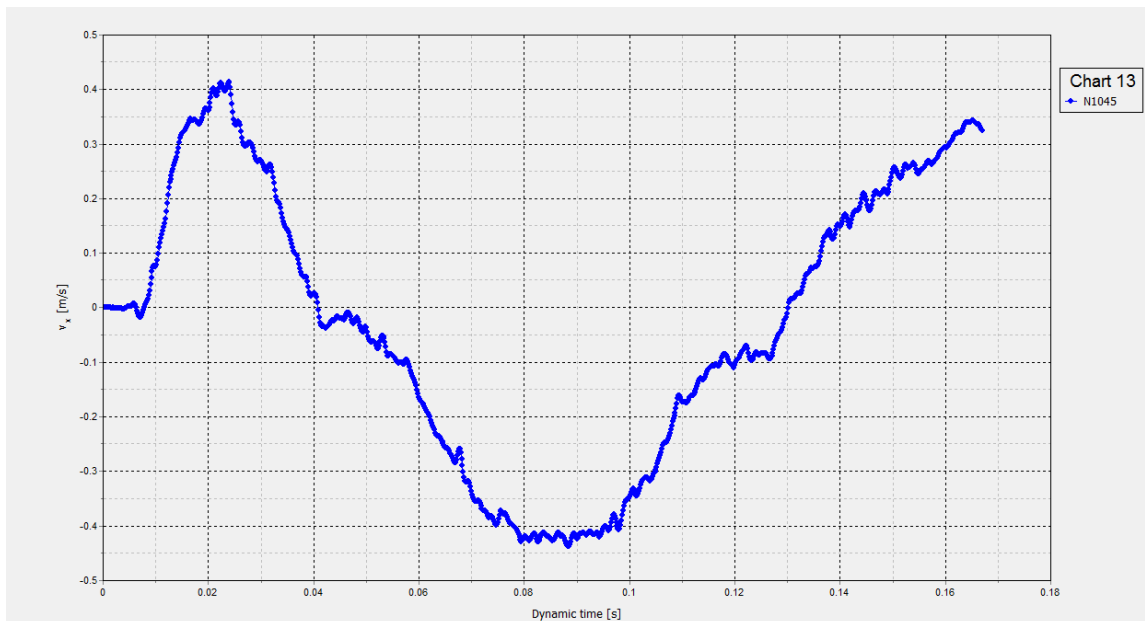
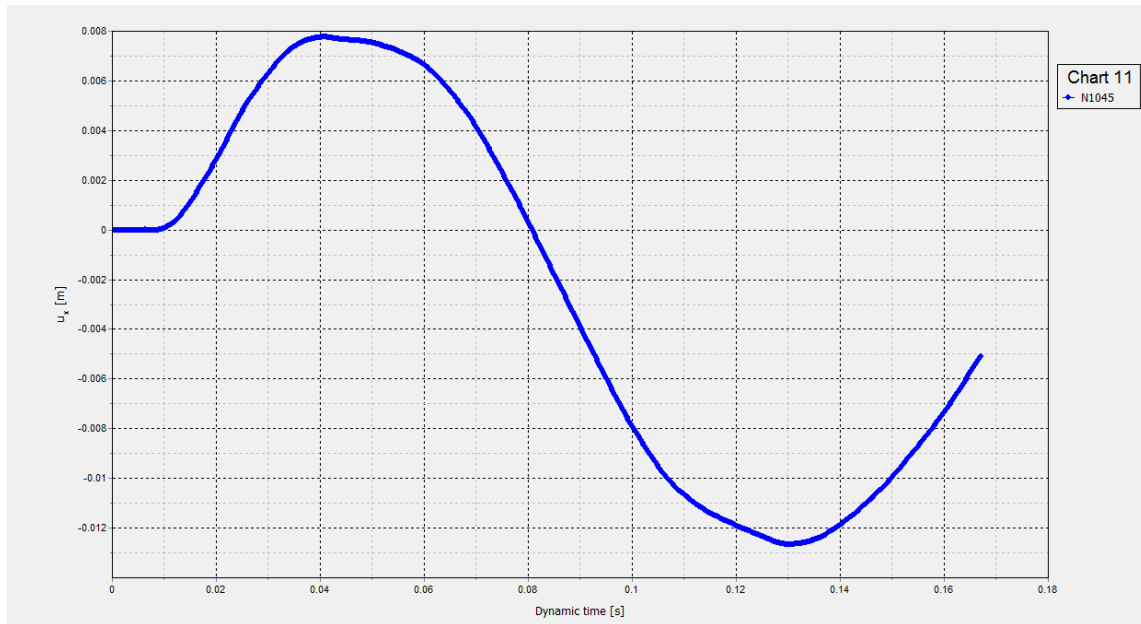


Figure 42 Time history of lower layer response to 6 Hz (top: displacement, bottom: velocity)

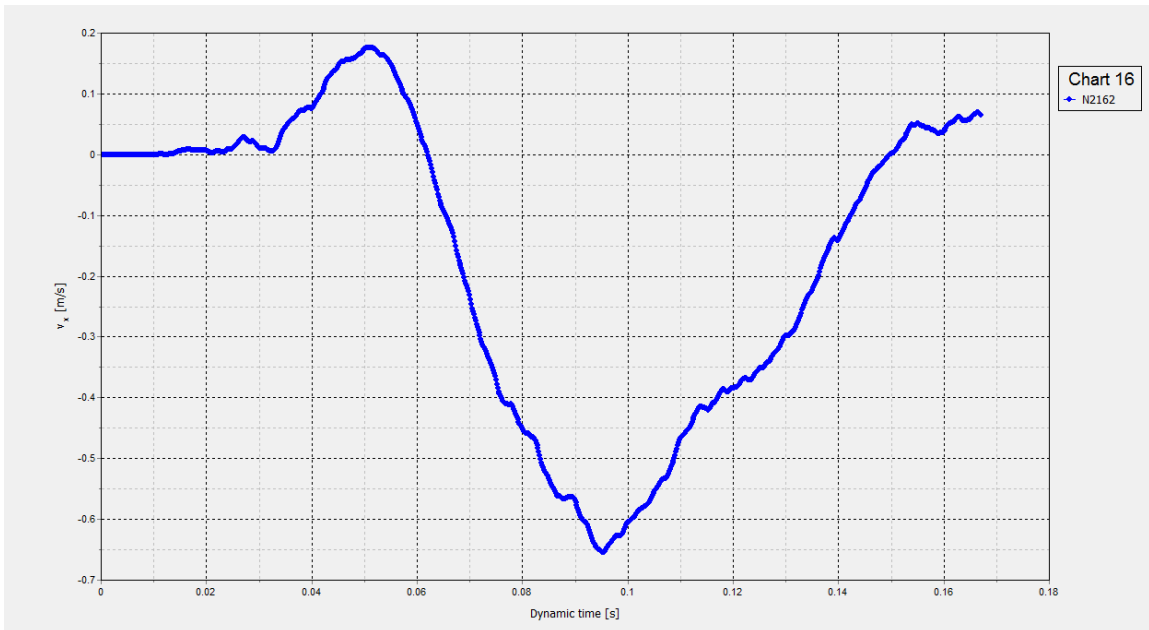
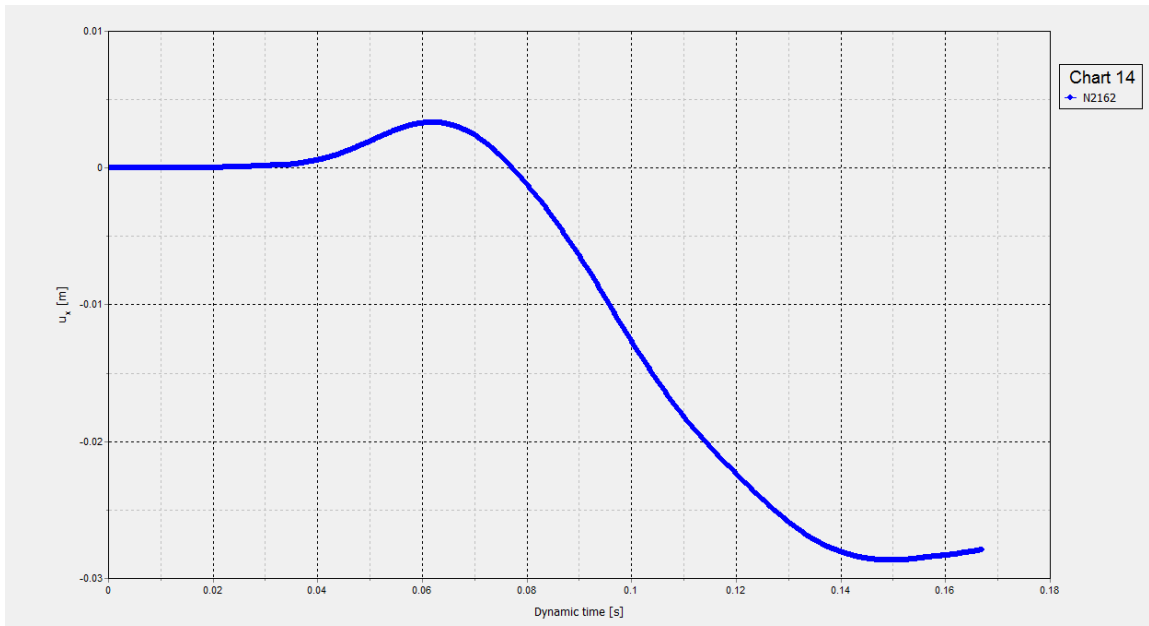


Figure 43 Time history of upper layer response to 6 Hz (top: displacement, bottom: velocity)

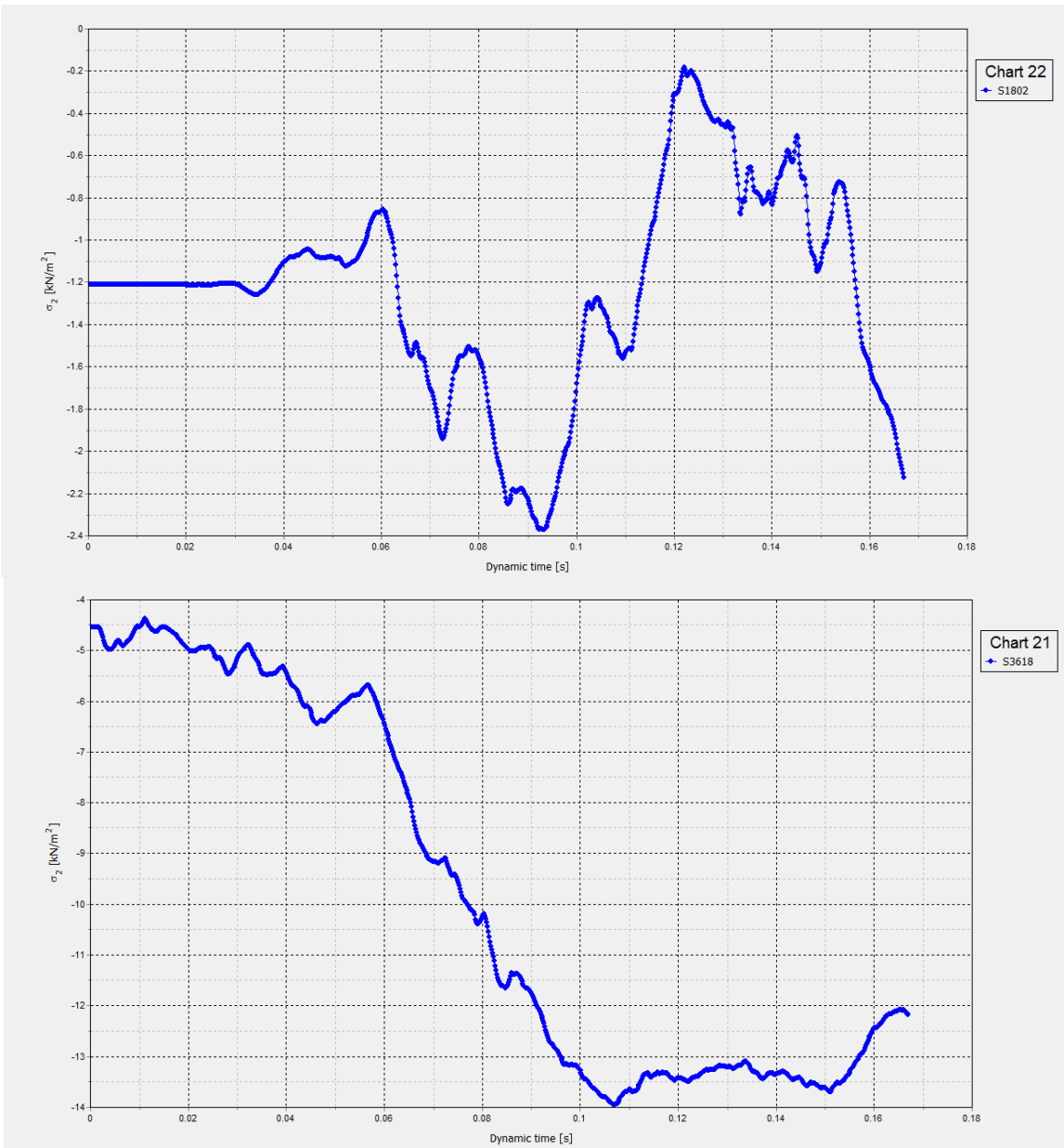


Figure 44 Time history of horizontal stress to 6 Hz (top: upper layer, bottom: lower layer)

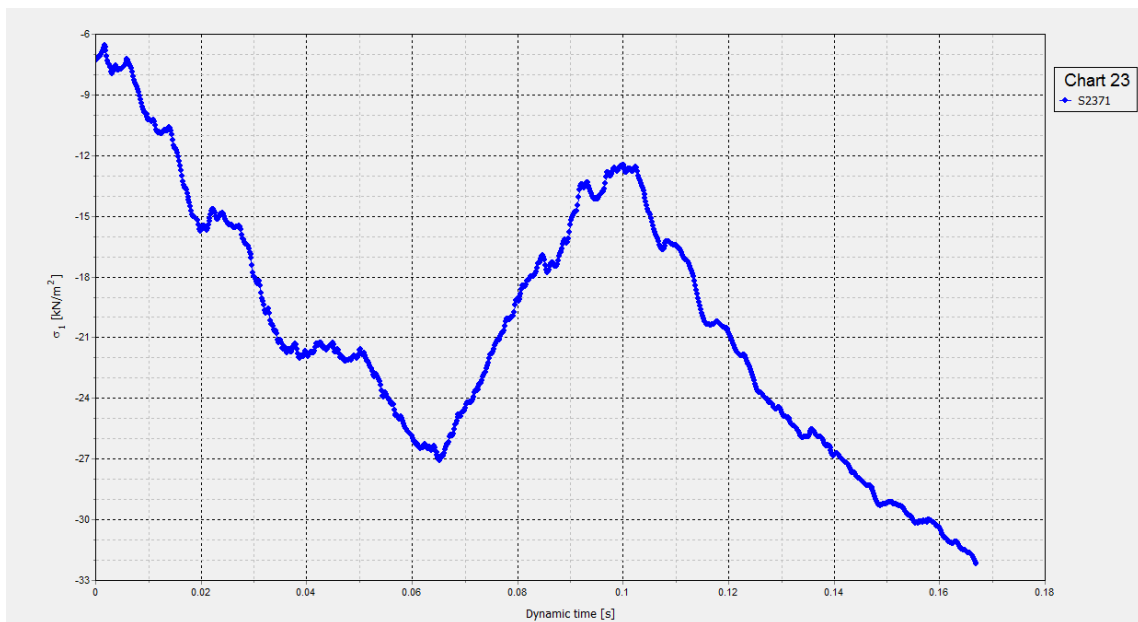
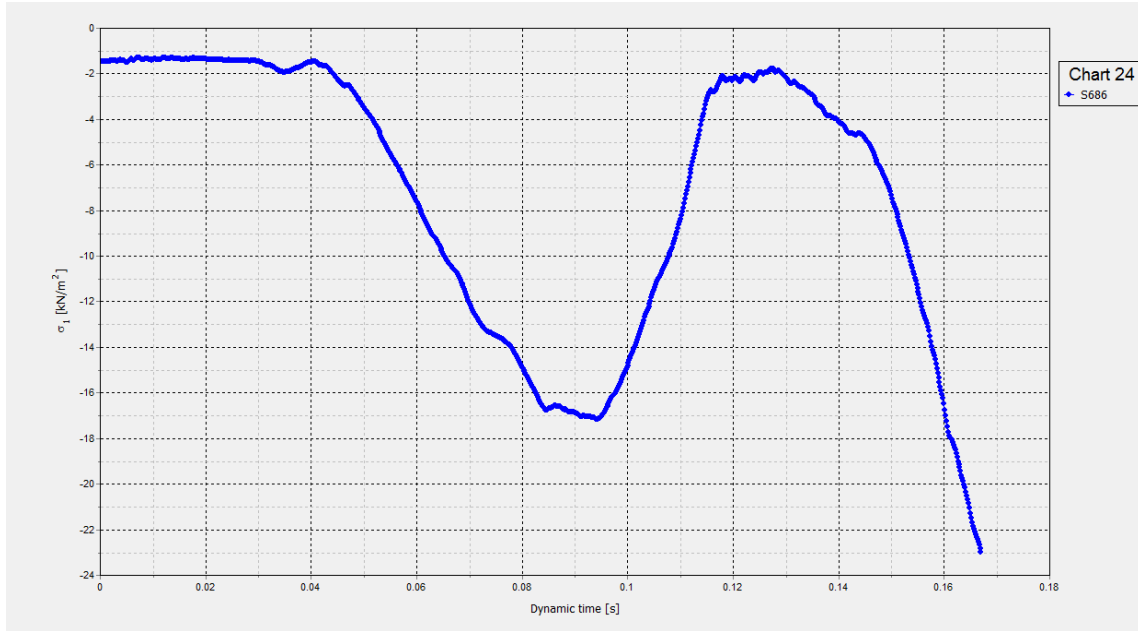


Figure 45 Time history of vertical stress to 6 Hz (top: upper layer, bottom: lower layer)

(3) TDA backfill, Northridge earthquake

(a) Shake Table Test

After the shake table testing, the MSE wall with TDA backfill did not have noticeable damage. And there were no noticeably excessive settlement and lateral spreading of the wall. Figure 46 shows the lateral deflections (displacements) of the MSE wall measured at the top, middle, and bottom layers in the shake table test. It shows increased lateral deflections from the bottom toward the top of the wall. In the first cycle of the simulated Northridge earthquake, the maximum horizontal deflection was approximately 5.8 cm, while it reached 7.3 cm in the repeated Northridge simulation. Figure 47 shows the vertical deformations of the MSE wall in the shake table testing. The two LVDTs recorded similar settlements in the repeated Northridge earthquake simulations, and the maximum vertical deformation was approximately 2.2 cm.

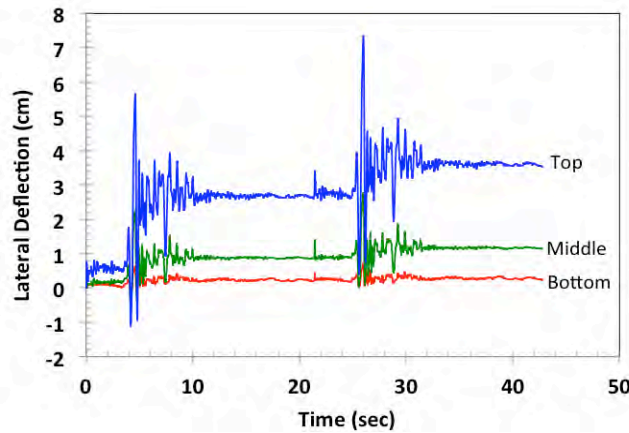


Figure 46. Lateral deflections of the MSE wall with TDA backfill, from Northridge earthquake

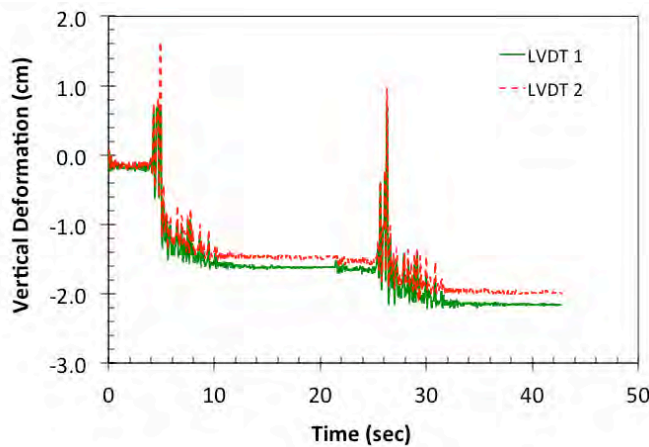


Figure 47. Vertical deformations of the MSE wall with TDA backfill, from Northridge earthquake

Figure 48 presents the lateral pressures on the TDA backfill, and Figure 49 shows the vertical stresses in the TDA backfill.

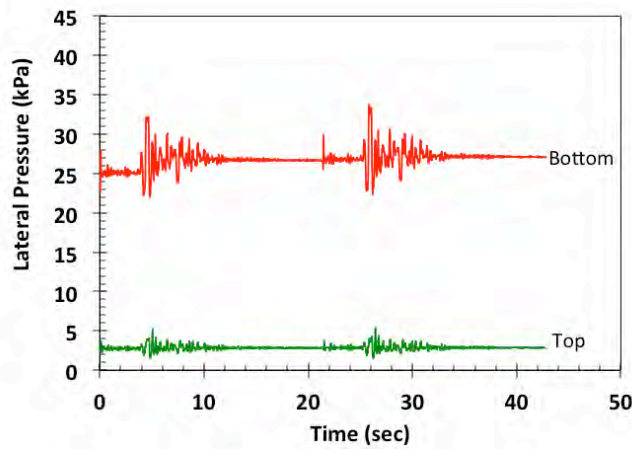


Figure 48. Lateral pressures on the TDA backfill of the MSE wall, from Northridge earthquake

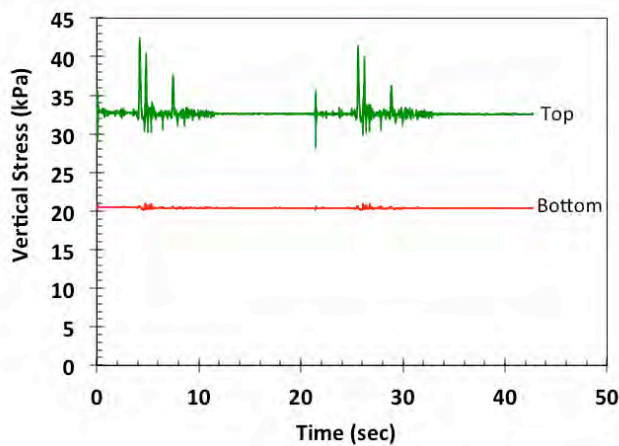


Figure 49. Vertical stresses in the TDA backfill of the MSE wall, from Northridge earthquake

The accelerometers recorded the acceleration ~ time histories of each layer, the table and the box. The maximum accelerations and their time of occurrence are listed in Table 7. Non-linear distribution of accelerations with the depth of the wall was observed.

Table 7. Maximum accelerations and time of occurrences

Location	Layer 1 (bottom)	Layer 2	Layer 3	Layer 4	Layer 5 (top)	Table	Box
Acc (g)	1.322	1.471	1.358	1.382	1.605	1.254	1.377
Time (sec)	4.67	26.69	26.7	4.71	4.73	21.41	21.41

(b) Numerical Model

The response of the MSE system with TDA backfill to the Northridge earthquake record is shown using time history of deformation and stress at various layers.

While, the general deformed shape confirms to experimental observations, the analytical results indicate higher deformations in comparison to experimental results. It appears that material characteristics, including the modulus of elasticity, have great impact on numerical analysis. Therefore, simplifications in estimating input values and testing procedures could be the source of observed discrepancy.

Further, lack of convergence in PLAXIS is manifested in high frequency fluctuations in the response time histories, even though; such short-duration noises do not have substantial impact on average results.

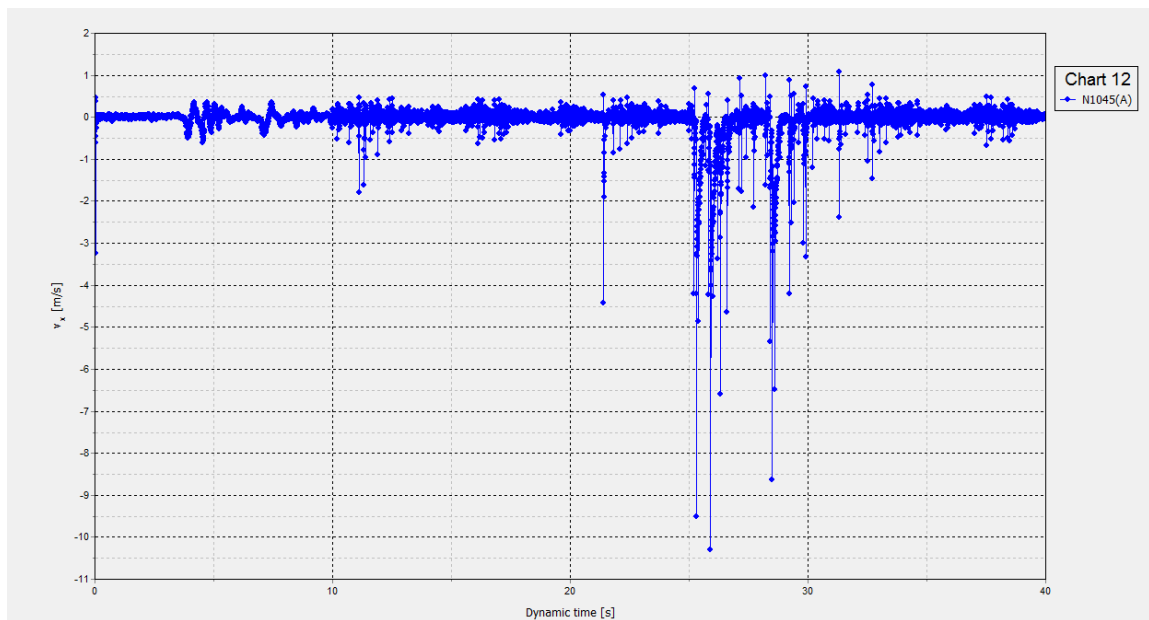
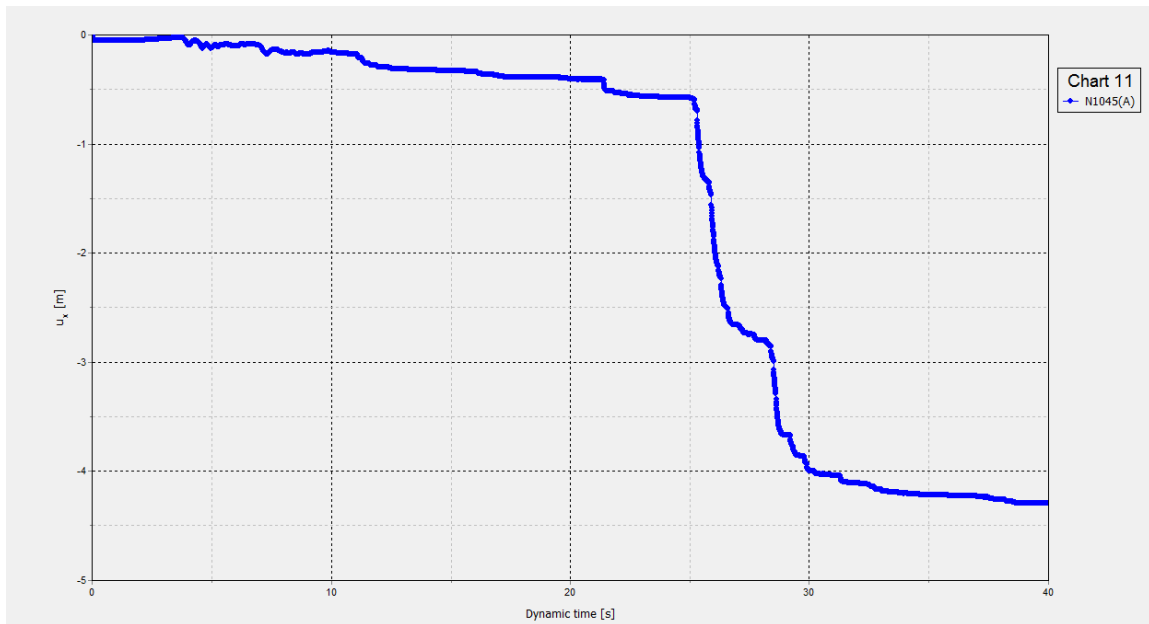


Figure 50 Time history of lower layer response to Northridge earthquake (top: displacement, bottom: velocity)

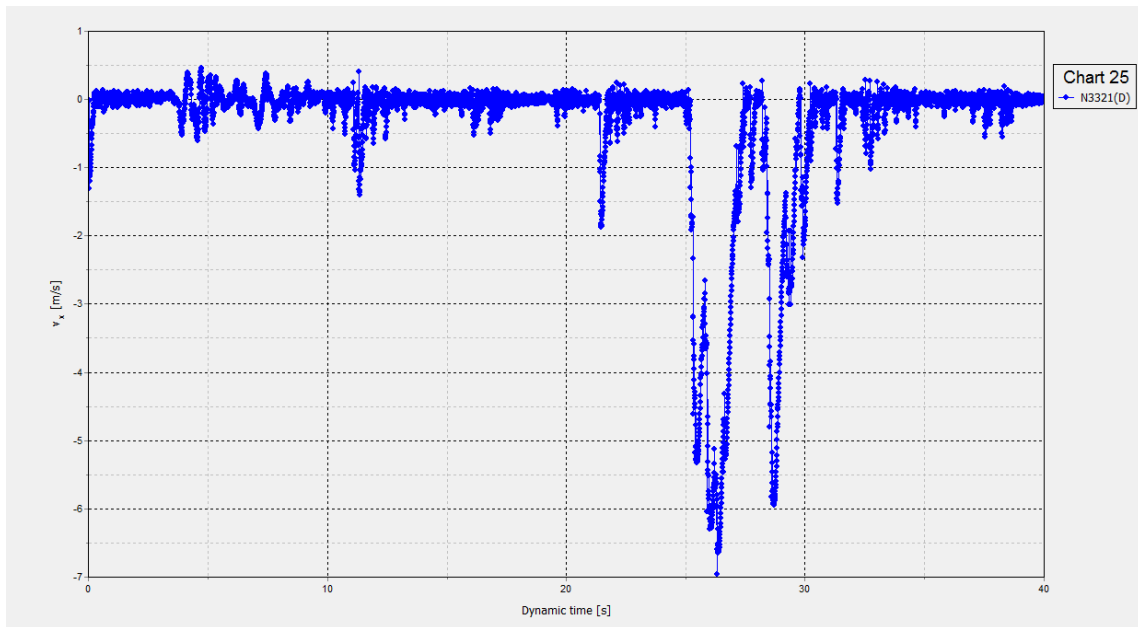
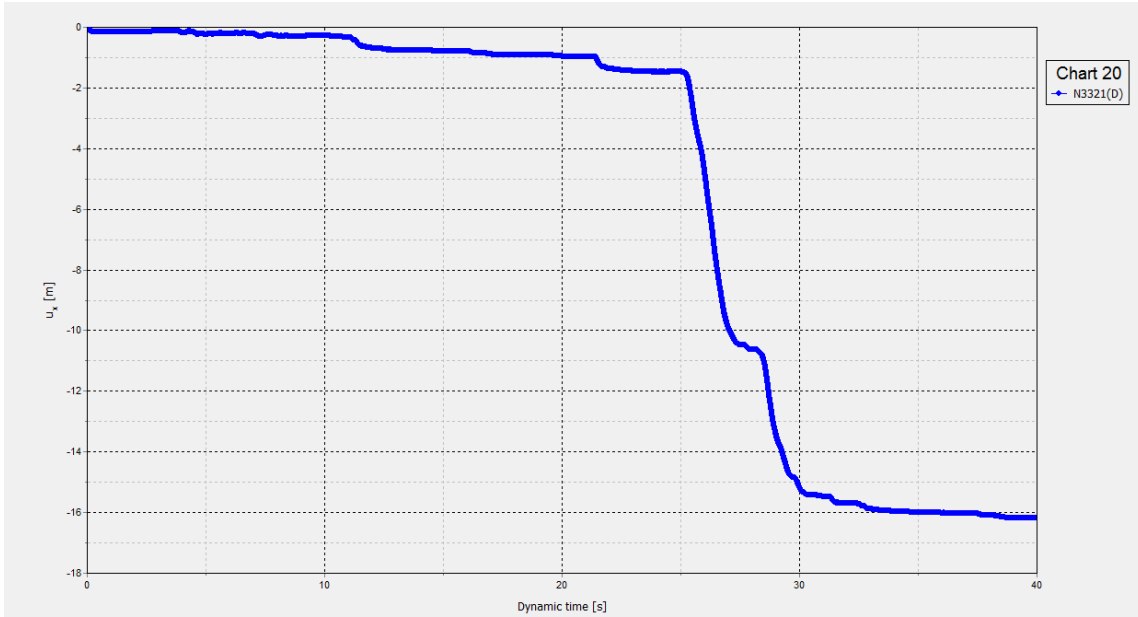


Figure 51 Time history of upper layer response to Northridge earthquake (top: displacement, bottom: velocity)

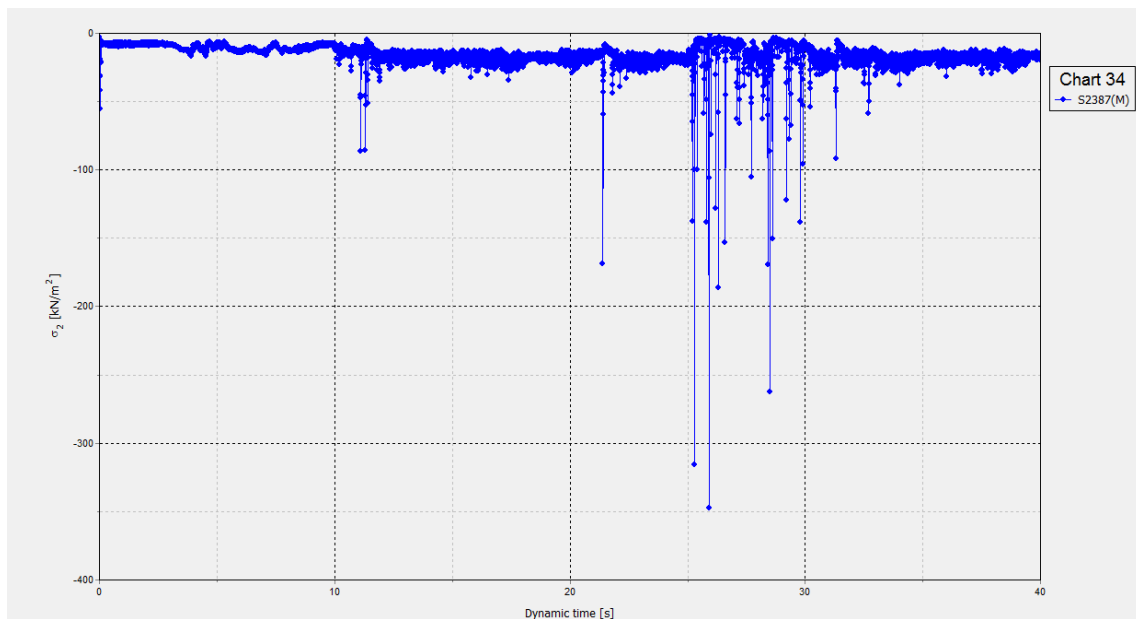
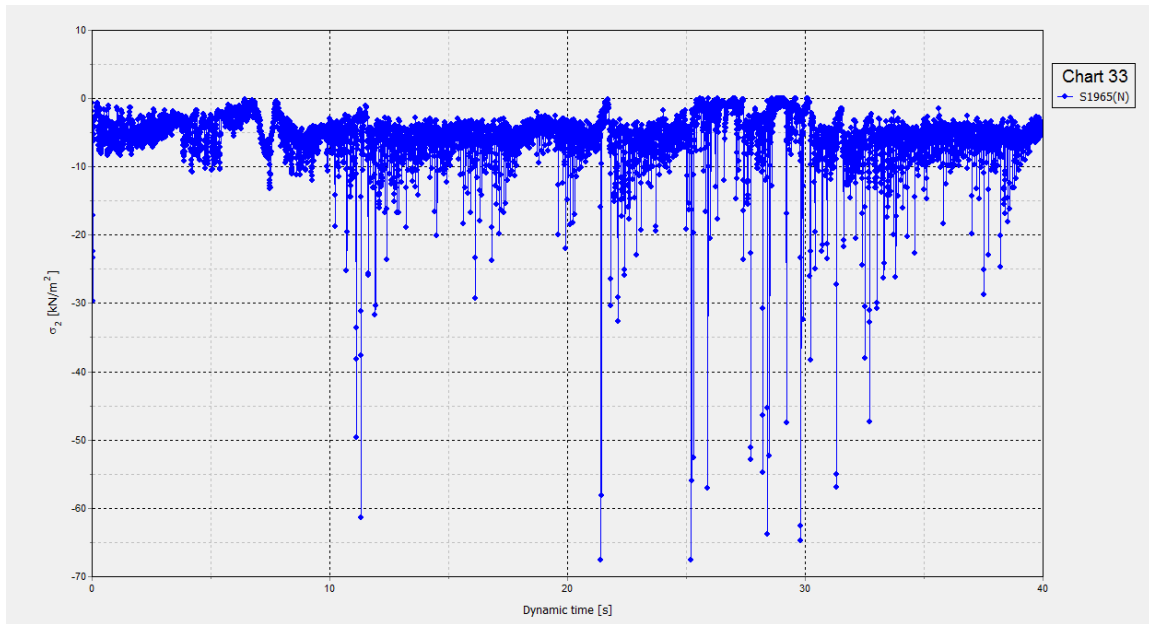


Figure 52 Time history of horizontal stress to Northridge earthquake (top: upper layer, bottom: lower layer)

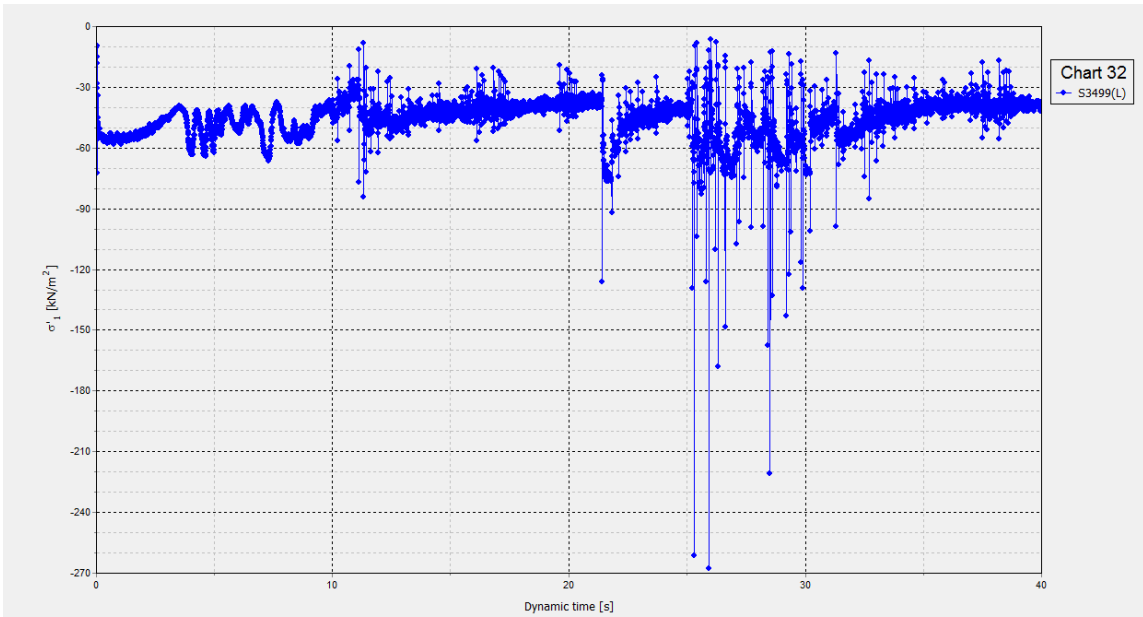
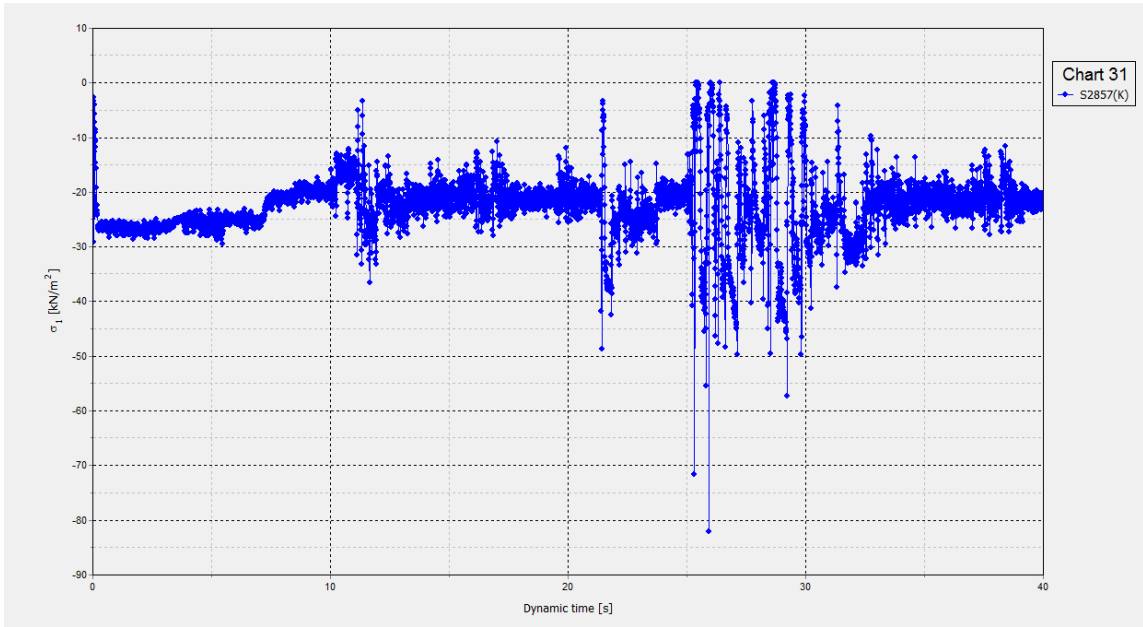


Figure 53 Time history of vertical stress to Northridge earthquake (top: upper layer, bottom: lower layer)

(4) TDA backfill, sinusoidal sweep-frequency motions

(a) Shake Table Test

Immediately after the simulated Northridge earthquake, sinusoidal sweep-frequency motions were run on the same MSE wall. After the strong shaking, the MSE wall with TDA backfill did not have noticeable damage. Figure 54 shows the lateral deflections (displacements) of the MSE wall measured at the top, middle, and bottom layers in the shake table test. It shows increased lateral deflections from the bottom toward the top of the wall and increased lateral deflection with the frequency. The maximum horizontal deflection was approximately 4.2 cm. Figure 33 shows the vertical deformations of the MSE wall in the shake table testing. The two LVDTs recorded similar settlements in the sinusoidal motions, and the maximum vertical deformation was approximately 1.5 cm.

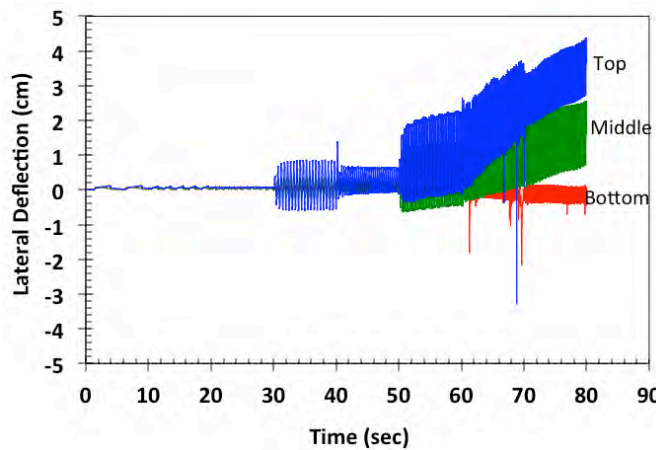


Figure 54. Lateral deflections of the MSE wall with TDA backfill, from sinusoidal sweep-frequency motions, after Northridge earthquake

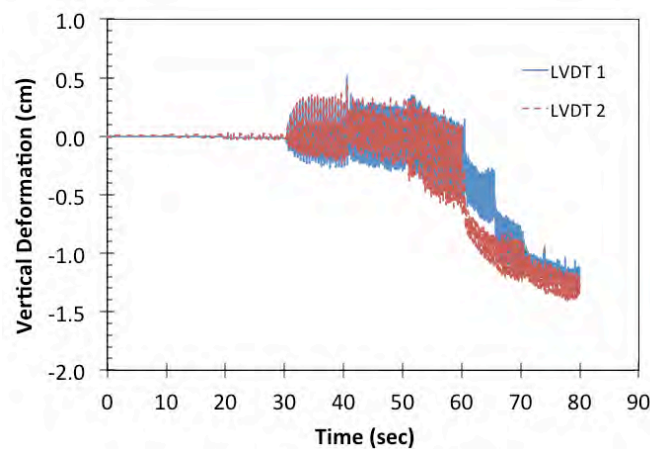


Figure 55. Vertical deformations of the MSE wall with TDA backfill, from sinusoidal sweep-frequency motions, after Northridge earthquake

Figure 56 presents the lateral pressures on the TDA backfill, and Figure 57 shows the vertical stresses in the TDA backfill. It is noted that vertical stress at the top is higher than that at the bottom. The investigators believe the vertical pressure measurements may be incorrect.

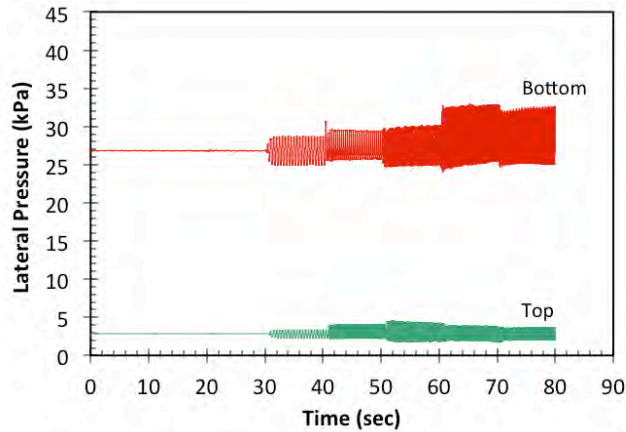


Figure 56. Lateral pressures on the TDA backfill of the MSE wall, from sinusoidal sweep-frequency motions, after Northridge earthquake

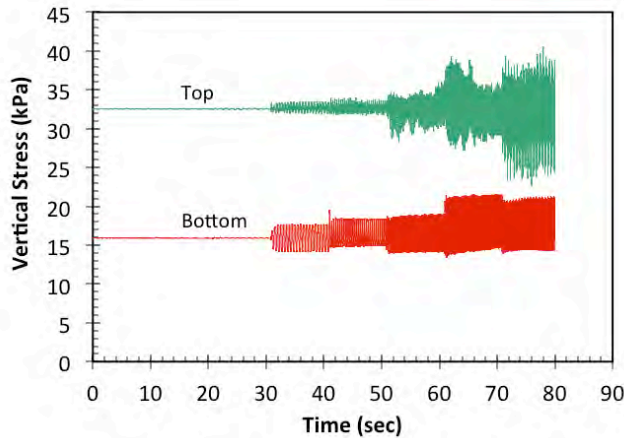


Figure 57. Vertical stresses in the TDA backfill of the MSE wall, from sinusoidal sweep-frequency motions, after Northridge earthquake

The accelerometers recorded the acceleration ~ time histories of each layer, the table and the box. The maximum accelerations and their time of occurrence are listed in Table 5. The accelerations showed a decreasing trend from the bottom to top, except for the top layer. This is the same trend as in Test 3.

Table 8. Maximum accelerations and time of occurrences

Location	Layer 1 (bottom)	Layer 2	Layer 3	Layer 4	Layer 5 (top)	Table	Box
Acc (g)	2.322	2.112	2.046	1.523	1.612	2.226	2.071
Time (sec)	70.5	69.86	69.91	70.09	59.66	79.4	78.59

(5) LWA backfill, Loma Prieta earthquake

(a) Shake Table Test

After the shake table testing, the MSE wall with LWA backfill did not have noticeable damage. And there were no noticeably excessive settlement and lateral spreading of the wall. Figure 58 shows the lateral deflections (displacements) of the MSE wall measured at the top, middle, and bottom layers in the shake table test. It shows increased lateral deflections from the bottom toward the top of the wall. The maximum horizontal deflection was approximately 4.8 cm, higher than the MSE wall with TDA backfill under the same shaking. Also important to note is that the LWA backfill tended to oscillate laterally: both movements into and away from the backfill occurred. This is different from the TDA backfill, which only moved away from the backfill.

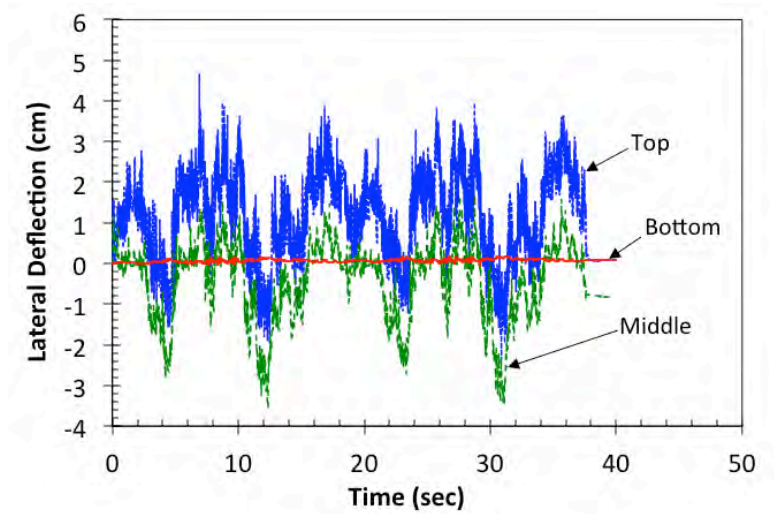


Figure 58. Lateral deflections of the MSE wall with LWA backfill, from Loma Prieta earthquake

Figure 59 shows the vertical deformations of the MSE wall in the shake table testing. One LVDT malfunctioned, so only the readings from the other LVDT were shown. The maximum vertical deformation was approximately 0.84 cm.

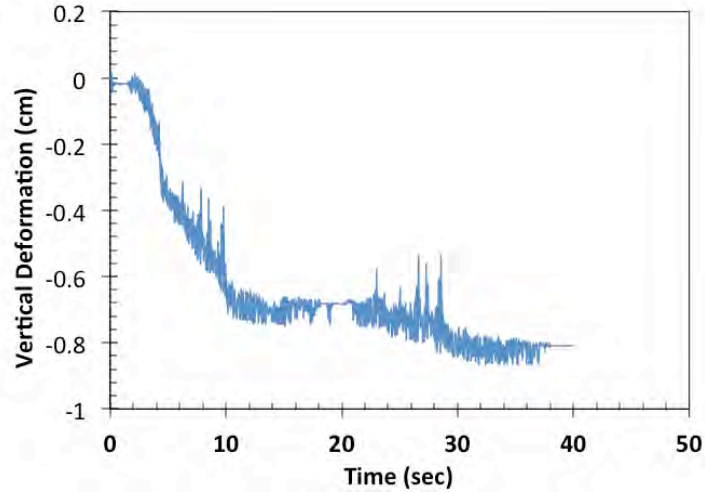


Figure 59. Vertical deformations of the MSE wall with LWA backfill, from Loma Prieta earthquake

Figure 60 presents the lateral pressures on the LWA backfill, and Figure 61 shows the vertical stresses in the LWA backfill.

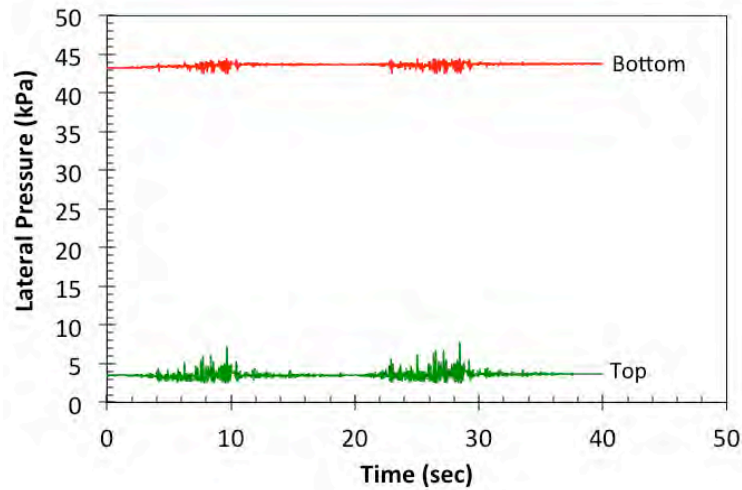


Figure 60. Lateral pressures on the LWA backfill of the MSE wall, from Loma Prieta earthquake

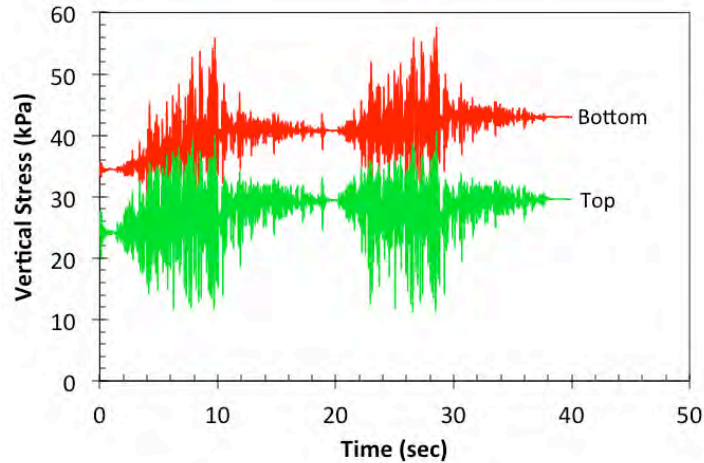


Figure 61. Vertical stresses in the LWA backfill of the MSE wall, from Loma Prieta earthquake

The accelerometers recorded the acceleration ~ time histories of each layer, the table and the box. The maximum accelerations and their time of occurrence are listed in Table 9. The accelerations showed a general increasing trend from the bottom to top. This is different from the TDA backfill under the same shaking, which showed a non-linear distribution of acceleration with depth.

Table 9. Maximum accelerations and time of occurrences

Location	Layer 1 (bottom)	Layer 2	Layer 3	Layer 4	Layer 5 (top)	Table	Box
Acc (g)	0.718	0.702	0.794	1.141	1.421	0.653	0.643
Time (sec)	28.32	27.13	27.48	28.44	28.44	28.31	28.32

(c) Numerical Model

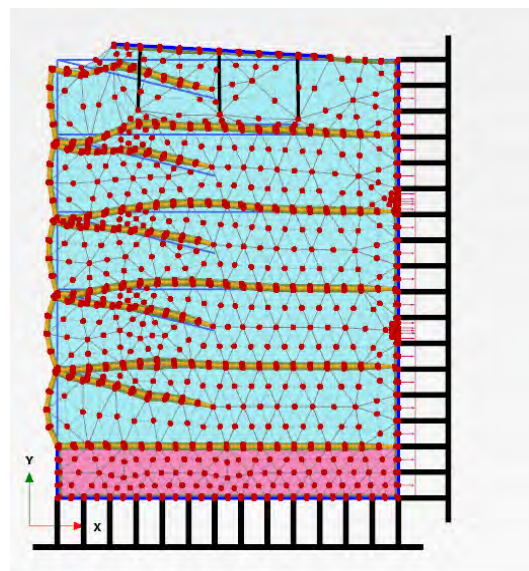


Figure 62 Typical deformed mesh (Loma Prieta)

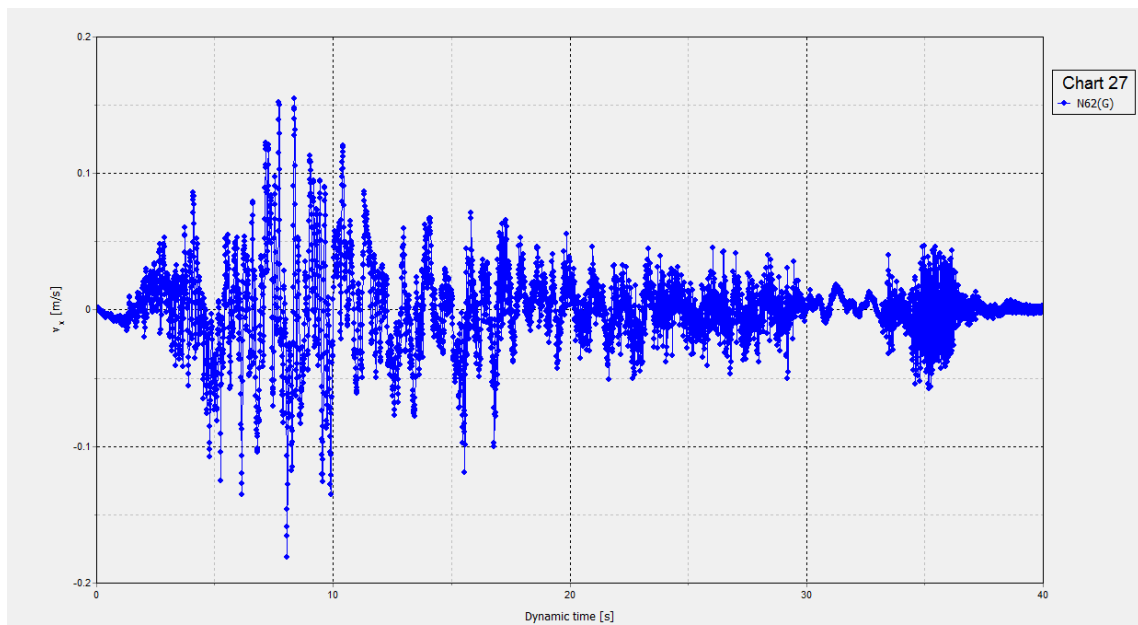
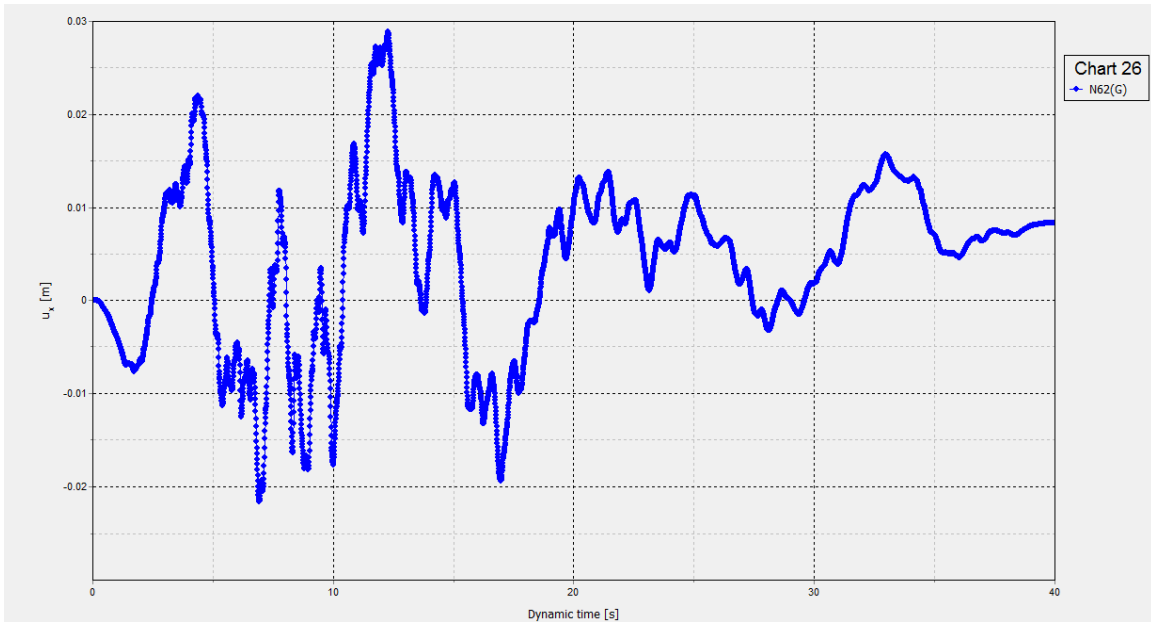


Figure 63 Time history of ground to Loma Prieta earthquake (top: displacement, bottom: velocity)

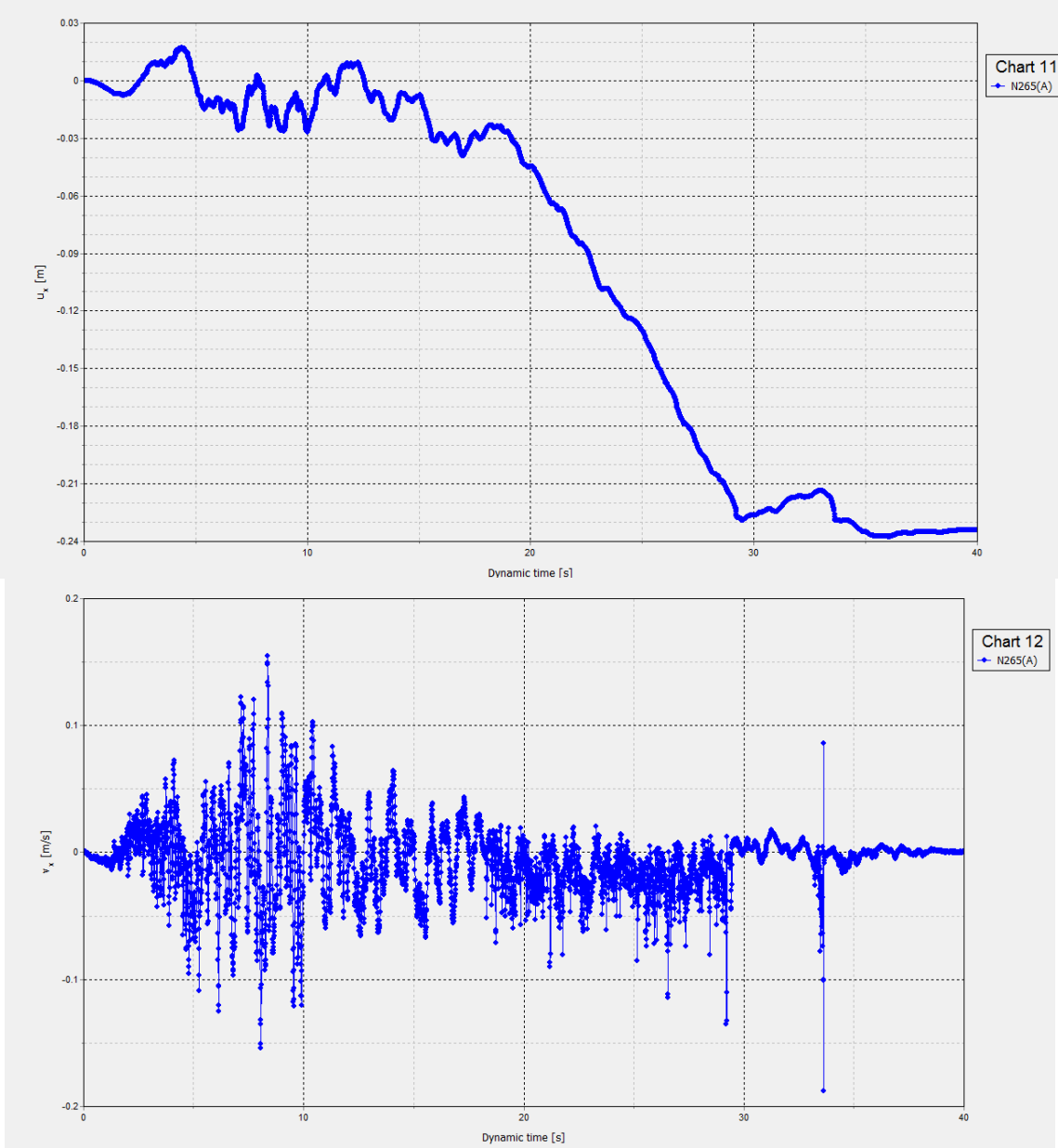


Figure 64 Time history of lower layer response to Loma Prieta earthquake (top: displacement, bottom: velocity)

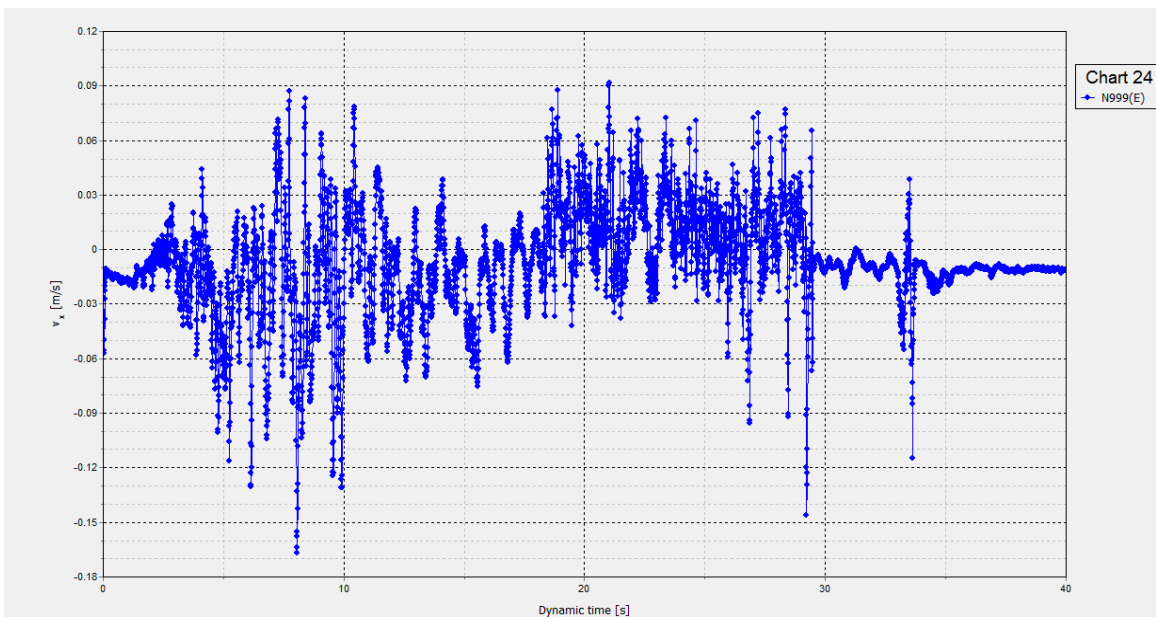
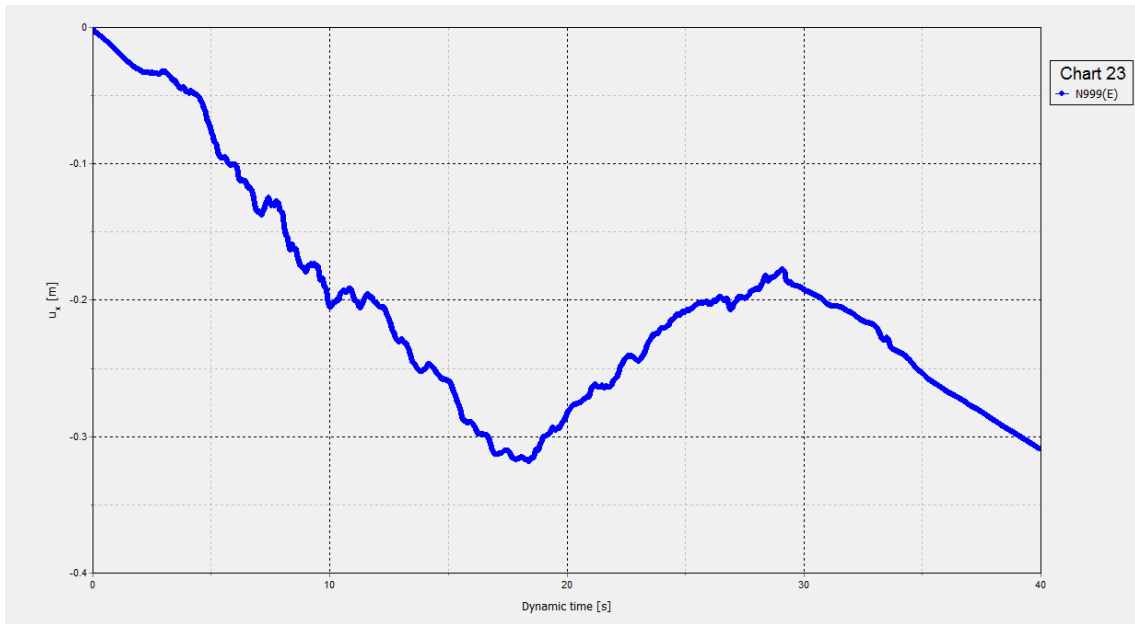


Figure 65 Time history of upper layer response to Loma Prieta earthquake (top: displacement, bottom: velocity)

(6) LWA backfill, sinusoidal sweep-frequency motions

(a) Shake Table Test

Immediately after the simulated Loma Prieta earthquake, sinusoidal sweep-frequency motions were run on the same MSE wall. The MSE wall failed during shaking frequency of 6 Hz: the MSE wall spread laterally and collapsed on the side panel in front of it, as shown in Figure 66.



(a) Before sinusoidal shaking



(b) After sinusoidal shaking

Figure 66. Illustration of MSE wall failure with LWA backfill

Figure 67 shows the lateral deflections (displacements) of the MSE wall measured at the top, middle, and bottom layers in the shake table test. It shows increased lateral deflections from the bottom toward the top of the wall and increased lateral deflection with the frequency. Since the wall collapsed and leaned against one side of the box, the lateral deflection measurements are less useful. Figure 68 shows the vertical deformations of the MSE wall in the shake table testing. The two LVDTs recorded similar settlements in the sinusoidal motions. But at $t = 48$ sec, the LVDT rods fell out of the LVDT tubes, thus no further measurements were available.

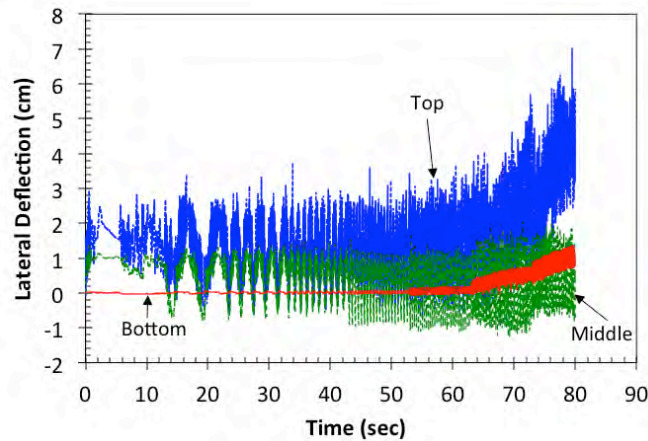


Figure 67. Lateral deflections of the MSE wall with LWA backfill, from sinusoidal sweep-frequency motions, after Loma Prieta earthquake

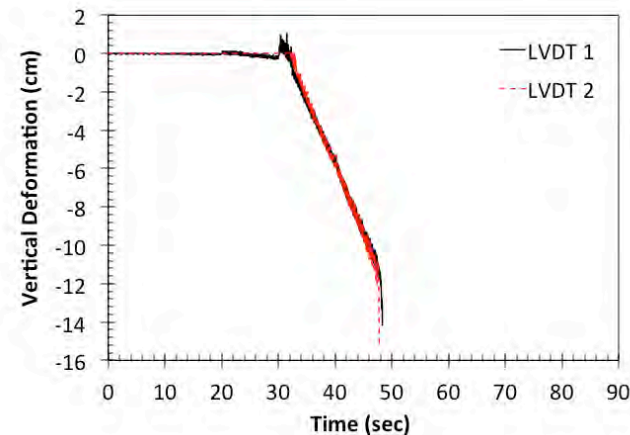


Figure 68. Vertical deformations of the MSE wall with LWA backfill, from sinusoidal sweep-frequency motions, after Loma Prieta earthquake

Figure 69 presents the lateral pressures on the LWA backfill, and Figure 70 shows the vertical stresses in the LWA backfill.

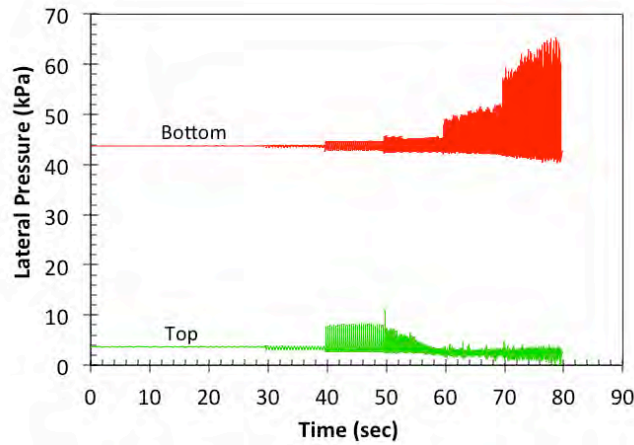


Figure 69. Lateral pressures on the LWA backfill of the MSE wall, from sinusoidal sweep-frequency motions, after Loma Prieta earthquake

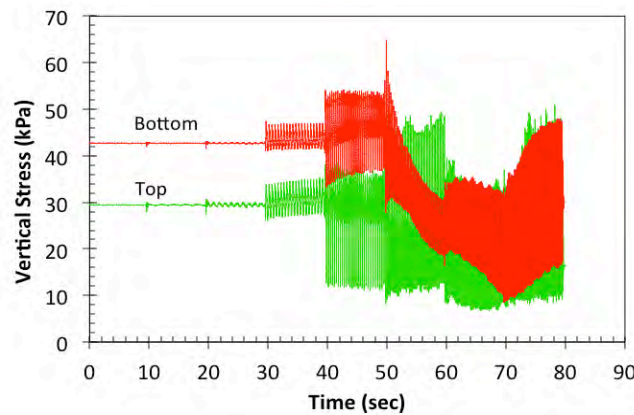


Figure 70. Vertical stresses in the LWA backfill of the MSE wall, from sinusoidal sweep-frequency motions, after Loma Prieta earthquake

The accelerometers recorded the acceleration ~ time histories of each layer, the table and the box. The maximum accelerations and their time of occurrence are listed in Table 10. Non-linear distribution of accelerations with the depth of the wall was observed. Since the maximum accelerations occurred after the failure of the MSE wall, the acceleration trend in Table 10 does not reveal the seismic performance.

Table 10. Maximum accelerations and time of occurrences

Location	Layer 1 (bottom)	Layer 2	Layer 3	Layer 4	Layer 5 (top)	Table	Box
Acc (g)	2.429	3.179	4.814	3.014	3.224	2.28	1.883
Time (sec)	71.81	70.33	70.67	74.16	50.49	74.65	71.74

(b) Numerical Model

The response of the MSE system with LWA backfill to the harmonic load is shown using time history of deformation, velocity, and stresses at various layers.

The results indicate an increase in maximum deflection of model as the frequency is increased from 0.2 Hz to 6 Hz. This qualitative outcome confirms experimental observations. But, quantitative maximum results overestimate experimental records, as they present failure of the system.

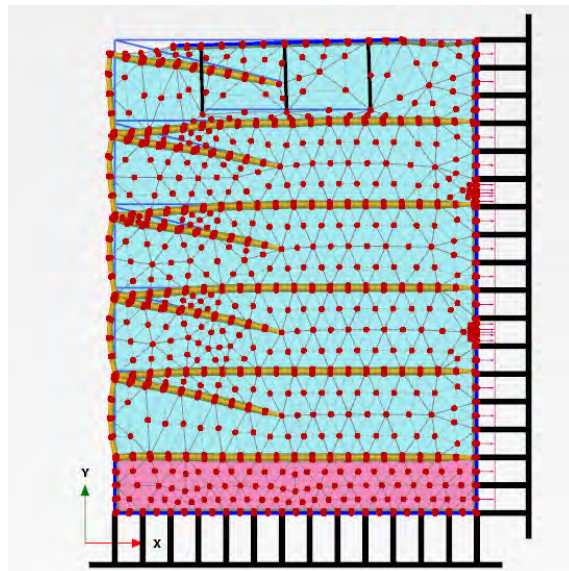


Figure 71 Typical deformed mesh, 0.2 Hz

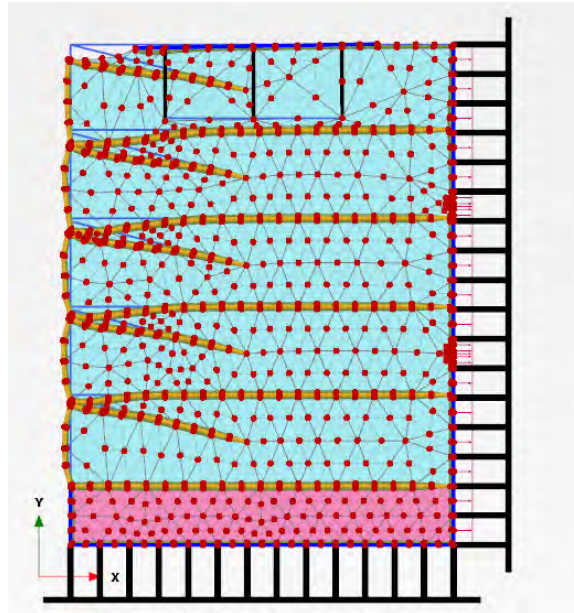


Figure 72 Typical deformed mesh, 4 Hz

Closer observations reveal that overall PLAXIS results for displacement and velocity follow a harmonic pattern, even though, results include noises in velocity time history due to lack of convergence. In general, it can be seen that the model tested with LWA shows less convergence than the model tested with TDA. These graphs appear to show a straight line but are actually harmonic. This cannot be clearly seen from these representations due to the lower amount of time steps used in order to shorten the run time of the model.

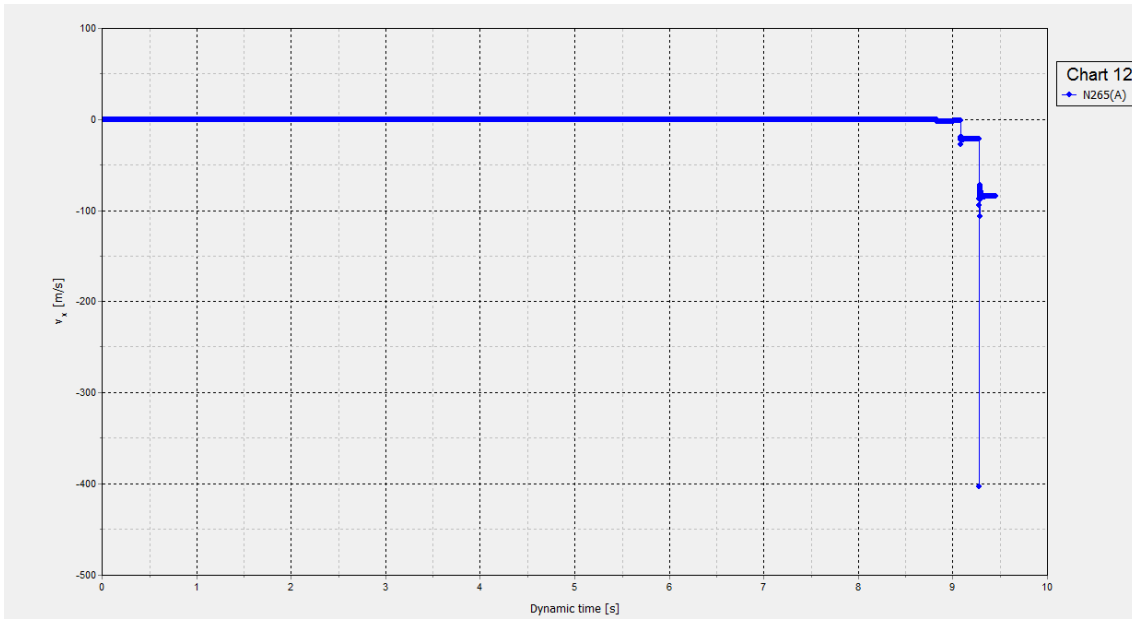
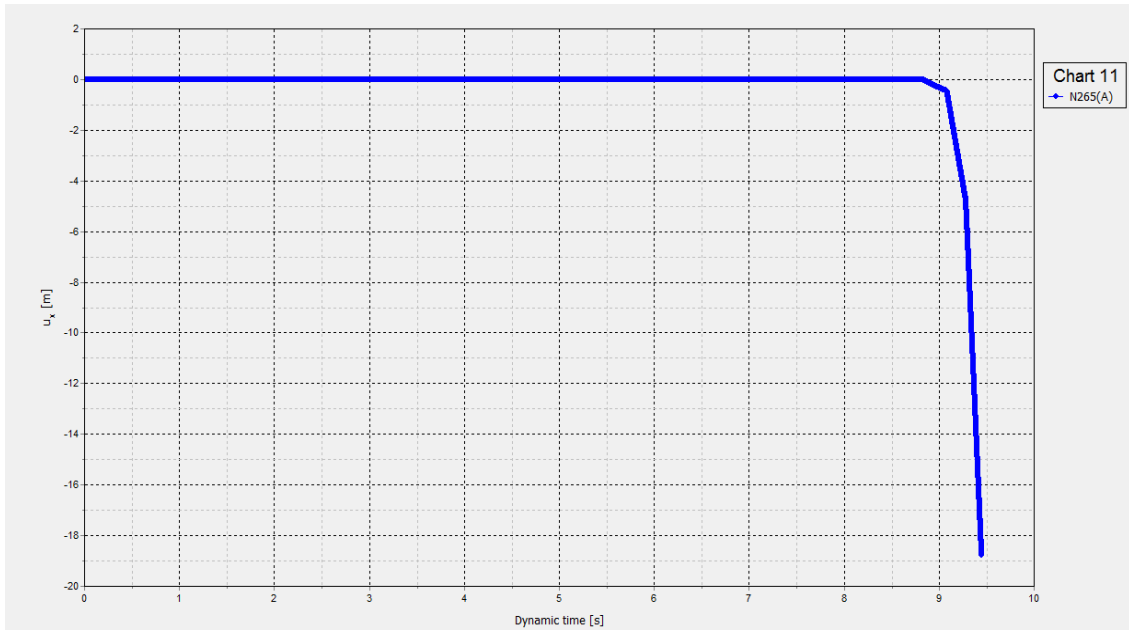


Figure 73 Time history response of lower layer to 0.2 Hz (left: displacement, right: velocity)

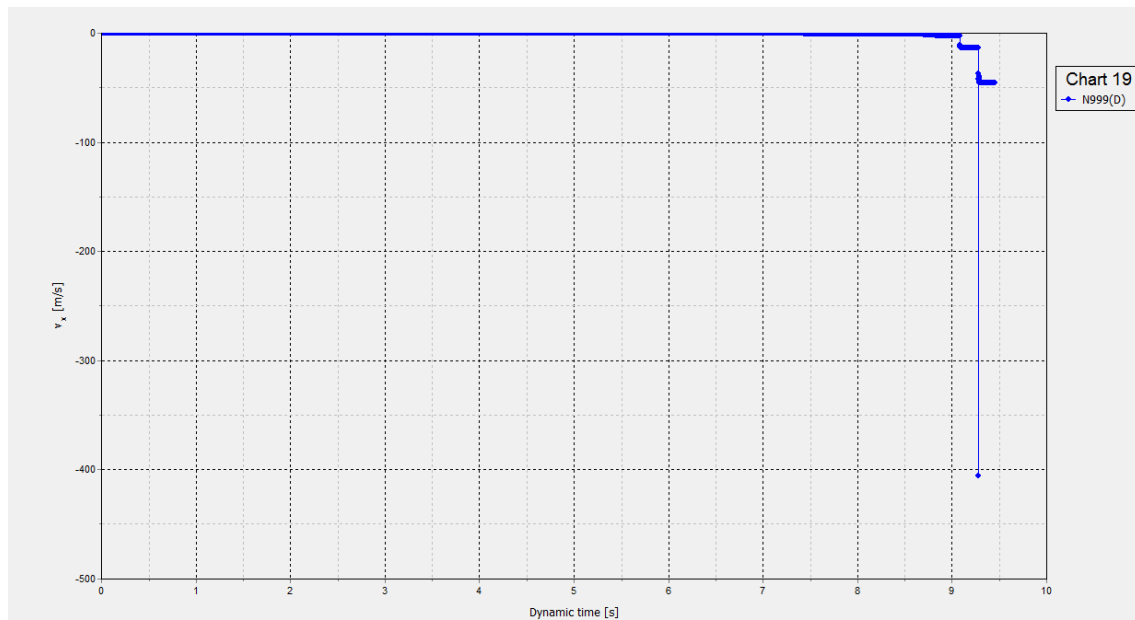
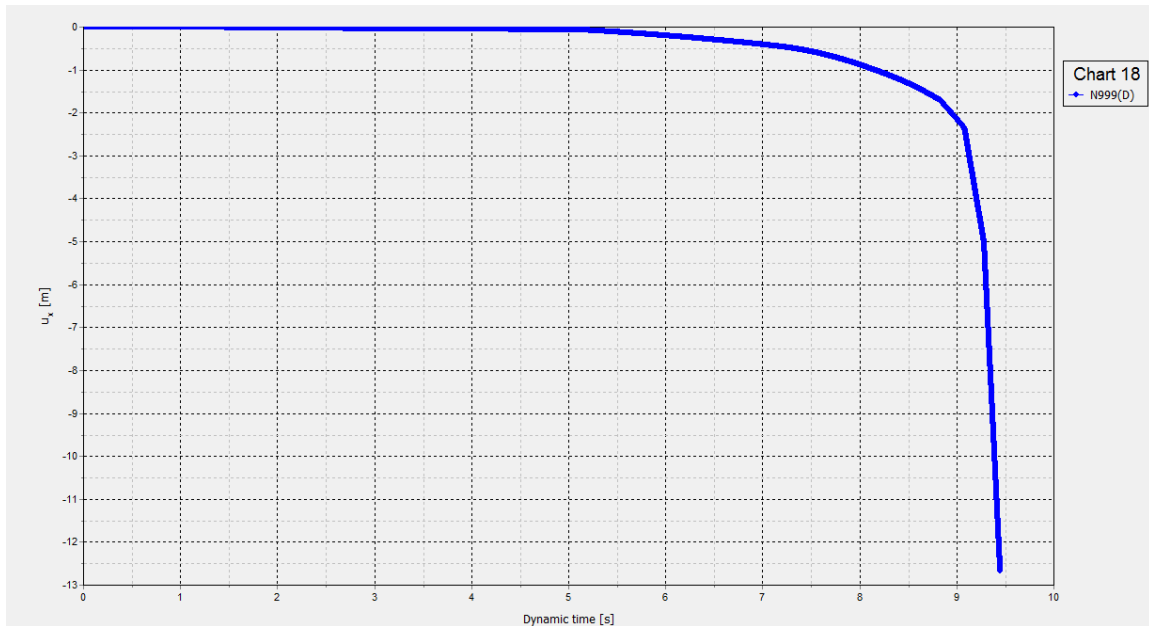


Figure 74 Time history of upper layer response to 0.2 Hz (left: displacement, right: velocity)

Time histories of horizontal and vertical stresses are subject to the same convergence issues as for velocity. Nevertheless, the average values indicate acceptable results. The sudden drop in these graphs indicates failure of the model, which occurs during the last excitation.

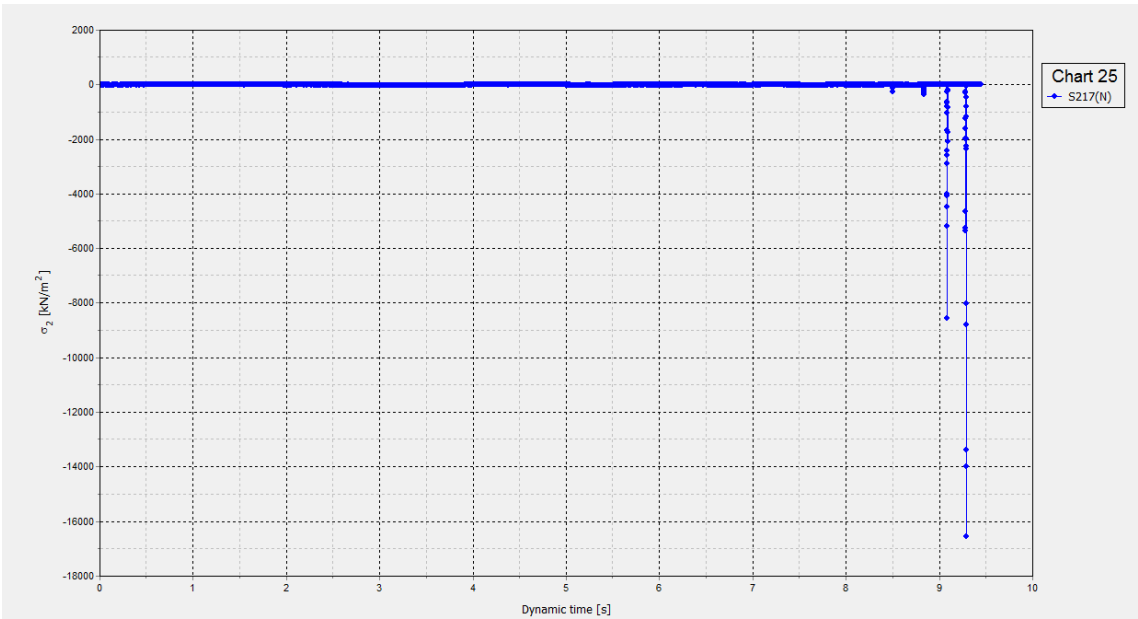
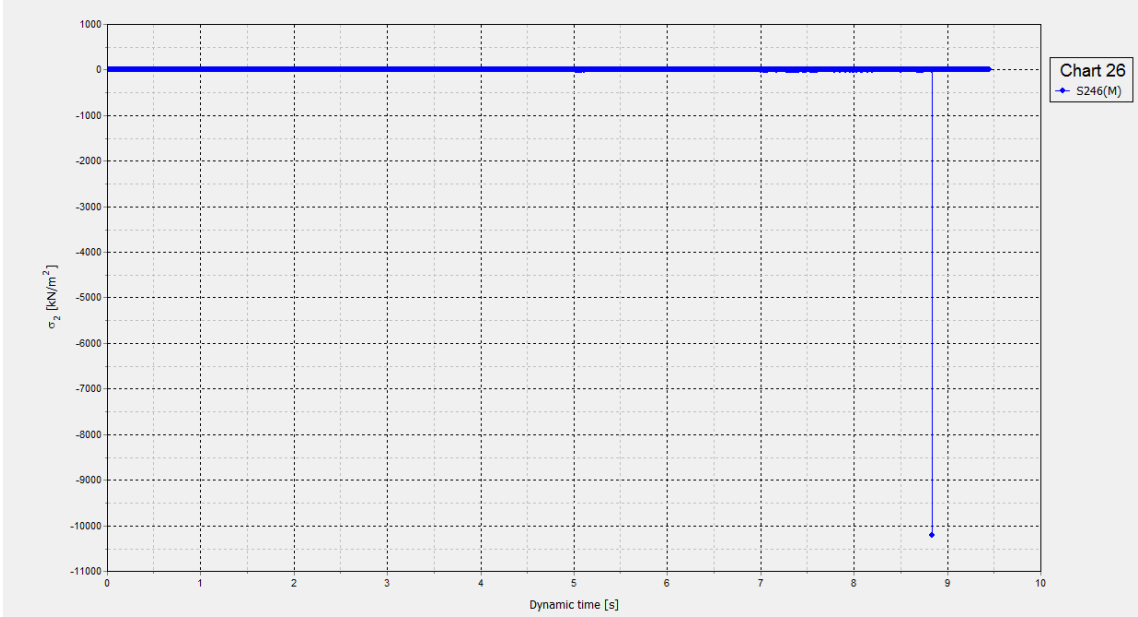


Figure 75 Time history of horizontal stress (top: upper layer, bottom: lower layer)

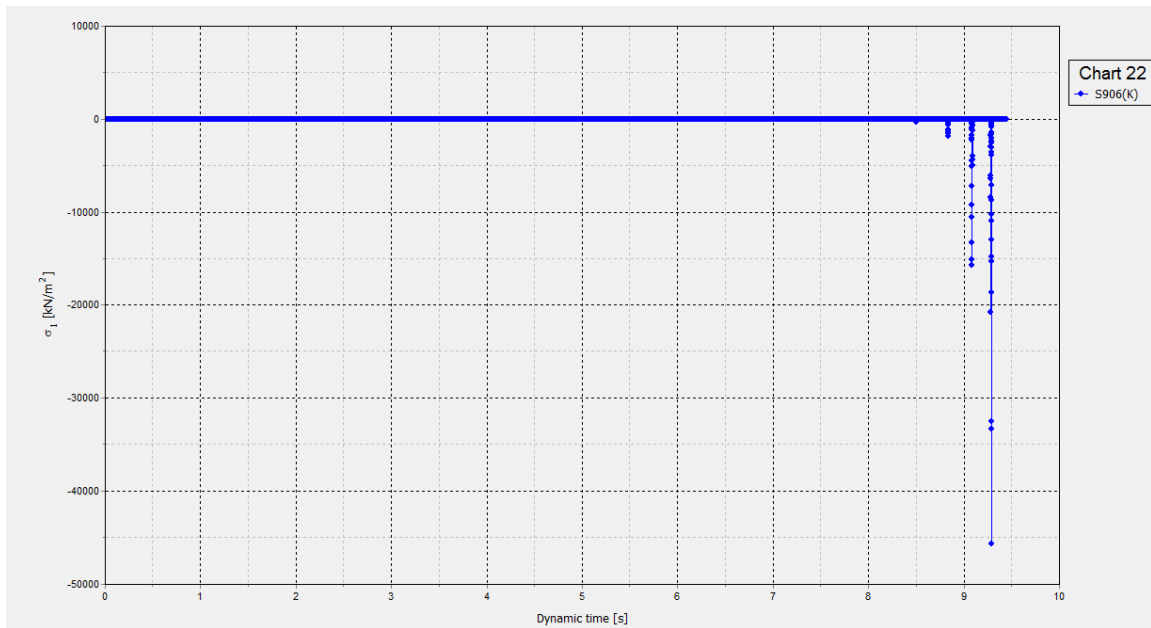
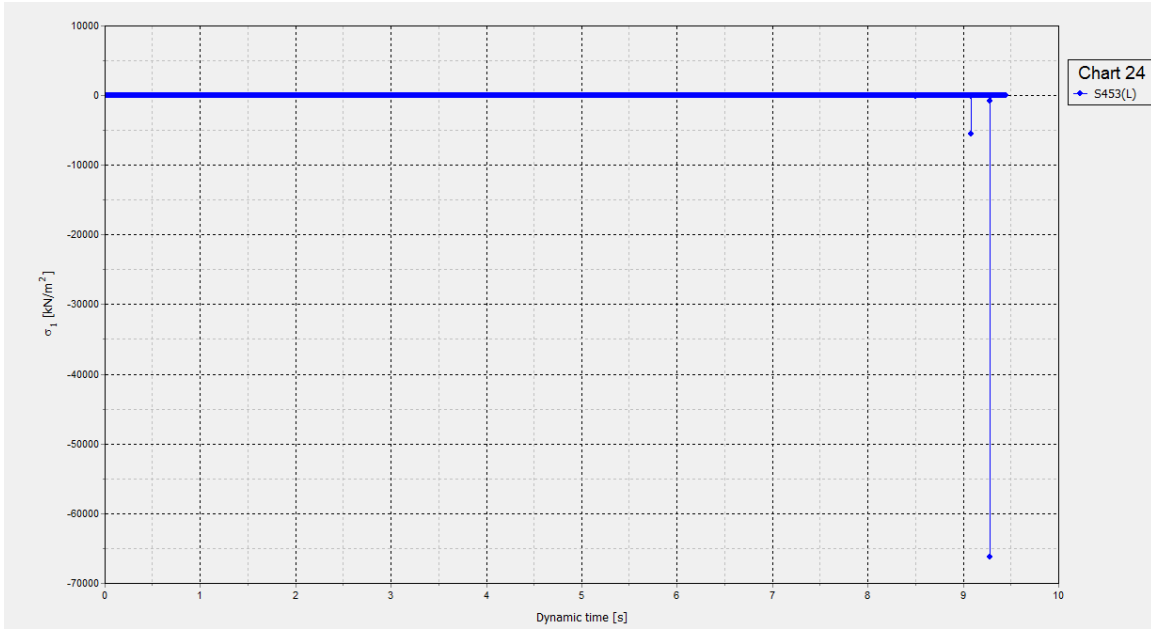


Figure 76 Time history of vertical stress (top: upper layer, bottom: lower layer)

(7) LWA backfill, Northridge earthquake

(a) Shake Table Test

After the shake table testing, the MSE wall with LWA backfill did not have noticeable damage. Noticeable lateral deflections were noticed. Figure 77 shows the lateral deflections (displacements) of the MSE wall measured at the top, middle, and bottom layers in the shake table test. It shows increased lateral deflections from the bottom toward the top of the wall. The maximum horizontal deflection was approximately 7.9 cm, higher than the MSE wall with TDA backfill under the same shaking. Also important to note is that the LWA backfill tended to oscillate laterally: both movements into and away from the backfill occurred. The same behavior occurred under the simulated Loma Prieta earthquake. This is different from the TDA backfill, which only moved away from the backfill.

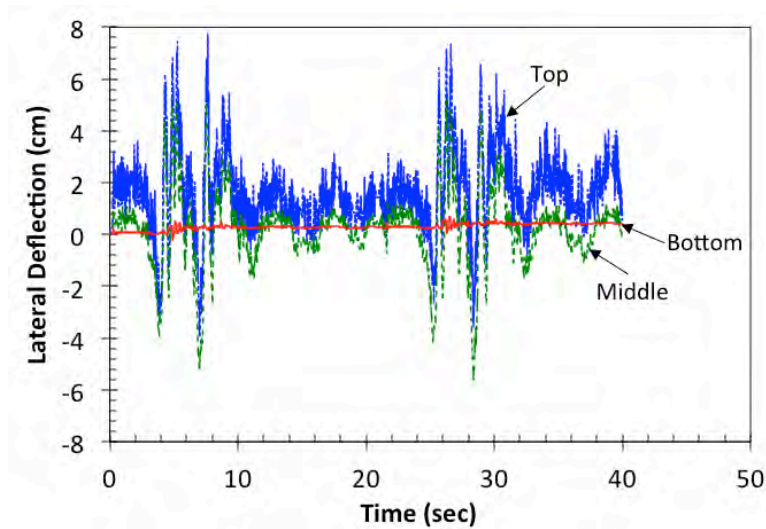


Figure 77. Lateral deflections of the MSE wall with LWA backfill, from Northridge earthquake

Figure 78 shows the vertical deformations of the MSE wall in the shake table testing. Both LVDT showed similar settlements. The maximum vertical deformation was approximately 2.0 cm.

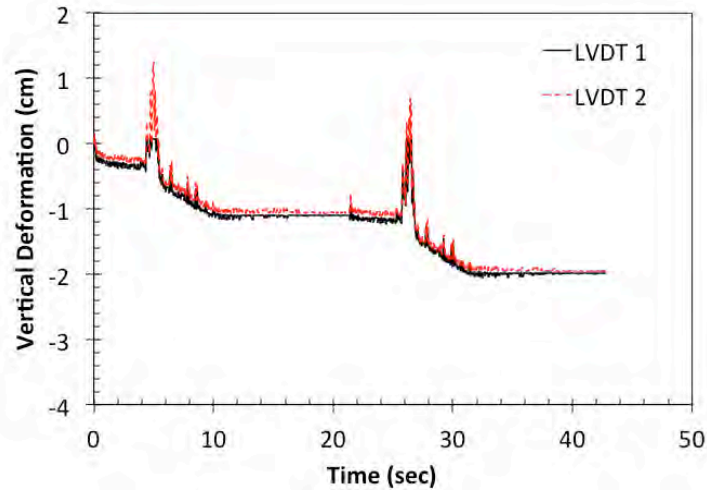


Figure 78. Vertical deformations of the MSE wall with LWA backfill, from Northridge earthquake

Figure 79 presents the lateral pressures on the LWA backfill, and Figure 80 shows the vertical stresses in the TDA backfill. It is noted that vertical stress at the top is higher than that at the bottom. The same trend occurred during the simulated Loma Prieta earthquake. Nevertheless, the investigators believe the vertical pressure measurements may be incorrect.

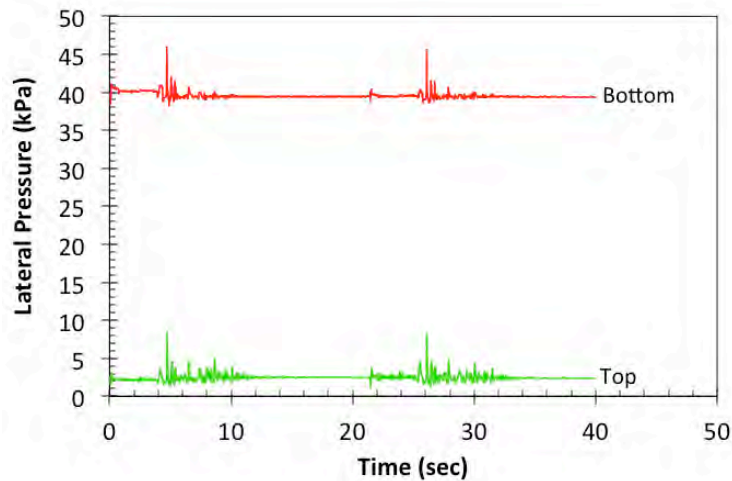


Figure 79. Lateral pressures on the LWA backfill of the MSE wall, from Northridge earthquake

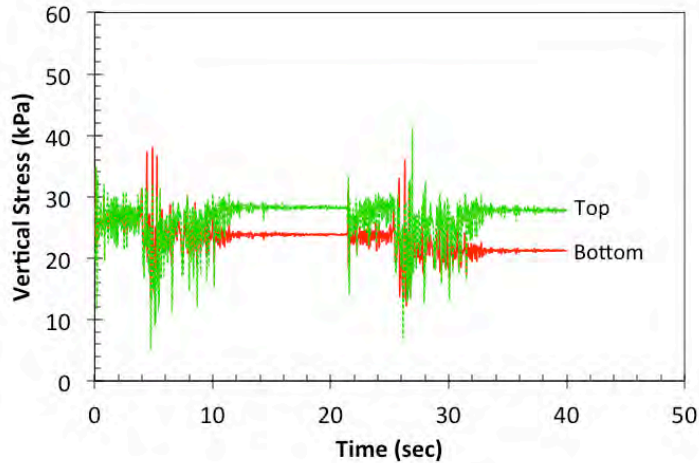


Figure 80. Vertical stresses in the LWA backfill of the MSE wall, from Northridge earthquake

The accelerometers recorded the acceleration ~ time histories of each layer, the table and the box. The maximum accelerations and their time of occurrence are listed in Table 10. The accelerations showed a clear increasing trend from the bottom to top. The same trend occurred under the simulated Loma Prieta earthquake. But this is different from the TDA backfill under the same shaking, which showed a non-linear distribution of acceleration with depth.

Table 11. Maximum accelerations and time of occurrences

Location	Layer 1 (bottom)	Layer 2	Layer 3	Layer 4	Layer 5 (top)	Table	Box
Acc (g)	1.466	1.821	2.152	3.014	3.033	1.214	1.319
Time (sec)	26.05	26.05	26.05	5.07	5.07	26.05	4.67

(8) LWA backfill, sinusoidal sweep-frequency motions

(a) Shake Table Test

Immediately after the simulated Northridge earthquake, sinusoidal sweep-frequency motions were run on the same MSE wall. The MSE wall failed during shaking frequency of 6 Hz: the MSE wall spread laterally and collapsed on the side panel in front of it, as shown in Figure 81.



(a) Before sinusoidal shaking



(a) After sinusoidal shaking

Figure 81. Illustration of MSE wall failure with LWA backfill

Figure 82 shows the lateral deflections (displacements) of the MSE wall measured at the top, middle, and bottom layers in the shake table test. It shows increased lateral deflections from the bottom toward the top of the wall and increased lateral deflection with the frequency. Since the wall collapsed and leaned against one side of the box, the lateral deflection measurements are less useful. Figure 83 shows the vertical deformations of the MSE wall in the shake table testing. The two LVDTs recorded similar settlements in the sinusoidal motions. But at $t = 36$ sec, the LVDT rods fell out of the LVDT tubes, thus no further measurements were available.

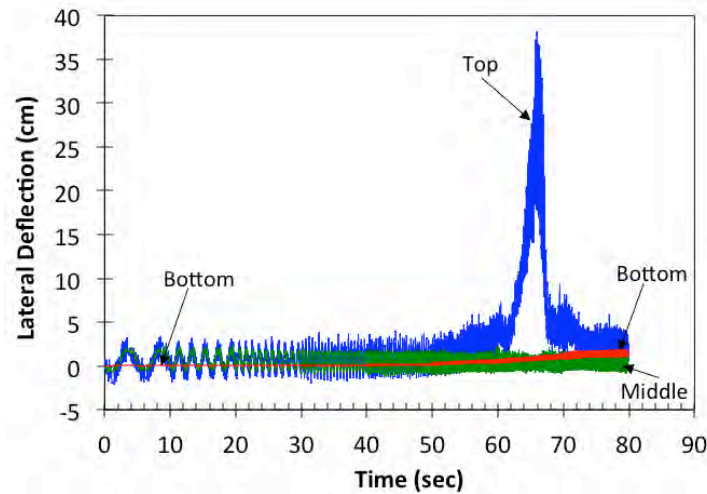


Figure 82. Lateral deflections of the MSE wall with LWA backfill, from sinusoidal sweep-frequency motions, after Northridge earthquake

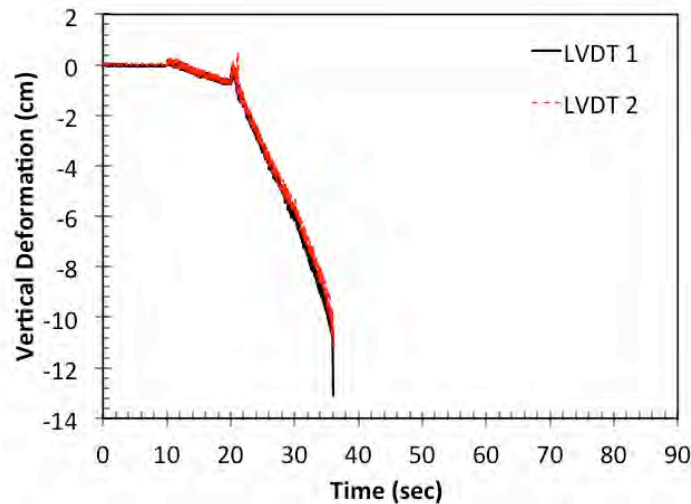


Figure 83. Vertical deformations of the MSE wall with LWA backfill, from sinusoidal sweep-frequency motions, after Northridge earthquake

Figure 84 presents the lateral pressures on the TDA backfill, and Figure 85 shows the vertical stresses in the TDA backfill.

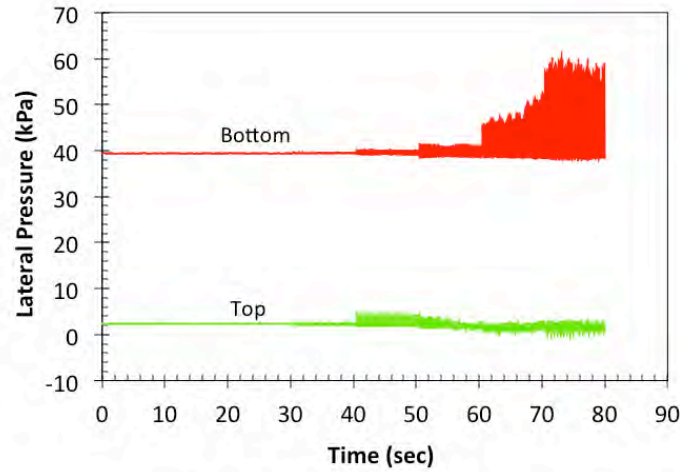


Figure 84. Lateral pressures on the LWA backfill of the MSE wall, from sinusoidal sweep-frequency motions, after Northridge earthquake

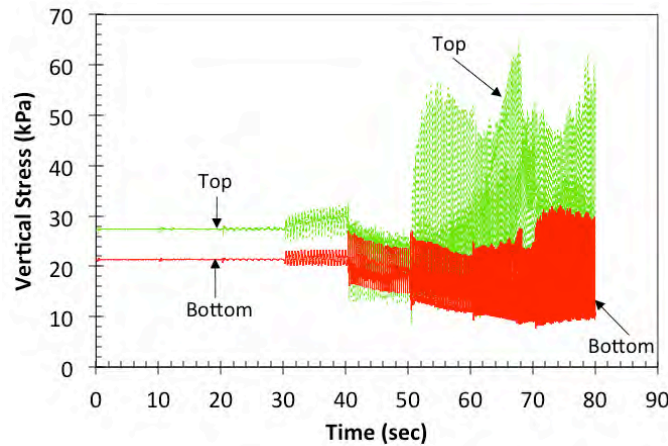


Figure 85. Vertical stresses in the LWA backfill of the MSE wall, from sinusoidal sweep-frequency motions, after Northridge earthquake

The accelerometers recorded the acceleration ~ time histories of each layer, the table and the box. The maximum accelerations and their time of occurrence are listed in Table 12. Non-linear distribution of accelerations with the depth of the wall was observed. However, all the maximum accelerations occurred after the wall failed and are, therefore, less useful.

Table 12. Maximum accelerations and time occurrences

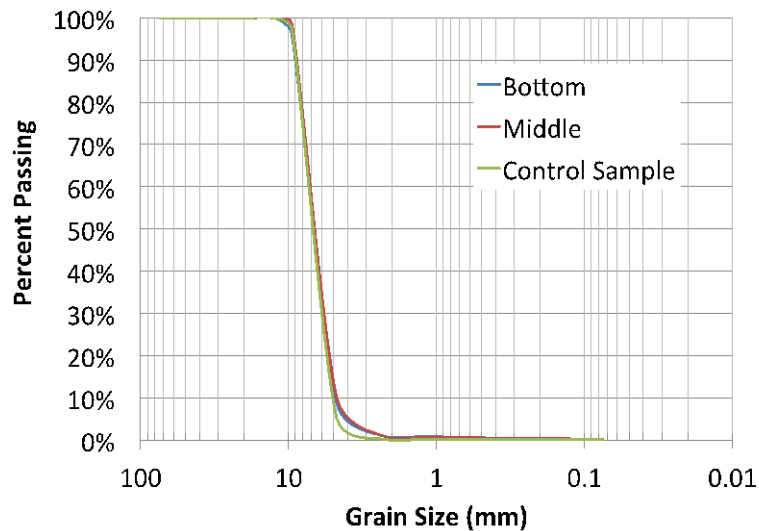
Location	Layer 1 (bottom)	Layer 2	Layer 3	Layer 4	Layer 5 (top)	Table	Box
Acc (g)	2.28	2.973	3.894	3.759	2.513	2.233	1.78
Time (sec)	70.47	71.00	71.53	60.21	78.25	73.99	71.16

(b) Numerical Model

The results for the model with LWA subject to the Northridge earthquake are not presented here. The model was run for this earthquake but the model would not converge under this loading even after the addition of 10,000 steps in PLAXIS, which took over 12 days to run.

(9) Post-Shake Evaluation of LWA

In order to evaluate whether the LWA were crushed due to the seismic shaking, LWA samples were retrieved from the middle and the bottom of the layer 1 (bottom), 3, and 5 (top), after Test 6 and after Test 8, respectively. Sieve analyses were performed and compared with the control sample that did not experience seismic shaking. The grain size distributions after the Test 6 are shown in Figure 86; the grain size distributions after the Test 8 are shown in Figure 87. The test results showed the grain sizes became slightly smaller after the shaking. However, the majority of the grains remained the same sizes as the control sample.



(a) Bottom layer

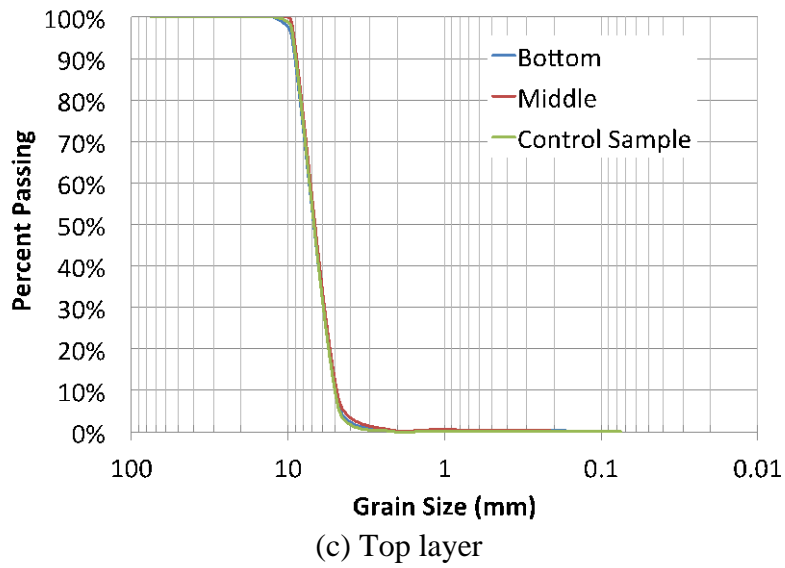
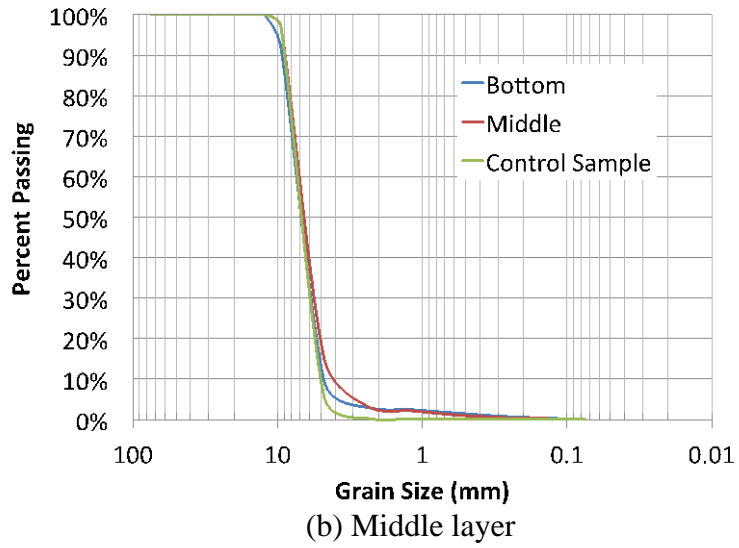
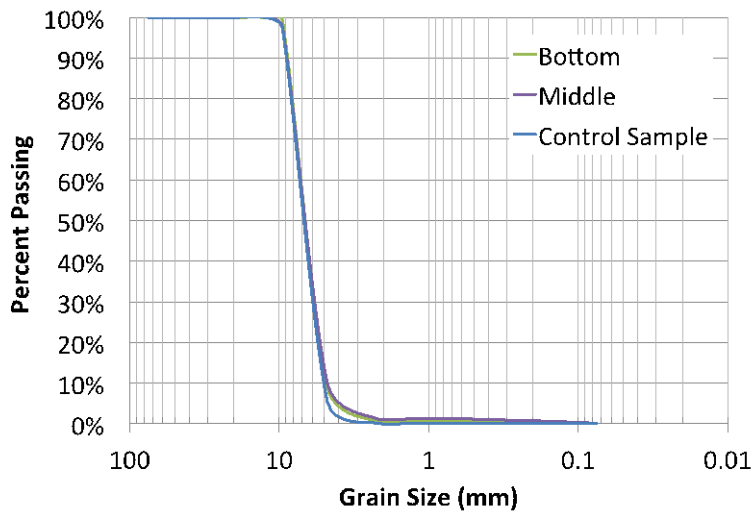
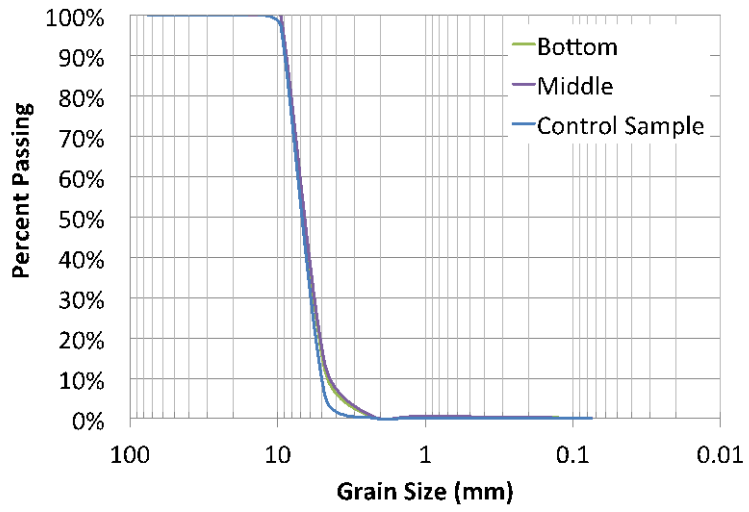


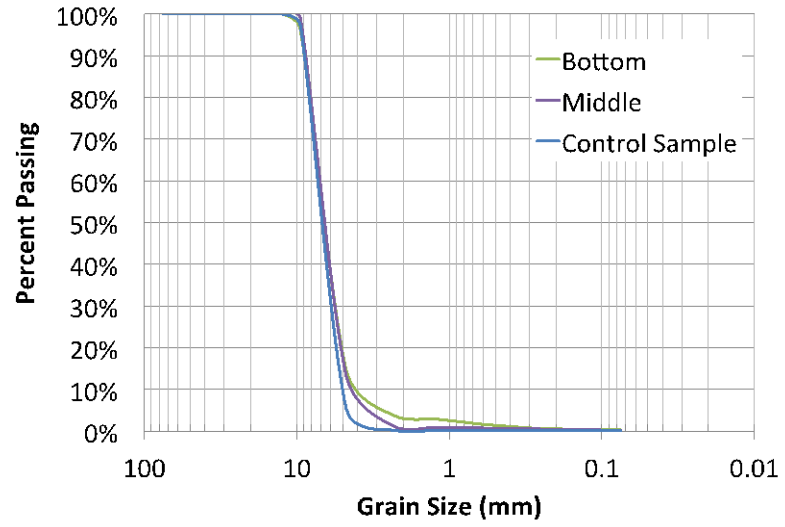
Figure 86. Grain size distributions of LWA after Test 6 (sinusoidal shaking following Loma Prieta excitation)



(a) Bottom layer



(b) Middle layer



(c) Top layer

Figure 87. Grain size distributions of LWA after Test 8 (sinusoidal shaking following Northridge excitation)

5. CONCLUSIONS

This project investigated the seismic performances of MSE walls with two alternative backfill materials: tired derived aggregates (TDA) and lightweight aggregates (LWA). Small-scale shake table testing and numerical model analyses using Plaxis were used as investigation tools. Seismic design was used in the model MSE wall construction and flexible boundary was incorporated in the shake table testing. Simulated full-scale Loma Prieta earthquake, Northridge earthquake, and sinusoidal sweep-frequency motions (0.2 to 6 Hz) were used in the shake table testing and numerical modeling. The following conclusions and observations were obtained from this project.

- (1) When properly designed, MSE walls with TDA backfill can sustain strong seismic shaking without excessive deformation and lateral spreading. No pullout, tensile overstress, or internal sliding failure occurred. The MSE wall with TDA backfill sustained sinusoidal shaking with maximum acceleration of 2.2 g. Non-linear distribution of accelerations with the depth of the wall was observed
- (2) The MSE walls with LWA backfill sustained the simulated full-scale Loma Prieta earthquake and Northridge earthquake. No pullout, tensile overstress, or internal sliding failure occurred. The wall had some vertical deformation, about 2.0 cm or 1.3% of the wall height, and noticeable lateral deflection, about 8.0 cm or 1.5% of wall height. The lateral deflections increased from the bottom to the top of the wall. LWA backfill tended to oscillate laterally: both movements into and away from the backfill occurred. Maximum accelerations increased from the bottom to the top of the wall.
- (3) The MSE wall with LWA backfill failed under sinusoidal shaking with maximum acceleration of 2.2 g.
- (4) When comparing the seismic performances, TDA is clearly a more suitable backfill material than LWA in seismic regions.
- (5) Breaking (crushing) of LWA during strong seismic motions was insignificant. The majority of the lightweight aggregates were not affected by the shaking.
- (6) The concrete slab was used to secure the top geogrid reinforcement in the MSE wall with TDA backfill. When the concrete slab was removed and the MSE wall was subjected to sinusoidal shaking with maximum acceleration of 2.2 g, the geogrid reinforcement in the top layer pulled out during the strong seismic motion, causing the TDA backfill in the top layer to spill.
- (7) The FHWA seismic design methodology for MSE walls with traditional backfill may be suitable for TDA and LWA backfill.
- (8) Numerical model verified the validity of the spring-supported panel as flexible boundary to simulate dense sand. The numerical model showed the lateral

deflections of the MSE wall matched well with the artificial flexible boundary and the true boundary of vast dense sand.

- (9) The discrepancy between the numerical and the experimental results may be due to the input values of the material characteristics. In the future study, the shake table tests can be used to calibrate the numerical model, which can then be used to verify the boundary conditions used in the shake table testing and further predict seismic performances of in-situ MSE walls with TDA backfill.
- (10) The numerical results warrant further studies to incorporate other soil models for alternative backfill materials. The model parameters might be obtained from either conventional testing or experimental results of shake table studies.

6. DESIGN and CONSTRUCTION RECOMMENDATIONS

- (1) The type-A TDA backfill should be compacted at least 43 lb/ft³. No moistening of TDA is needed. The LWA backfill should be compacted to 95% of its maximum dry density at optimum water content.
- (2) The shear strength of the large-sized aggregates (TDA and LWA) should be experimentally obtained.
- (3) The FHWA “Mechanically Stabilized Earth Walls and Reinforced Soil Slopes Design and Construction Guidelines” (FHWA-SA-96-071) may be used to design the MSE walls with TDA and LWA backfills.
- (4) When constructing MSE walls with TDA backfill, particular efforts should be made to secure the top reinforcement layer into the backfill, if using a wrap-around configuration.
- (5) Tire derived aggregates (TDA) may be a suitable alternative backfill material for MSE walls in seismic regions. More study should follow to investigate the seismic performances of this type of MSE walls in full scale, using experimentally calibrated numerical model.

7. REFERENCES

- ACCT, FHWA (2005). "ACCT II–The Second Year Report of the Accelerated Construction Technology Transfer Program." March 2005.
- ACCT, FHWA (2006). "ACCT III–The Third Year Report of the Accelerated Construction Technology Transfer Program." Publication No. FHWA-IF-06-028. January 2006.
- ACCT, FHWA (2007). "Accelerated Construction Technology Transfer, Building on Success." Publication No. FHWA-IF-07-015. January 2007.
- Bathurst, R. J., and Cai, Z. (1995). "Pseudo-static seismic design of geosynthetic-reinforced segmental retaining walls." *Geosynthet. Int.*, 2(5), 787–830.
- Bosscher, P. J., Edil, T. B., and Eldin, N. N. (1992). "Construction and performance of a shredded waste tire test embankment." *Transportation Research Record. 1345*, Transportation Research Board, Washington, D.C., 44–52.
- Bosscher, P.J., Edil, T.B., and Kuraoka, S. (1997). "Design of highway embankments using tire chips." *ASCE J. Geotech. and Geoenviron. Eng.*, 123(4), 295-304.
- CalRecycle (2010). <http://www.calrecycle.ca.gov/tires/>. Last accessed on Aug 28, 2010.
- Collin, J. G., Chouery-Curtis, V. E., and Berg, R. R. (1992). "Field observations of reinforced soil structures under seismic loading." *Proc., Int. Symp. on Earth Reinforcement Pract., Earth reinforcement practice*, H. Ochiai, N. Yasufuku, and K. Omine, eds., Vol. 1, Balkema, Rotterdam, The Netherlands, 223–228.
- Doven, A.G., and Pekrioglu, A. (2005). "Material Properties of High Volume Fly Ash Cement Paste Structural Fill." *ASCE J. Mat. in Civ. Engrg.* 17(6), 686-693.
- Eliahu, U., and Watt, S. (1991). "Geogrid-reinforced wall withstands earthquake." *Geotech. Fabrics Rep.*, 9(2), 8–13.
- Federal Highway Administration, U.S. Department of Transportation. (2006). "Accelerated Construction Technology Transfer (ACTT)." FHWA-HRT-06-054.
- Federal Highway Administration (FHWA), Elias, V., Christopher, B.R., 1998. Mechanically Stabilized Earth Walls and Reinforced Soil Slopes Design and Construction Guidelines. FHWA-SA-96-071, Washington, DC, September, 371pp.
- Foose, G.J., Benson, G.H., Bosscher, P.J. (1996). "Sand reinforced with shredded waste tires." *ASCE J. Geotech. Eng.*, 122(9), 760-767.
- Helwany, M.B., and McCallen, D. (2002). "Seismic analysis of segmental retaining walls. II: effects of facing details." *ASCE J. Geotech. and Geoenviron. Engrg.*, 127(9), 750-756.
- Helwany, M.B., Wu, J.T.H, and Kitsabunnarat, A. (2007). "Simulating the behavior of GRS bridge abutments." *ASCE J. Geotech and Geoenviron. Engrg.*, 133(10), 1229-1240.
- Holm T. A. and Valsangkar A. J., "Lightweight Aggregate Soil Mechanics: Properties and Applications," Transportation Research Board, National Research Council, Washington, D.C., Transportation Research Record 1422: Soils Geology and Foundations: Lightweight Artificial and Waste Materials for Embankments Over Soft Soils, 1993, Reprinted 2001.
- Huang, C.C. and Tatsuoka, F. (2001). "Stability analysis of the geosynthetic-reinforced modular block walls damaged during the Chi-Chi Earthquake." *Proc. Fourth Int. Conf. on Recent Advances in Geotech. Earthquake Engrg. and Soil Dyn.*, San Diego.
- Humphrey, D. N. (1998). "Highway applications of tire shreds." *New England Transportation Consortium Rep.*, September.

- Humphrey, D. N., and Manion, W. P. (1992). "Properties of tire chips for lightweight fill." *Proc. Conj. on Grouting, Soil Improvement, and Geosynthetics*, 2 ASCE, New York, 1344-1355.
- Itasca Consulting Group (2000). *FLAC version 4.0 User's Guide*. Minneapolis, MN.
- Lee, J.H., Salgado, R., Bernal, A., and Lovell, C.W. (1999). "Shredded tires and rubber-sand as lightweight backfill." *ASCE J. Geotech. and Geoenviron. Eng.*, 125(2), 132-141.
- Lindquist, D.D. (2008). "Seismic modeling of a 135-foot-tall MSE wall." Proceedings of the Geotechnical Earthquake Engineering and Soil Dynamics IV (CD), ASCE GSP 181.
- Ling, H. I., Leshchinsky, D., and Perry, E. B. (1997). "Seismic design and performance of geosynthetic-reinforced soil structures." *Geotechnique*, 47(5), 933-952.
- Ling, H. I., and Leshchinsky, D. (1998). "Effects of vertical acceleration on seismic design of geosynthetic-reinforced soil structures." *Geotechnique*, 48(3), 347-373.
- Ling, H.I., Liu, H., and Mohri, Y. (2004). "Parametric studies on the behavior of retaining walls under earthquake loading." *J. Engineering Mechanics*, 131(10), 1056-1065.
- Ling, H.I., Hohri, Y., Leshchinsky, D., Burke, C., Matsushima, K., Liu, H. (2005). "Large-scale shaking table tests on modular-block reinforced soil retaining walls." *ASCE J. Geotech and Geoenviron. Engrg.*, 131(4), 465-476.
- Ling, H.I. Leshchinsky, D., Wang, J.P., Hohri Y., and Rosen, A. (2008). "Seismic responses of geocell retaining walls: experimental studies." *J. Geotech. and Geoenviron. Engrg.*, 135(4), 515-524.
- Ling, H.I., Leshchinsky, D., Chou, N.S. (2001). "Post-earthquake investigation on several geosynthetic-reinforced soil retaining walls and slopes during the Ji-Ji earthquake of Taiwan." *Soil Dynamics and Earthquake Engineering*, 21, 297-313.
- Mirdamadi, A., Shamsabadi, S.S., Kashi, M.G., Nemati, M., and Shekarchizadeh, M. (2009). "Geotechnical Properties of Controlled Low Strength Materials (CLSM) Using Waste Electric Arc Furnace Dust (EAFD)." *Slope Stability, Retaining Walls, and Foundations (GSP 197)*, Proceedings of the 2009 GeoHunan International Conference.
- National Concrete Masonry Association (NCMA). (1997). *Design Manual for Segmental Retaining Walls*. Collin, J.G. (Ed.), Herndon, VA, 289pp.
- Richardson, G.N., and Lee, K.L. (1975). "Seismic design of reinforced earth walls." *ASCE J. Geotech. Eng. Div.*, 101(2), 167-188.
- Sandri, D. (1994). "Retaining walls stand up to the Northridge earthquake." *Geotech. Fabrics Rep.*, 12(4), 30-31.
- Shamsabadi, A., Rollins, K.M., Kapuska, M. (2007). "Nonlinear soil-abutment-bridge structure interaction for seismic performance-based design." *ASCE J. Geotech. and Geoenviron. Eng.*, 133(6), 707-720.
- Siddharthan, R.V., Ganeshwara, V., Kutter, B. El-Desouky, M., and Whitman, R. (2004). "Seismic deformation of bar mat mechanically stabilized earth walls. I: centrifuge tests." *ASCE J. Geotech. and Geoenviron. Engrg.*, 130(1), 14-25.
- Strenk, P.M., Wartman, J., Grubb, D.G., Humphrey, D.N., Natale M.F. (2007). "Variability and scale-dependency of tire-derived aggregate." *ASCE J. Materials in Civil Engineering*, 19(3), 233-241.
- Tandon, V., Velazco, D.A., Nazarian, S., and Picornell M. (2007). "Performance monitoring of embankments containing tire chips: case study." *ASCE J. of Performance of Constructed Facilities*, 21(3), 207-214.

- Tatsuoka, F., Tateyama, M., and Koleski, J. (1996). "Performance of soil retaining walls for railway embankments." *Soils and Foundations, Special Issue*, Japanese Geotechnical Society, 311-324.
- Tatsuoka, F., Koseki, J., and Tateyama, M. (1997). "Performance of reinforced soil structures during the 1995 Hyogo-ken Nanbu Earthquake." *Earth reinforcement*, H. Ochiai et al., eds., Balkema, Rotterdam, The Netherlands, 973–1008.
- Tehrani F. (1998) "Raah-nama-ie Jaame-e Leca" (Leca Handbook, in Persian), Leca Co. LTD.
- Tsang, H. H. (2008). "Seismic isolation by rubber-soil-mixtures for developing countries." *Earthquake Engineering and Structural Dynamics*, 37, 283-303.
- Turner-Fairbank Highway Research Center (TFHRC), FHWA. (2010). <http://www.tfhrc.gov/hnr20/recycle/waste/st1.htm>. Last accessed on Aug 28, 2010.
- Tweedie, J.J., Humphrey, D.N., Sandford, T.C. (1998). "Tire shreds as lightweight retaining wall backfill: active conditions." *ASCE J. Geotech. and Geoenviron. Eng.*, 124(11), 1061-1070.
- Wartman, J., Natale, M.F., and Strenk, P.M. (2007). "Immediate and time-dependent compression of tire derived aggregate." *ASCE J. Geotech. and Geoenviron. Eng.*, 133(3), 245-256.
- Watn, Arnstein, et al. (2004). "LWAgeolight: LWA for Roads and Railways." Internordic research and Development Project Final Technical Report. SINTEF Civil and Environmental Engineering.